

The effect of seasonal temperature variations on the quay walls in the Port of Rotterdam

Konstantinos Patrikis



The effect of seasonal temperature variations on the quay walls in the Port of Rotterdam

by

Konstantinos Patrikis

to obtain the degree of Master of Science
at the Delft University of Technology,
to be defended publicly on Monday January 16, 2023.



Student number: 5372372
Project duration: March 2022 – November 2022
Supervisors: Prof. Dr. Kenneth Gavin TU Delft [*Chair*]
Ir. Kevin Duffy TU Delft
Ir. Jasper Sluis Witteveen+Bos
Dr. Ir. Alfred Roubos Port of Rotterdam - TU Delft
Dr. Federico Pisanò TU Delft

An electronic version of this thesis is available at <http://repository.tudelft.nl/>.

Preface

This research concludes my studies for the degree of Master of Science in Geo-Engineering at Delft University of Technology. This project was a combination of data analysis and modelling in PLAXIS 2D. I was lucky to have access to data from the Port of Rotterdam. During my Thesis, which is focused on the quay walls, I was able to better understand the operation of the quay walls. Throughout the process of conducting my research, I received tremendous support from my supervisors, who helped me tackle the engineering difficulties and uncertainties that come with any research project. Their valuable feedback motivated me and helped me develop critical thinking.

For that reason, I would like to thank my University's supervisors, Ken Gavin, Federico Pisano and Kevin Duffy for sharing their knowledge and guiding me throughout the Thesis. Kevin, thank you for our weekly meetings, continuous support and advice. It has always been a pleasure to talk to you!

Moreover, I would like to express my gratitude to Alfred Roubos and the Port of Rotterdam for giving me the opportunity to work with data from five different quay walls. Furthermore, I would like to thank Witteveen+Bos, specifically Jasper Sluis, for providing me with everything I needed to accomplish this Thesis. Jasper, thank you for our weekly meetings and for sharing your expert opinion with me, which helped me deal with the difficulties.

Last but not least, I would like to express my gratitude to my family and friends. Thank you to all for supporting me throughout the entire process.

*Konstantinos Patrikis
Delft, January 2023*

Summary

Quay walls are often designed with Finite Element models (FE models) to take into account the complex soil-structure interaction and highly non-linear soil behaviour. However, the effect of temperature variations is uncertain if it is taken into account in the design of the quay walls at the Port of Rotterdam.

Nowadays, new quay walls are often equipped with sensors that collect information about their behaviour. These quay walls are known as smart quay walls. The measurement data of smart quay walls could be used to validate FE models and reduce parameter uncertainties. This could lead to an optimisation of the functionality of the quay walls.

Smart quay walls have been observed to show much higher strain levels in the anchors during summer compared to the winter period. According to strain records, differences of up to 10% and 20% seem to be present, which is quite high. The objective of this thesis is to verify the effect of temperature on anchor force in quay walls using the data of smart quay walls.

The data analysis that took place analysed data from five different quay walls (HHTT, SIF, EMO, Brammen terminal, Britanniëhaven). Deformations, strains, anchor forces, groundwater levels and temperatures are some of the measurements that were investigated in order to understand the quay wall reaction to the seasonal temperature fluctuation effect. The most useful measurement data proved to be the deformations of the combi walls and the anchor forces in the MV-piles.

This research will eventually highlight the results of the extensive data analysis from different smart quay walls, while it will further prove that quay walls are affected by the effect of seasonal temperature fluctuation. The gain is that with the available data it is verified that the wall is moving back and forth depending on the season. However, the deformations are minor compared to the deformations of the dredging period.

After data analysis, a FE model was set up to predict the deformations and anchor forces of the quay wall during seasonal temperature fluctuations. For the parameter determination, CPTs, later research projects, design records and triaxial tests were used. Regarding the FE model, the case that was used is the HES Hartel Tank Terminal (HHTT-quay), which is a smart quay wall in the port of Rotterdam. HHTT quay wall was selected as the most well monitored quay wall regarding the needs of this research. Moreover, the HHTT-quay consists of sections with and without a relieving platform. Both types were considered in this thesis.

Then comes the validation of the FE model with the measurement data. Moreover, having a FE model in PLAXIS 2D which can realistically model the cycle heating effects, could be used both to estimate deformations due to climate change effect, as well as the anchor forces leading to better quay wall design for the future.

As with all of the cycle effects, heating and cooling of the quay wall could cause deformations that after many years of operation of a quay wall could lead to excessive deformations. Additionally, increasing temperature will cause higher temperature fluctuations, which means larger cycles and severe degradation of the quay walls. Therefore, a new research with more cycles, better quality data and a FEM that could calculate the cycle heating effects is crucial to a better understanding of the cycle phenomenon.

Contents

Preface	i
Summary	ii
1 Introduction	1
1.1 Problem description	1
1.2 Project Background	2
1.3 Research objective and questions	2
1.4 Method of approach	3
1.5 Chapter organisation	4
2 Background information	5
2.1 General information about the quay wall design	5
2.2 Description of the measurement methods of smart quay walls	8
2.2.1 Fiber Bragg Grating sensors	9
2.2.2 Manual inclinometers	12
2.2.3 Shape Accel Array inclinometer (S.A.A.)	14
2.3 Temperature in PLAXIS 2D	15
2.3.1 Constitutive model for quay wall in PLAXIS 2D	15
3 Data processing from measurement data in quay walls	17
3.1 Location of the five quay walls	17
3.2 Location of sensors for each quay wall	18
3.3 Anchor forces analysis	19
3.4 Combi wall analysis	22
3.5 Temperature analysis	31
3.6 Conclusions	33
4 Parameters for the model set up	35
4.1 Soil profile and geotechnical parameters	35
4.2 Site investigation	36
4.3 Soil parameters	41
4.3.1 Volumetric unit weights	42
4.3.2 Relative density	42
4.3.3 Peak friction angle, dilatancy angle and cohesion	43
4.3.4 Stiffness moduli	43
4.3.5 Power parameter	45
4.4 Geotechnical cross section	45
4.5 Structure parameters	46
4.6 Structural elements in PLAXIS 2D	46
4.7 Definition of the material properties	48
5 Set up and validation of the developed model	50
5.1 Set up of the geotechnical model in PLAXIS 2D	50
5.1.1 Drainage type	50
5.1.2 Temperature input	51
5.1.3 Calculation types	52
5.1.4 Project properties	52
5.1.5 Boundary conditions	53
5.2 Description of the Geometry	54
5.3 Validation of the developed model	55
5.3.1 Analysis with model A	55

5.3.2	Analysis with model B	59
5.3.3	Analysis with model C	60
5.4	Heating phase	61
5.5	Sensitivity analysis of the thermal parameters	65
5.6	Concluding remarks	65
6	Conclusions and Recommendations	67
6.1	Conclusions	67
6.2	Recommendations	70
6.2.1	Measurement data	70
6.2.2	FE modelling	70
6.2.3	The overall contribution of this research study to the industry is summarised below	70
	References	71
	A Data	73
	B FEM	78

List of Figures

1.1	Five different climate models for the planet’s future average temperature increase	2
1.2	Working plan	3
2.1	A cross section of a structure with a deep relieving platform [6].	6
2.2	Various horizontal cross-sections for combined walls [6].	6
2.3	Various horizontal cross-sections for combined walls [6].	7
2.4	A schematic cross section of section B from HHTT quay wall and a detailed cross section of the MV pile with the location of the sensors.	8
2.5	Structure of FBG sensor [4].	9
2.6	Fundamentals of FBG sensor: (a) principle of FBG sensor; (b) wavelength shift due to temperature and/or elastic strain change [11].	10
2.7	(a) Cross section of an of FBG, (b) Working principle of FBG (c) Output of the FBG.	11
2.8	Principles of inclinometer configuration of inclinometer equipments [22].	12
2.9	Illustration of inclinometer operation [22].	13
2.10	Illustration of rotation error [22].	13
2.11	Schematic diagram showing arrangment of shape accelerometer array in 27 mm ID electrical conduit with webbing to seat the accelerometer against the conduit wall [5].	14
2.12	SAAV Extend is the most versatile ShapeArray	15
2.14	Hardening Soil parameters for stiffness at PLAXIS 2D	16
3.1	Locations of the 5 quay walls at the port of Rotterdam (Google Maps, 2022)	18
3.2	The location of the sensors at the HHTT quay wall (Google Maps, 2022)	18
3.3	Location of the section P4 where the SAA sensor is located at SIF quay wall (Google maps, 2022)	19
3.4	Locations from the monitored sections(PUT-1, PUT-2 and PUT-3) of the Brammenterminal quay wall	19
3.5	Measured temperatures from the section D01 at the HHTT quay wall	20
3.6	Temperature from anchors (MV piles) and KNMI temperature from 11/2020 to 11/2021	20
3.7	Anchor forces from the right bottom sensor of the MV piles A11, B14 and C02 during the period from 11/2020 to 03/2022	21
3.8	Anchor forces from the right bottom sensors of the MV piles A11, B14 and C02 during the period from 10/2020 to 10/2022 having as a reference measurement day 01/10/2020	21
3.9	Anchor forces from two different quay walls, HHTT and Britanniehaven	22
3.10	Section B and section D from the HHTT quay wall	23
3.11	Combi wall deformation at section D01 at the HHTT quay wall	24
3.12	Combi wall deformation at section D01 for depth = -5.60m+NAP	24
3.13	A combined graph with the deformations of the combi wall and the anchor forces from 11/2019 to 07/2022 at Section D	26
3.14	A combined graph with the deformations of the combi wall and the anchor forces from 11/2019 to 07/2022 at Section D	27
3.15	Combi wall deformation at section B03 at the HHTT quay wall	27
3.16	Combi wall deformation at section B03 for depth = -5.50m+NAP	28
3.17	A combined graph with the deformations of the combi wall and the anchor forces from 11/2019 to 07/2022 at Section B	28
3.18	Deformations vs Time from P4 at the SIF quay wall	29
3.19	Deformations, anchor forces and anchor temperature vs time at SIF quay wall from 01/2022 to 10/2022	29
3.20	Deformations from the Brammenterminal from 2018 until today	30
3.21	Cross section of SIF quay wall	32

3.22	Temperatures from the combi wall of the SIF quay wall along the entire depth	32
3.23	Temperatures along the depth during all the seasons in Alexandria, Egypt [21]	33
4.1	The H.H.T.T quay wall	35
4.2	Section D at the HHTT quay wall is annotated with the yellow box	36
4.3	Location of the CPTs for the soil investigation at HHTT - section D [Dinoloket]	36
4.4	Section D of the HHTT quay wall along the coast	37
4.5	Section D of the HHTT quay wall along the coast	38
4.6	Modelled results for CPT 000000155926	39
4.7	Graph for the identification of the soils [16].	40
4.8	Soil identification regarding the Robertson graph	41
4.9	Simplified soil profile of at the section D of HHTT quay wall	46
4.10	Table with the input parameters for plate elements	49
5.1	Tab sheet for filling the table for the temperature input of PLAXIS 2D	51
5.2	Boundary conditions that used for the heating phase in PLAXIS 2D	53
5.3	Air temperatures from KNMI station	54
5.4	Different models in PLAXIS 2D	55
5.5	Input temperature in PLAXIS 2D	56
5.6	Temperature at the stress point 1162	56
5.7	Depth vs Temperature for 1 year of the model A	57
5.8	Depth vs Temperature for 1 year of the model A	57
5.9	Real data from combi wall at the SIF quay wall compared with model A in PLAXIS 2D	58
5.10	Temperature at the surface of the model and at the seabed of the model	59
5.11	Comparison between the real measurements from Section D01 at the HHTT quay wall and the results from PLAXIS 2D model B	60
5.12	Comparison between the real measurements from Section B03 at the HHTT quay wall and the results from PLAXIS 2D model C	61
5.13	Two different scenarios for the heating phase of the model	62
5.14	Model with relieving platform and with the cycle input approach	63
5.15	Model with relieving platform and with the climate input approach	63
5.16	Model without relieving platform and with the cycle input approach	64
5.17	Model with relieving platform and with the climate input approach	64
A.1	Dredging records from section B and D at the HHTT quay wall [19]	73
A.2	Anchor forces from the right bottom sensor of the MV piles A11, B14 and C02 during the period from 11/2020 to 03/2022	74
A.3	Brittanniëhaven anchor 7929, temperature sensor 791 and KNMI temperatures from 05/2020 to 05/2021	74
A.4	Section B HHTT	76
A.5	Section D HHTT	77
B.1	Model without a relieving platform	79
B.2	Model without a relieving platform	80
B.3	Nodes for analysing the deformations of the combi wall and the axial forces of the MV pile	81
B.4	Sensitivity analysis changing the value of the heat capacity	82
B.5	Sensitivity analysis changing the value of the thermal conductivity	83

List of Tables

2.1	Specification of Zones A,B,C and D of the HHTT quay wall appendix ??).	8
2.2	Monitoring systems	9
3.1	Name and Location of the quay walls that were investigated	17
3.2	Measurements at Brittannihaven	22
3.3	Table of deformations for each measurement of combi wall at Section D-01 at depth = -5.50 m+NAP	25
3.4	Table of deformations for each measurement of combi wall at Section D-01 at depth = -5.50 m+NAP	25
3.5	Table of deformations for each measurement of combi wall at Section D-01 at depth = -5.50 m+NAP	26
3.6	Deformations for each measurement of combi wall at Section PUT-1 having as a reference measurement the 15/12/2017	30
3.7	Deformations for each measurement of combi wall at Section PUT-2 having as a reference measurement the 15/12/2017	31
3.8	Deformations for each measurement of combi wall at Section PUT-3 having as a reference measurement the 15/12/2017	31
4.1	Parameters based on the CPT values	41
4.2	Soil identification based on Robertson's graph	42
4.3	Unit weights and relative density of the soil layers	43
4.4	Peak friction angle, dilatancy angle and cohesion values for the soil layers	44
4.5	Stiffness parameters for the soil layers	45
4.6	Table with the structural element parameters of the HHTT quay wall	47
4.7	Thermal properties of soil types and other components [24]	49
5.1	Constitutive model and drainage type for each soil material	51
5.2	Calculation types for each phase of the model in PLAXIS 2D	52
5.3	Structural elements applied on the quay wall	54
5.4	Coordinates of the Nodes from the model with relieving platform	62
5.5	Coordinates of the Nodes from the model without relieving platform	63
5.6	Sensitivity analysis input parameters	65
A.1	Table of deformations for each measurement of combi wall at Section B-03 at depth = -5.50 m+NAP	73
A.2	Table of deformations for each measurement of combi wall at Section PUT-1	75
A.3	Table of deformations for each measurement of combi wall at Section PUT-2	75
A.4	Table of deformations for each measurement of combi wall at Section PUT-3	76

1

Introduction

The M.Sc. Thesis project with the title “The effect of seasonal temperature variations on the quay walls in the Port of Rotterdam” is a joint venture of the University of TU Delft and the company Witteveen+Bos.

1.1. Problem description

The port of Rotterdam is one of the most approachable ports due to its favourable geographical position right on the North Sea and at the mouth of the Rhine River. The terminals are directly adjacent to deep water and can be accessed from the open sea quickly and safely. Due to the strategic position, the port allows the vessels to be unloaded and loaded in no time, so that they can be on their way to their next destination quickly. Consequently, the port of Rotterdam continues to grow in container throughput. Due to this growth, the demand for quay wall and terminal capacity space increases. According to the World Economic Forum in 2019, the Netherlands has the first place in Europe in terms of the quality of its transport infrastructure [20].

Quay walls play an important role in the functionality of a port, as they are used for the loading and unloading of ships. Moreover, quay walls can have complex soil-structure interaction, due to the presence of (inclined) retaining walls, anchors, relieving platforms and bearing piles.

Nowadays, new quay walls are often equipped with sensors, such as fiber optic strain sensors on anchors or inclinometers that measure horizontal deformations. These quay walls are known as smart ones. In the port of Rotterdam, the new quay walls are mainly smart quay walls. The idea is that the measurement data that are collected by a smart quay wall could be used for design, construction and maintenance. The measurement data which are obtained by the sensors show how quay walls are affected by weight and pressure, water level, temperature, wind and weather influence. Several researches used these data in the past and that knowledge can be integrated into design guidelines. This M.Sc. thesis will try to achieve conclusions and results that could be useful for future design guidelines.

Besides ports, quay walls also exist in cities. In the Netherlands, thousands of kilometres of quay walls have been built. Although engineers have gained a lot of experience and knowledge over the years regarding the design and the construction of these type of structures, still there are few topics that are not fully investigated. One of the main challenges lies in the description and modelling of the soil and its interaction with the structural elements due to the seasonal fluctuation of the temperature (summer-winter). Therefore, this M.Sc thesis will investigate that effect. Also, another aspect that this M.Sc. thesis will try to investigate is the effect of the increase of the temperature in the quay walls due to climate change (warmer summers).

According to the IPCC (Intergovernmental Panel on Climate Change) summary for policymakers in 2022, five different climate models mention that our planet's average temperature could be between 1.2 and 4.5 °C warmer in 2100 than it is today [23]

According to the Royal Netherlands Meteorological Institute ("KNMI'14"): Climate Change scenarios for the 21st Century – A Netherlands perspective" [8], The Netherlands will face mild winters and hotter summers. Also, precipitation in general will increase with extreme precipitation during winters.

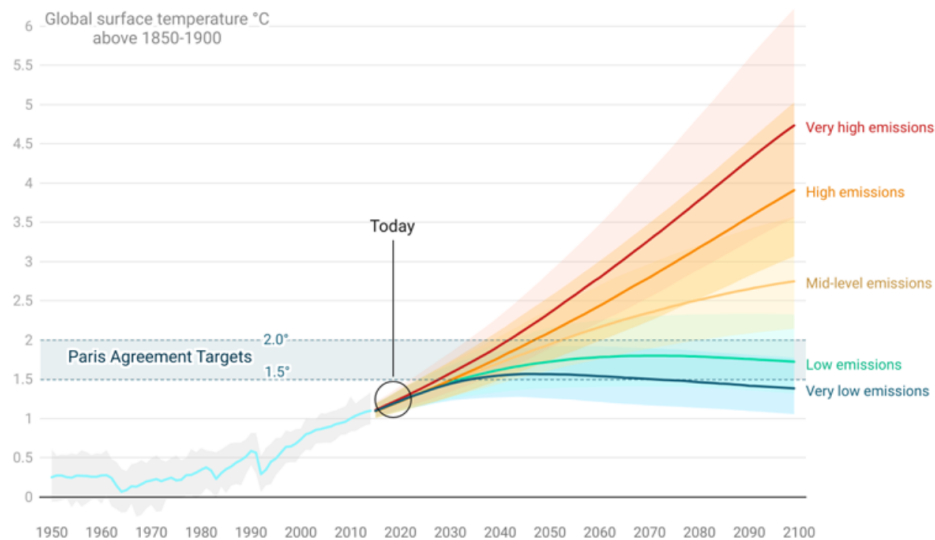


Figure 1.1: Five different climate models for the planet's future average temperature increase

1.2. Project Background

Since the quay walls are increasingly equipped with sensors, a great deal of data has become available. According to some research conducted by TU Delft and other engineering companies so far, they noticed that smart quay walls from the Port of Rotterdam show higher strain levels in the anchors during summer compared to the winter period.

Although engineers can explain most of the quay wall data, a clear explanation for the effect of temperature on anchor forces is still lacking. It is not clear to what extent the quay wall itself is influenced by temperature and to what extent the translation from strain to force influences the results. The effect of temperature is currently not taken into account during the design process of the quay wall in the port of Rotterdam.

1.3. Research objective and questions

In this section, the main research question that this M.Sc. Thesis will attempt to answer is given. This research aims to evaluate the impact of seasonal temperature fluctuations on the quay walls and to show how structural elements react to that fluctuation.

The central research question of this thesis is therefore defined as follows.

Main research question:

What is the influence of seasonal temperature fluctuation on a quay wall and how could this be modelled using finite element method models like PLAXIS 2D?

Sub questions:

1. What is the outcome of the installed monitoring system and how accurate are the results?
2. How do structural elements (diaphragm wall, combi wall, MV-piles, SI-piles) respond to seasonal temperature fluctuations?
3. Can a finite element method program, e.g. PLAXIS 2D, capture the mechanical and thermal behaviour of a quay wall?
4. To what extent should the temperature effects be included in quay-wall design considering climate change effects?

Ideally, this thesis should provide a new and well-structured data analysis regarding smart quay walls, to evaluate the response of the structural elements. Furthermore, the results must be verified with more than one smart quay wall and should also be verified with different types of measurements.

To be successful, the research output should be a clear answer to how the wall moves through seasonal changes. It should also provide port authorities or terminals with more information regarding the deformations of the combi wall and the anchor forces.

To improve the applicability of the study, the insights acquired should be shared with the industry. A more technical success factor of this study is validating the available data using PLAXIS 2D, one of the most advanced finite element models currently used in quay-wall engineering. Afterwards, having a working model, a future prediction could take place due to climate change and the increase of the temperature, which could be beneficial for the design quay wall designing companies.

1.4. Method of approach

The general steps to be followed in the analysis of this Thesis in order to check the movement of the quay wall and validate the results with a FE model are depicted in Figure 1.2.

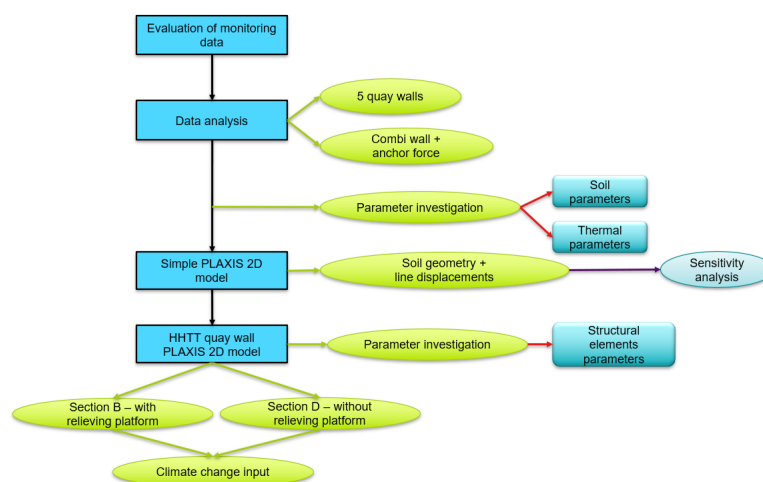


Figure 1.2: Working plan

1.5. Chapter organisation

The main chapters to be presented in this study are listed below:

- Chapter 1 : Introduction
- Chapter 2 : Background information
- Chapter 3 : Data processing from measurement data in quay walls
- Chapter 4 : Parameters for the model set up
- Chapter 5 : Set up and validation of the developed model
- Chapter 6 : Conclusions and recommendations

2

Background information

The literature study accompanying this thesis outlines the design details of a quay wall and the monitoring systems that are used at the Port of Rotterdam. As mentioned above, the walls of the city play an important role in our daily lives. Moreover, the lifetime of the quay walls is very important. However, engineers are still lacking information on the influence of temperature on quay walls. In this chapter, a detailed explanation of what this thesis refers to is provided.

2.1. General information about the quay wall design

There are different types of quay walls. This research will focus on two of them. Quays with a combi-wall with a relieving platform and without a relieving platform. In general, the whole structure of a quay wall consists of bearing and earth-retaining sheet piling on the water side and a foundation system of tension and bearing piles on the land side.

The relieving platform is supported by the foundation elements. On the water side, a retaining and bearing sheet pile structure (combi-wall) and on the land side, one or two rows of prefabricated concrete bearing piles (SI-piles) and one row of tension piles (MV-piles or Muller Verfahren). By using cast iron saddles between the relieving platform and sheet pile wall a hinge is created [6]. The piles and the sheet piling can be positioned at an angle. A schematic overview of a typical cross section of a quay wall is illustrated in Figure 2.1.

With very high retaining heights, the final stability of the quay wall can be ensured by a row of MV piles (steel tension piles with grout injection). These MV piles are driven at an inclination of approximately 42.5° - 45° to take up the horizontal anchor forces and the horizontal soil pressures of the superstructure. Figure 2.1 illustrates a typical cross section of a quay wall, with all the details mentioned above.

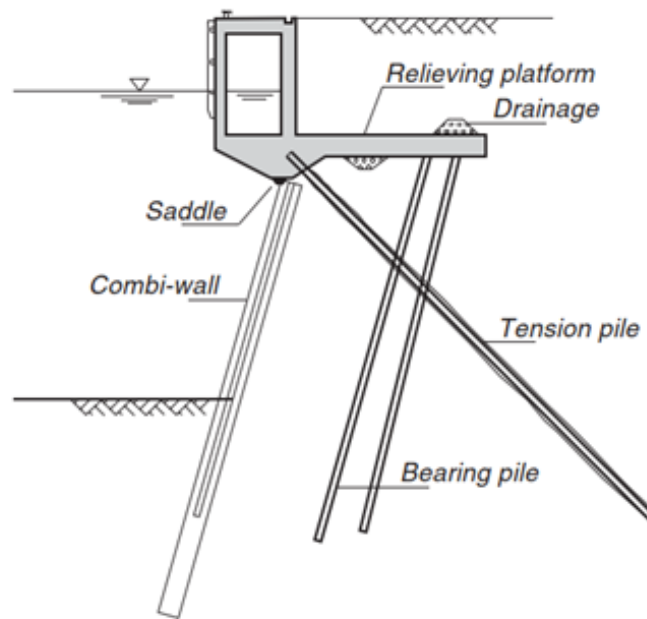


Figure 2.1: A cross section of a structure with a deep relieving platform [6].

Moreover, for quay walls with high retaining height that must bear considerable loads, heavy structures are needed that may consist of various types of combined wall. Figure 2.2 shows a number of examples of combined walls. A combined wall consists of heavy primary elements that are deeply embedded in the subsoil at a set distance from each other.

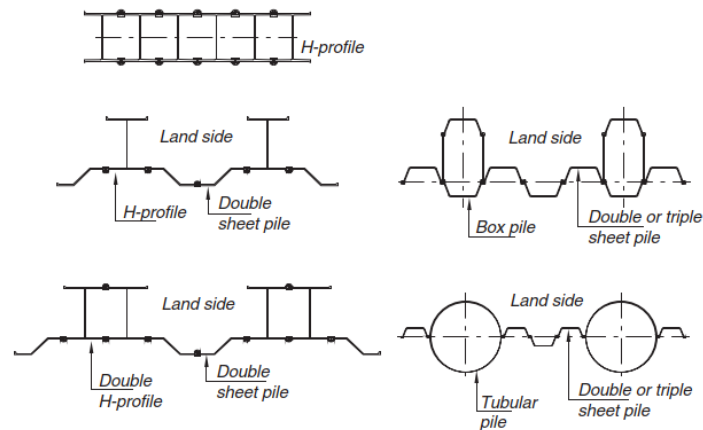


Figure 2.2: Various horizontal cross-sections for combined walls [6].

Combined walls have been used in the Netherlands since the 1980s. With this system, the primary elements are round, open, high quality steel tubular piles. Tubular piles are more desirable from both a construction and an economic point of view than box piles. It became possible to use these piles when the interlocks could be welded to tubular piles. Moreover, this construction system is economically attractive. The open tubular piles can be relatively easily vibrated or driven through the firm sand layers [6].

The resistance of the quay wall against the horizontal pressure must be sufficient to avoid displacements. This is happening with the anchors. There are several types of anchors. There are horizontal anchors, anchors with grout body and tension anchors.

Sheet piling can be anchored by tension piles that may be part of a pile trestle system. Closed piles, open steel tubular piles, steel H-Piles and MV-piles can be used. In all of these types, the tensile force is supplied by shaft friction. Figure 2.3 illustrates the different types of tension piles.

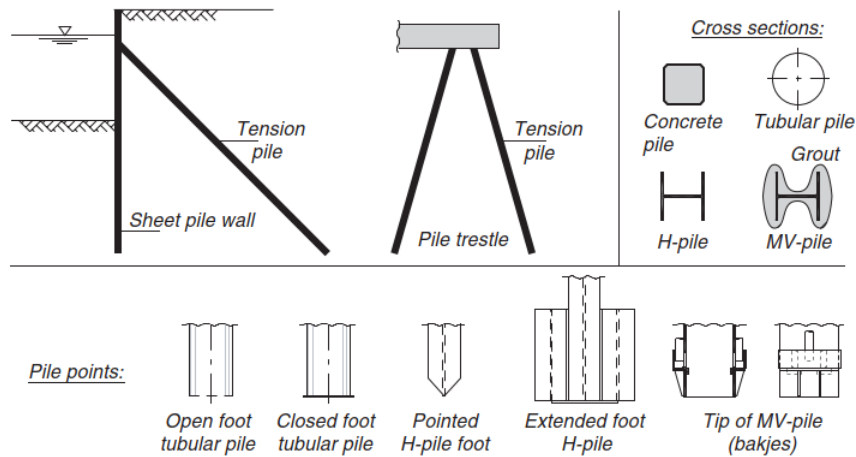


Figure 2.3: Various horizontal cross-sections for combined walls [6].

Regarding the bearing piles (SI-piles), the main function of them is creating horizontal and vertical stability for the quay wall. To ensure the vertical stability of the quay wall, the relieving platform must be supported by a system of bearing piles that transfer vertical forces to deeper sand layers that have a larger bearing capacity than the top layers.

The MV piles, which were used at the HES Hartel Tank Terminal quay wall, have often been used in quay designs on the Maasvlakte since 1984 [6]. The piles are formed by introducing a layer of grout around the steel H-pile during the driving process with the aid of a foot plate or tray welded onto the point of the pile.

Concerning the M.Sc. thesis, the quay wall that will be investigated and afterwards modelled in PLAXIS 2D is the HES Hartel Tank Terminal (HHTT) quay wall. This choice was made because this quay wall is the best instrumented according to the data that were available at the moment and there is enough literature available regarding the construction stages. The HHTT consists of a 2200 metres long quay wall, of which 1200 metres for large seagoing vessels and 1000 metres for smaller inland vessels.

Moreover, the HHTT quay wall is designed for different types of ships like VLCC, Suezmax and MR2. Each of these ships according to the Nautical Guaranteed Depth (NGD), which indicates what is the minimum required depth that has to be guaranteed for a ship to safely moor at a quay, has its own retaining height requirements.

Table 2.1: Specification of Zones A,B,C and D of the HHTT quay wall appendix ??).

Zone	Ship type	Ground level NAP (m)	NGD (m)	Design depth (m)	Retaining height (m)	Relieving platform	Number of sections
A	Suezmax	+4.5	-19	-20.5	25	YES	11 (A1 to A11)
B	VLCC	+4.5	-23.6	-25.6	30.1	YES	20 (B1 to B20)
C	Suezmax	+4.5	-19	-20.5	25	YES	11 (C1 to C11)
D	MR2	+4.5	-14.6	-16.1	20.6	NO	8 (D1 to D8)

The quay wall of the HHTT platform was built with combi walls. Also, the HHTT quay wall is divided into 4 sections (A,B,C and D). Sections A, B, and C are constructed with a relieving platform and the D section is without. Detailed cross sections of the sections B and D platforms are in Appendix A.

In Figure 2.4 a schematic cross section is indicated from section B of the HHTT quay wall. Furthermore, at the right-hand site, a cross section (A-A') of the MV pile is provided with the location of the sensors [19]. With the blue rectangles at the cross section A-A', are illustrated the force sensors and with the red dot in the middle as the temperature sensor.

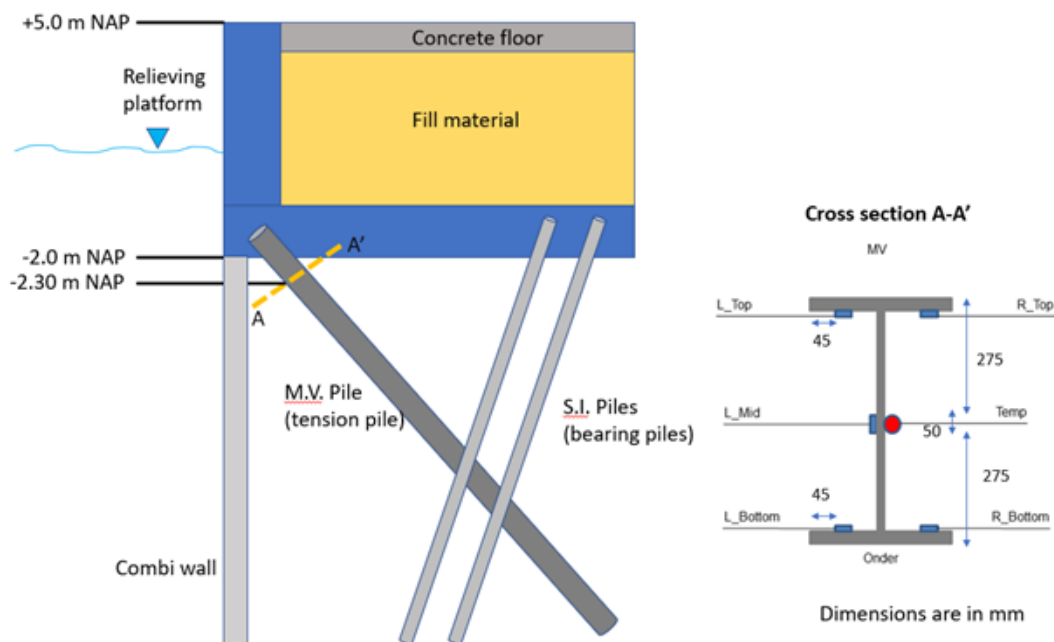


Figure 2.4: A schematic cross section of section B from HHTT quay wall and a detailed cross section of the MV pile with the location of the sensors.

2.2. Description of the measurement methods of smart quay walls

Nowadays, sensors on quay walls provide data on the condition of the quay. These quay walls are called smart quay walls. The way in which these data are obtained differs from each quay wall. The

goal of this paragraph is to explain which are the methods and how the measurement data are collected from all the quay walls. The methods are explained to gain insight into how the data are collected. Therefore, a better understanding of the measurement data will help to spot possible errors and think more critically about which data are sufficient for the research.

Sensors in quay walls can provide data on their condition. This knowledge benefits the quay owner and the users. Maintenance of existing quays can then be done more efficiently. Thus, costs can be saved and hindrance and downtime can be reduced. The data also reveal hidden capacities which allow customers to better utilise current quays. Finally, the information provided by the sensors can be used in the development and improvement of future quay walls.

The type of monitoring system differs with respect to the measured value. Table 2.2 shows the type of measurement, that each monitoring system measures.

Table 2.2: Monitoring systems

<i>measurement</i>	FBG*	SAA**	Manual inclinometer
Anchor force	X	X	
Temperature	X	X	
Horizontal deformation		X	X

*FBG : *Fiber Bragg Grating sensor*

**SAA : *Shape Accel Array*

2.2.1. Fiber Bragg Grating sensors

Fiber optic sensors are becoming increasingly popular for monitoring various types of infrastructure. The main attractive characteristics of these sensors are their long durability, high accuracy, high sensitivity and easy maintenance [7]. Therefore, they are used to monitor structural elements that are prone to small deformations.

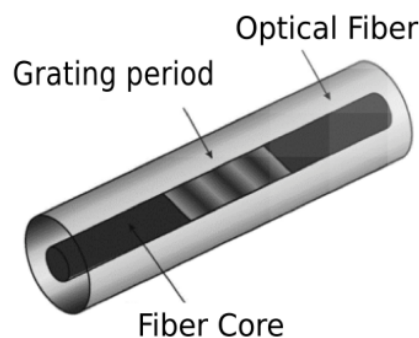


Figure 2.5: Structure of FBG sensor [4].

As 2.5 shows, the typical size of an FBG sensor is 5 mm - 7 mm with a typical grating period of 500

nm [4].

The way an FBG sensor works is by reflecting a particular wavelength and transmitting another wavelength by creating a periodic variation in the refractive index of the fiber core by irradiation with an ultraviolet laser. When the FBG sensor is exposed to a change in temperature or to an external load, there is a change in the physical properties of the FBG sensor that is caused by a change in the reflected wavelength [10].

However, the FBG sensor is manufactured from glass. Therefore, during the installation, sensors are easily damaged due to the fact that the sensors are fragile. Consequently, some form of protection is applied in order to avoid an unwilling situation. Figure 2.6 illustrates with a schematic diagram of an FBG sensor with the protections that are used and the wavelength shift due to deformation by change in temperature or external forces [11].

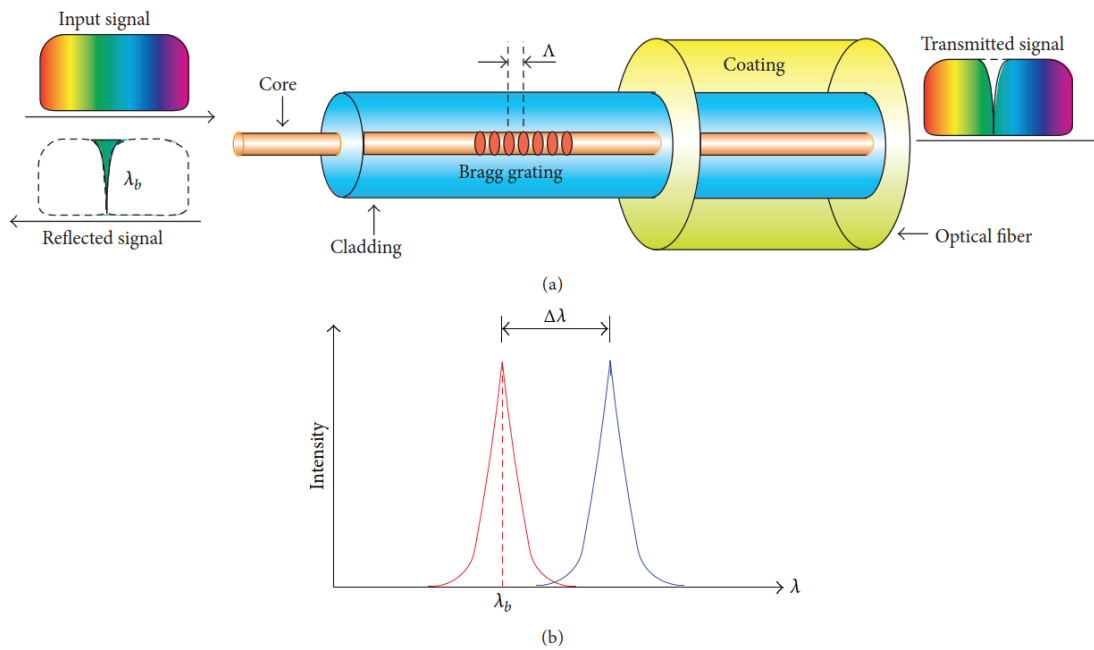


Figure 2.6: Fundamentals of FBG sensor: (a) principle of FBG sensor; (b) wavelength shift due to temperature and/or elastic strain change [11].

When the structure, for example an MV pile, is exposed to an external load or a temperature change, then at the installed FBG sensor, the reflected wavelength of the bragg grating changes, as illustrated at Figure 2.6 (b).

This change in the reflected wavelength is calculated using equation 2.1:

$$\Delta\lambda = \lambda\beta * ((1 - P_e) \Delta\varepsilon + (\alpha + \xi) * \Delta T) \quad (2.1)$$

Where $\lambda\beta$ is the initial reflected wavelength, P_e the effective strain-optic constant, $\Delta\varepsilon$ the change in strain, α the thermal expansion coefficient, ξ the thermo-optic coefficient and ΔT the change in temperature [10].

Regarding the MV-piles and the bearing piles, the FBG sensors are fixed to the steel and to the reinforcement, respectively. In particular, at the HHTT quay wall, there are six MV-piles equipped with

sensors. These piles are located in sections A5, A11, B4, B14, C2 and D1. Each of these piles has 6 FBG sensors as it is illustrated in Figure 2.4. Figure 2.4, on the right side, shows the cross section of each of the MV piles and where it is equipped with the 6 sensors. The location of the sensors is just below the relieving platform, approximately at depth NAP -2.30 *m*.

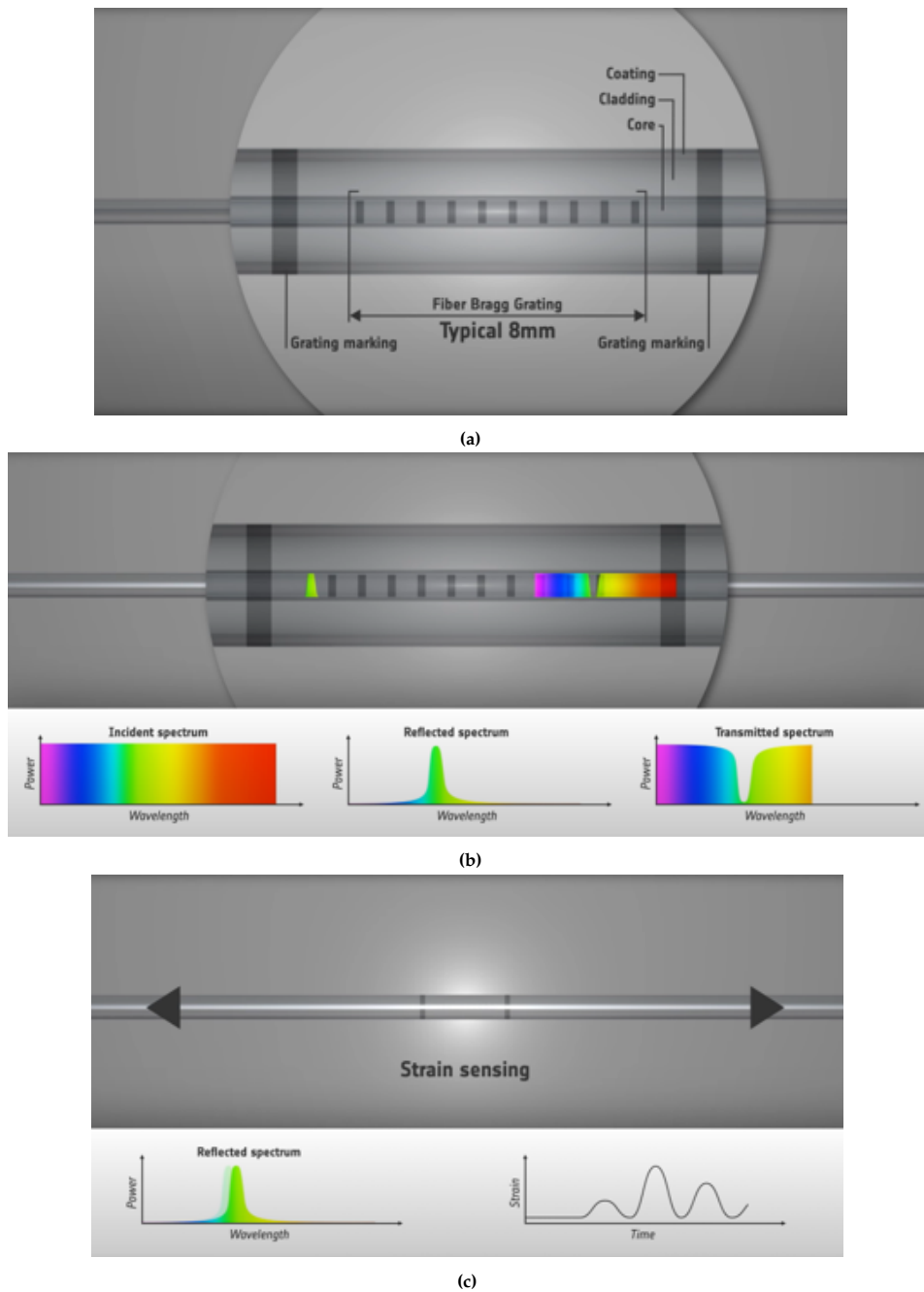


Figure 2.7: (a) Cross section of an of FBG, (b) Working principle of FBG (c) Output of the FBG.

Furthermore, Figure 2.7 explains how the FBG sensors work. When an incidence spectrum of light propagates through the grating, a specific wavelength is reflected back, whereas the rest of the spectrum is transmitted unaffected.

When an external axial strain is induced, the FBG recasts, accordingly, causing a proportional shift in the reflective Bragg of the wavelength. With a one-time instrument calibration, strain values and many other derived parameters can be measured dynamically. A key advantage of the FBGs technology

is that measurement points can be fabricated as an array of independent sensors along the same fiber, enabling multiplexed or even distributed measurements. These multiplex FBG sensors can also be used to monitor other physical parameters, such as temperature, in real time. In particular, this research takes into account the temperature measurements. Therefore, FBGs play an essential role.

The optical fiber containing the FBG sensor is glued to a thin steel plate. Also, to protect the sensors, a cap is placed over the FBG.

Moreover, each MV-pile has 1 FBG sensor that measures the temperature near the anchor. This sensor is not fixed to the steel profile and is therefore free to deform under temperature variations.

2.2.2. Manual inclinometers

The purpose of using manual inclinometers is to measure the relative magnitude and direction of the lateral deformation of the combined wall and the concrete bar (front wall). The inclinometer is inserted in the casing and it measures the inclination. At the HHTT quay wall, the casing is a hollow steel square casing and is attached to the tubular piles of the combined walls and the concrete bar (front wall).

The inclinometer probe contains two force-balanced accelerometers that measure the inclination. The inclination is measured in both planes, vertical and perpendicular [22]. The square hollow steel casing is placed in such a direction in order to have perpendicular and vertical measurements of the quay wall with the inclinometers.

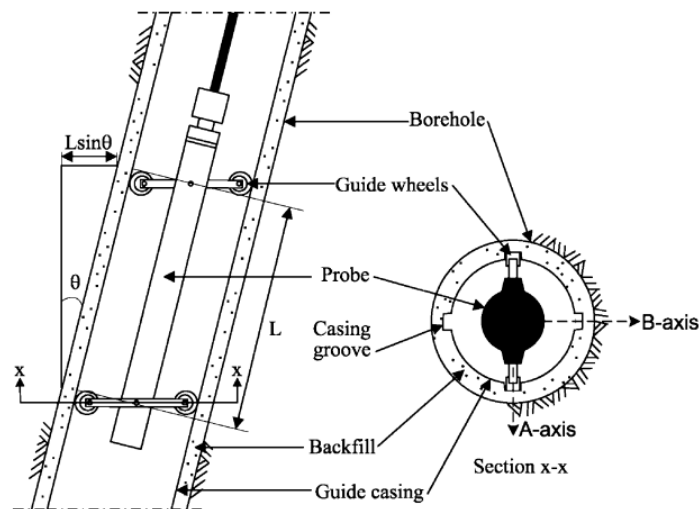


Figure 2.8: Principles of inclinometer configuration of inclinometer equipments [22].

Figure 2.8 illustrates a cross section of the inclinometer probe inside the casing and a plan view of the orientation of the square hollow steel casing. Measurements start from the bottom of the casing and measurements are made every 0.5m. As already mentioned, the inclinometer measures the inclination of the casing, not the horizontal deformation. Therefore, an equation is needed to convert the inclination to horizontal deformation. Hence, the relative horizontal deformation is calculated on the basis of the equation 2.2:

$$\text{deviation from vertical} = \sin \theta * L_{\text{internal}} \quad (2.2)$$

Figure 2.9 illustrates the operation of the inclinometer and better explains how equation 2.2 works.

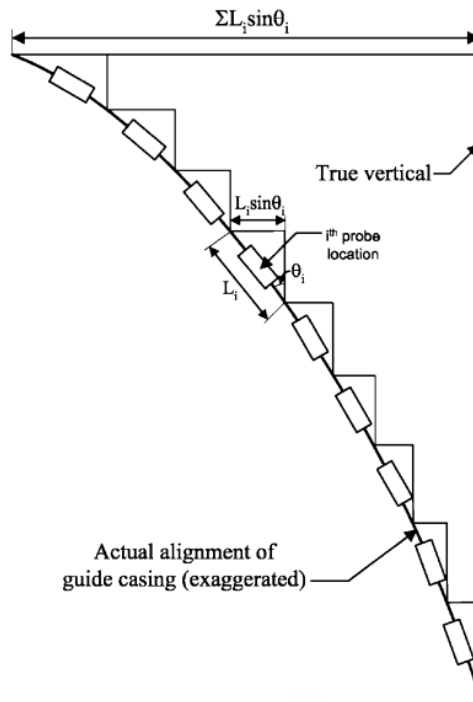


Figure 2.9: Illustration of inclinometer operation [22].

Worth mentioning is the fact that each measurement is carried out twice. This is the case because during the second measurement the probe is rotated 180. Therefore, systematic errors are reduced with the averaging of both measurements. According to [22] and to the manufacturer of the HHTT quay wall inclinometer, the inclinometer reports a system accuracy of $\pm 2\text{mm}/25\text{m}$. However, with respect to multiple case studies, the accuracy of the system is assumed to be $\pm 6.5\text{ mm} / 25\text{m}$.

Common types of systematic errors are the bias-shift and rotation errors. Figure 2.10 illustrates the rotation error that could occur. Moreover, rotation errors can occur when a replacement or a different inclinometer probe is used. Therefore, it is highly recommended to use the same probe during all phases of the project monitoring [22].

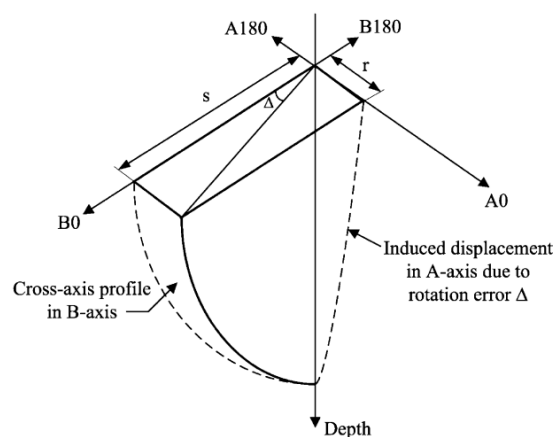


Figure 2.10: Illustration of rotation error [22].

As already mentioned, the aim of the inclinometer measurements is to investigate the horizontal

deformations of the combi wall at the HHTT quay wall. Regarding the measurements, it is assumed that the toe is fixed during the inclinometer measurements. Therefore, all the measurements along the combi-wall are relative to the assumption that the toe of the combi-wall is fixed. Later, in the chapter where the measurement data analysis is, the graphs that refer to the horizontal deformation of the combi-walls have as reference measurement the toe of the combi-wall -37 m+NAP.

2.2.3. Shape Accel Array inclinometer (S.A.A.)

An alternative way to determine horizontal displacements versus depth is using Shape accelerometer arrays. Typically, these arrays consist of triaxial chip-based accelerometers located at 0.3 m intervals within flexible waterproof tubing. The SAA can be inserted within a conventional PVC pipe which is concreted into place along the length of the pile [5]. In this research there is a quay wall which is instrumented with this type of sensor. This is the S.I.F. quay wall and there are measurements for the deformation, the temperature and for the anchor forces as well.

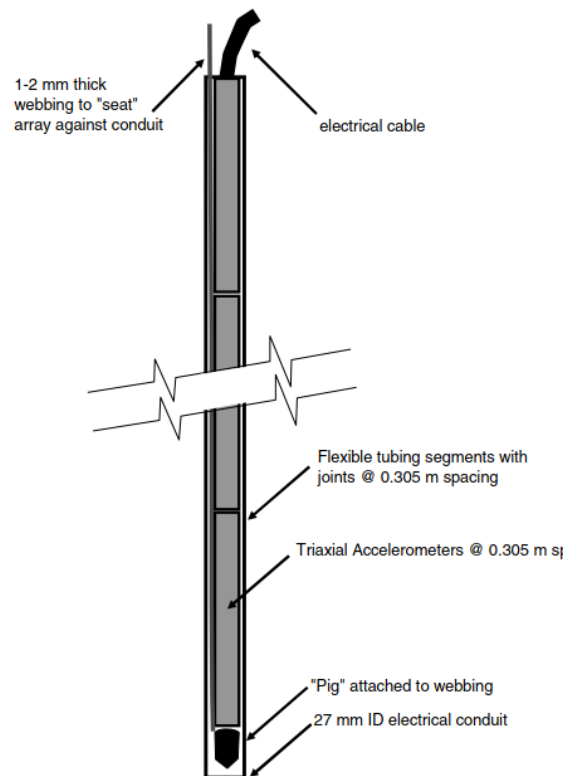


Figure 2.11: Schematic diagram showing arrangement of shape accelerometer array in 27 mm ID electrical conduit with webbing to seat the accelerometer against the conduit wall [5].

The accelerometer arrays are manufactured by Measurand, Inc. They contain MEMS (Micromachined Electro-Mechanical System) accelerometers with a range of $\pm 2g$ and a noise figure limited to.

A shape accel array, as illustrated in Figure 2.12, is a chain of rigid segments connected by flexible joints. The joints are designed to resist twist, but allow the segments to tilt in any direction.

Moreover, the advantage of SAA measurements compared to manual inclinometer measurements, is that there are everyday measurements. This is an advantage because manual inclinometer measurements are made a few times a year and are not favourable to understanding wall movement.

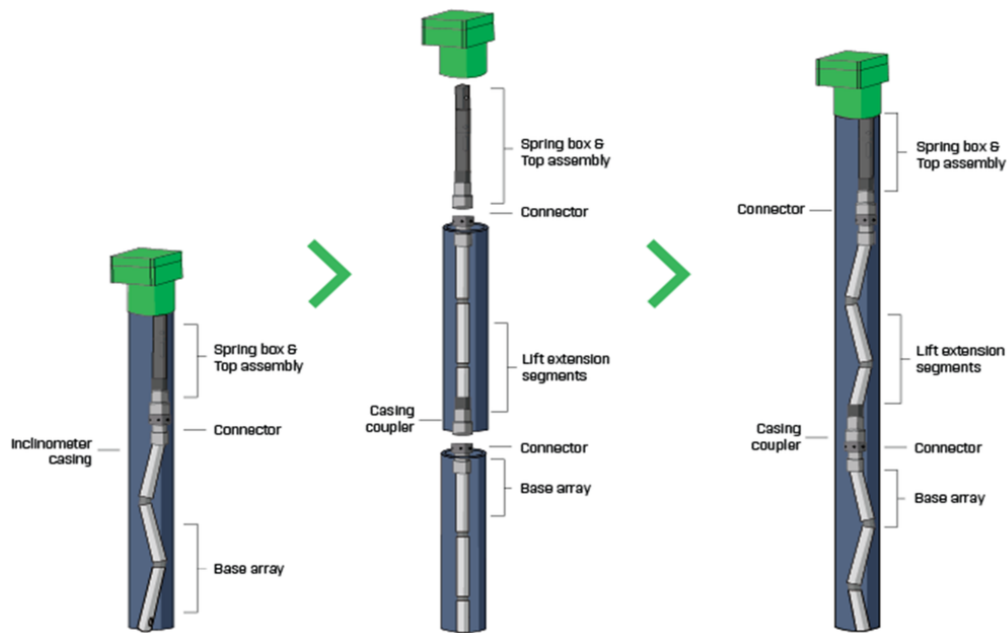


Figure 2.12: SAAV Extend is the most versatile ShapeArray

2.3. Temperature in PLAXIS 2D

In case temperature or a temperature change is of influence on the behaviour of soils or structures, PLAXIS 2D offers the possibility to take thermal effects into account. The calculation of the temperature distribution on the ground is based on the thermal calculations. Since groundwater flow plays an essential role in the transport of heat in the ground, thermal calculations are generally coupled with groundwater flow calculations (thermos-hydraulic (TH) coupling). Moreover, results of coupled steady-state TH calculations may be used to analyse the effects of changes of temperature on stress and deformation. More generally, PLAXIS 2D allows for fully coupled transient thermos-hydro-mechanical (THM) calculations of problems in which the time-dependent effect of changes of temperature on stress, deformation and groundwater flow are to be taken into account simultaneously [15].

2.3.1. Constitutive model for quay wall in PLAXIS 2D

There are multiple constitutive soil models available in PLAXIS 2D. The Hardening Soil model is considered the most suitable for analysing the behaviour of the quay wall [6] and [13]. The Hardening Soil Model also uses the Mohr-Coulomb failure criterion. However, the description of the soil stiffness is much more advanced. It includes shear hardening, compression hardening, stress-dependency of stiffness module, it allows for the introduction of pre-consolidation and it distinguishes between elastic behaviour during unloading and reloading [18].

The Hardening Soil model (HS) is an advanced model for the simulation of soil behaviour. The HS model is an elastoplastic type of hyperbolic model, formulated in the framework of shear hardening plasticity. Furthermore, the model involves compression hardening to simulate irreversible soil compaction under primary compression. This second order model can be used to simulate the behaviour of sands and gravel, as well as softer types of soil, such as clays and silts [15].

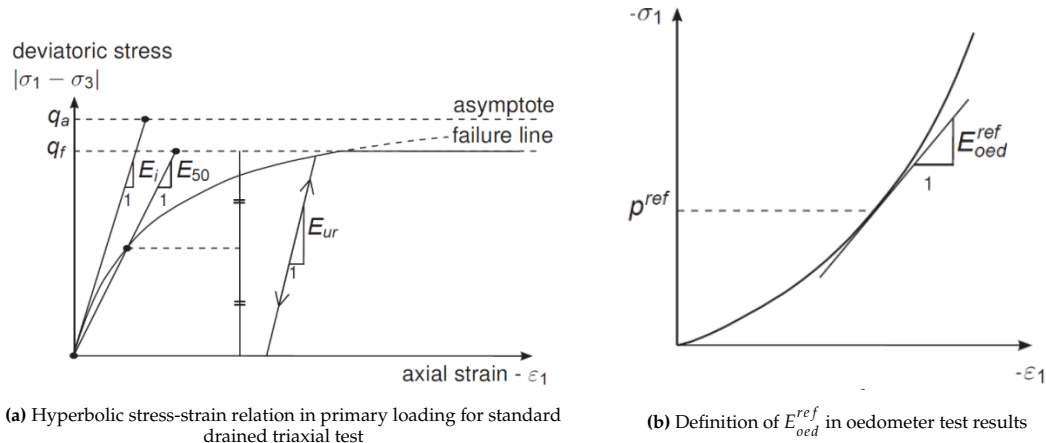


Figure 2.13: Characteristics of Hardening Soil model

Figure 2.14 illustrates how the parameter tab sheet for the Hardening soil model is for drained behaviour. The values are from the sand soil layer at the surface level of the model.

Property	Unit	Value
Stiffness		
E_{50}^{ref}	kN/m ²	58.00E3
E_{oad}^{ref}	kN/m ²	58.00E3
E_{ur}^{ref}	kN/m ²	172.0E3
power (m)		0.5000

Figure 2.14: Hardening Soil parameters for stiffness at PLAXIS 2D

The stiffness parameters of the Hardening Soil model are:

- E_{50}^{ref} - Secant stiffness in standard drained triaxial test [kN/m^2]
- E_{oad}^{ref} - Tangent stiffness for primary oedometer loading [kN/m^2]
- E_{ur}^{ref} - Unloading / reloading stiffness [kN/m^2]
- m - Power for stress-level dependency of stiffness [-]

In addition, advanced parameters can be defined for stiffness (it is recommended to use the default setting):

- ν_{ur} - Poisson's ration for unloading-reloading (default $\nu_{ur}=0.2$) [-]

3

Data processing from measurement data in quay walls

This section will answer the research question of how structural elements respond to seasonal temperature fluctuations. To achieve that, data from five different quay walls were analysed. In particular, diaphragm walls, piles, and anchors were analysed, intending to come up with some conclusions. Various graphs from the analysis and tables will also be available in this section.

3.1. Location of the five quay walls

Inventec B.V. company is responsible for some of the data measurements at the port of Rotterdam. Therefore, the data presented in this research are obtained from the database that Inventec B.V. has, and this is www.livesense.eu. The five quay walls which are illustrated in Figure 3.1 are the Hes Hartel Tank Terminal, the EMO kade, the SIF kade, the Brittanniehaven and the Bremmen terminal.

Table 3.1: Name and Location of the quay walls that were investigated

Name	Location
1) Hes Hartel Tank Terminal	Maasvlakte, Rotterdam
2) EMO-kade	Maasvlakte, Rotterdam
3) SIF - kade	Maasvlakte, Rotterdam
4) Brittanniehaven	Europoort, Rotterdam
5) Brammen terminal	Maasvlakte, Rotterdam

These five quay walls were selected because there were available data for them in the database from Inventec B.V..



Figure 3.1: Locations of the 5 quay walls at the port of Rotterdam (Google Maps, 2022)

3.2. Location of sensors for each quay wall

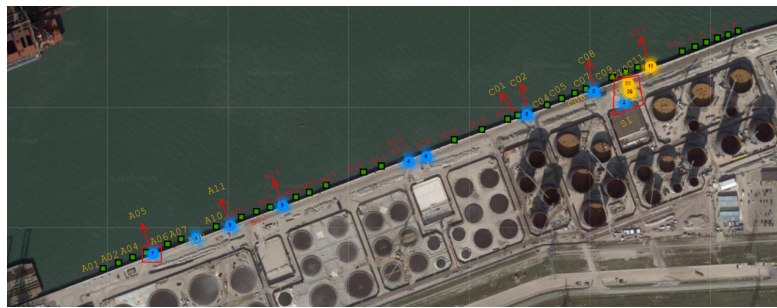


Figure 3.2: The location of the sensors at the HHTT quay wall (Google Maps, 2022)

Figure 3.2 shows the location of the sensors in a plan view of the HHTT quay wall. The combi-wall, the MV pile and the SI piles are equipped with various sensors. Sensor names have a specific format. The abbreviations for each measurement depend on which section the sensor refers to and on which part of the MV pile is located. For example, the names below refer to the MV-pile A05.

- A05 – L_{Top}
- A05 – R_{Top}
- A05 – L_{Mid}
- A05 – $Temp$
- A05 – L_{Bottom}
- A05 – R_{Bottom}

A ranking system was created for all the quay walls, depending on how well the data were measured. The comparison was made with respect to criteria such as data gaps (periods without measurements) and data coherency. The outcome was that the most well-instrumented quay wall is the HHTT. Therefore, later, for the modelling part of the thesis, the cross section of the HHTT quay wall will be used. However, in terms of data analysis, all the quay walls were used to understand the response of the structure of a quay wall to the seasonal effect of temperature.

The SIF quay wall is equipped with SAA monitoring system. However, not all the SAA systems work. Therefore, it was able to obtain data only from the section P4 of this particular quay wall.



Figure 3.3: Location of the section P4 where the SAA sensor is located at SIF quay wall (Google maps, 2022)

Another quay wall that was investigated with regard to the horizontal movements of the diaphragm wall is the Brammenterminal.



Figure 3.4: Locations from the monitored sections (PUT-1, PUT-2 and PUT-3) of the Brammenterminal quay wall

3.3. Anchor forces analysis

Regarding the temperature of the area, the data were obtained from the Royal Netherlands Meteorological Institute (KONINKLIJK NEDERLANDS METEOROLOGISCH INSTITUUT - KNMI). In particular, the data that were obtained were from the Hoek van Holland station from 01/2019 to 1/7/2022.

At the HHTT quay wall, the data that are available are temperatures from the groundwater, the ocean water and the MV piles. There are also measurements from the ocean water and groundwater levels. Additionally, there are measurements of the MV pile forces and there are measurements of the inclinometers that indicate horizontal deformation of the diaphragm wall.

Figure 3.5 illustrates a seasonal cycle from 11/2020 to 11/2021. The graph shows temperature on the y-axis and time on the x-axis. The atmospheric temperature is the blue line (KNMI), which is measured from the KNMI at Hook van Holand. The black line is the ocean water temperature (D01 O.W.T), which follows a pattern similar to the atmospheric temperature; however, it never reaches either the maximum value of the air temperature or the minimum. The green line displays the groundwater temperature

(D01 G.W.T.) that has a slight seasonal fluctuation, but the range is only between 7.5°C and 10°C . Regarding the anchor temperature, the red line follows the seasonal fluctuation pattern, but is slightly shifted to the right. This means that there is a late response at the anchor temperature compared to the air temperature. In addition, the anchor temperature cycles are smaller than the air temperature cycles, which was expected to happen.

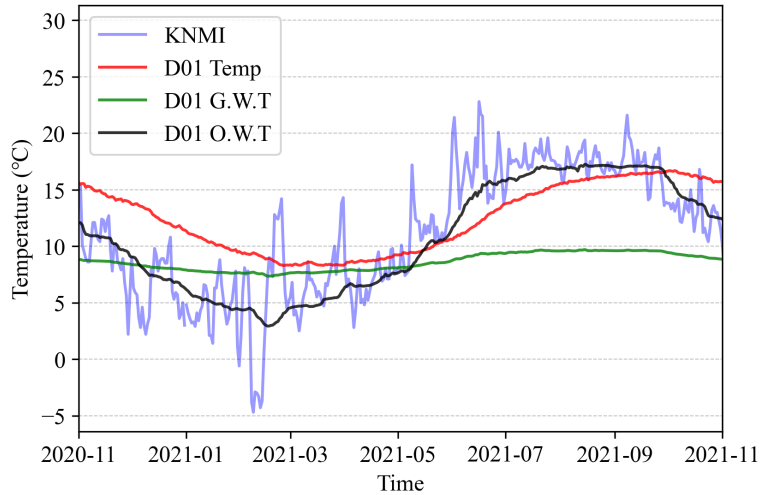


Figure 3.5: Measured temperatures from the section D01 at the HHTT quay wall

In February 2021, there were few days, approximately a week, when the temperature was constantly below 0 ° C. In that period, all canals in The Netherlands were frozen. For that reason, these days were analysed to check what was the reaction at the anchor temperature and what was the effect at the measurements.

Figure 3.6 shows that there is again this late response to anchor temperatures compared to air temperatures. In addition, the spikes are visible in the anchor measurements. These spikes are indicated by the faint black area during that week.

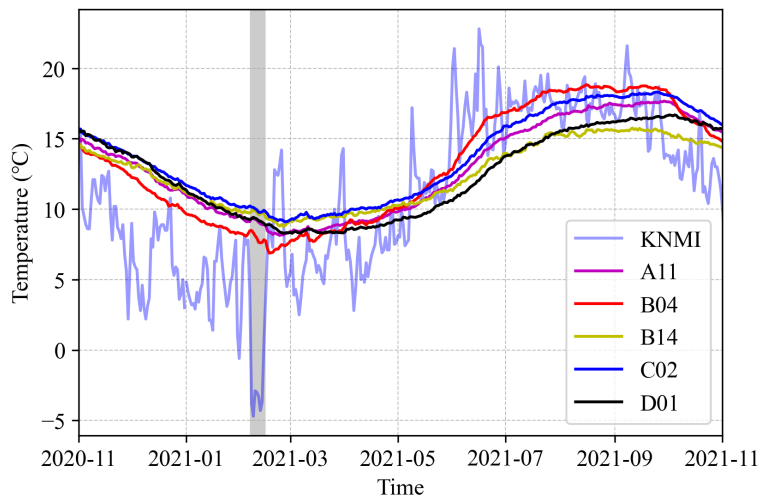


Figure 3.6: Temperature from anchors (MV piles) and KNMI temperature from 11/2020 to 11/2021

This means that the temperature sensors located on the MV piles are working well. In combination with results that are indicated by the sensors and that make sense, the measurements are reliable.

Regarding the anchor forces at the HHTT quay wall in Figure 3.7, it is visible that the forces follow the same pattern as the seasonal fluctuation of temperature. It is also detectable that during the summer period (June-July-August) there is an increase in the anchor forces. During the other periods, except for summer, there is a decrease in anchor forces. An increase in the anchor forces means that tension is increasing. Therefore, this indicates that the combi wall is pulling the anchor during that period. As will be discussed later, the quay wall reacts as a whole structure and not as each element individually. Therefore, a combination of the increase in the anchor forces with a possible move of the combi wall will verify that there is movement to the quay wall due to the seasonal effect of the temperature.

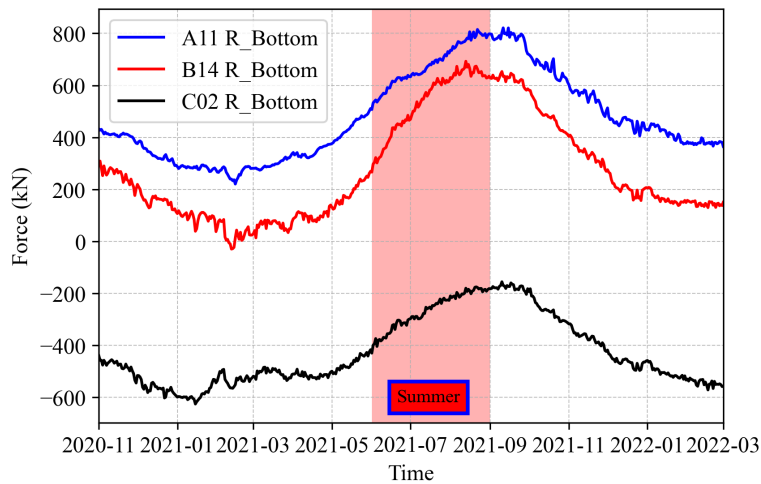


Figure 3.7: Anchor forces from the right bottom sensor of the MV piles A11, B14 and C02 during the period from 11/2020 to 03/2022

Figure 3.7 presents the anchor forces from 11/2020 to 03/2022. However, the reference measurement was taken long ago during the dredging period. Therefore, having as a reference measurement the 1/10/2020 it would be easier to understand the seasonal fluctuations. Figure A.2 illustrates this and presents the anchor forces for the MV piles A11, B14 and C02 for the period from 10/2020 to 10/2022.

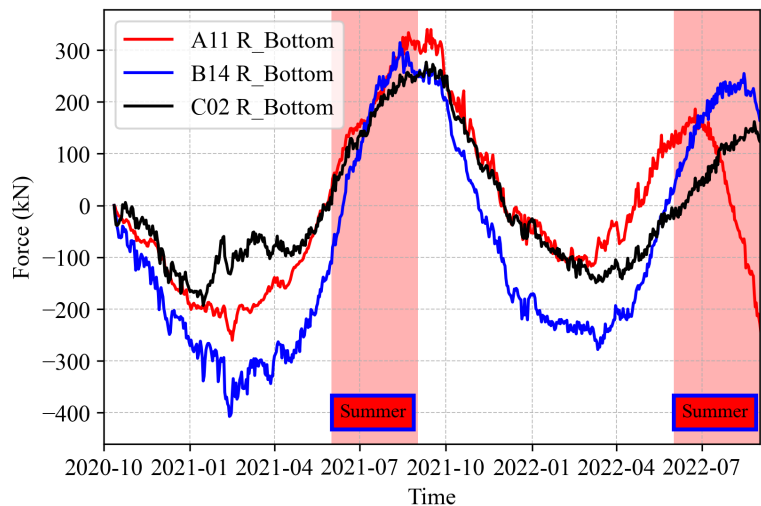


Figure 3.8: Anchor forces from the right bottom sensors of the MV piles A11, B14 and C02 during the period from 10/2020 to 10/2022 having as a reference measurement day 01/10/2020

The Britanniehaven quay wall has multiple sensors. The table below illustrates all the types of measurements that are obtained from this particular quay wall.

Table 3.2: Measurements at Britannihaven

Measurement types
Anchor sensors (force kN)
Pile head (strain $\mu\text{m}/\text{m}$)
Piezometer (gw1 m+NAP)
Temperature
Total pressure cell (kN/m^2)
Air pressure

Figure 3.9 represents the same phenomenon. An increase in anchor forces during the summer period. This graph combines both the HHTT and the Britanniehaven quay walls. This makes it clear that there is a pattern between anchor forces and temperature. The same is happening to the other quay walls as well.

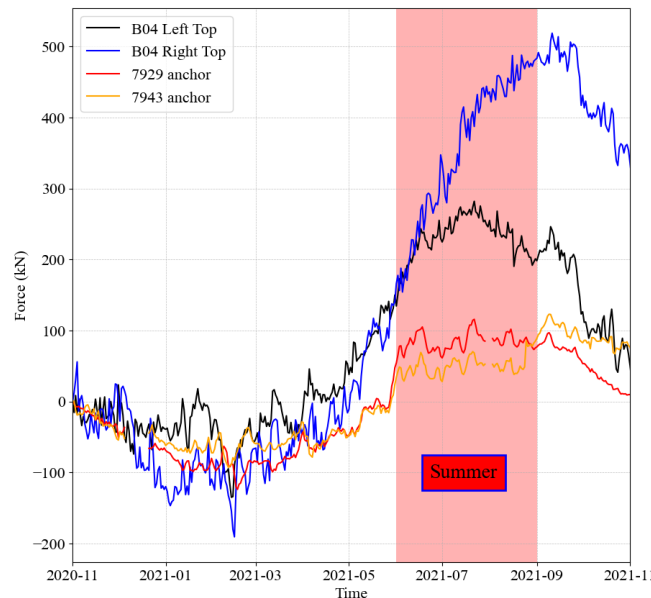


Figure 3.9: Anchor forces from two different quay walls, HHTT and Britanniehaven

Now that the correlation between anchor forces and temperature has already been verified, the next step is to investigate whether the temperature affects the entire structure of the quay wall and not only the anchors. Then there will be a verified answer to the research question of whether or not structural elements are influenced by temperature.

Therefore, the goal is to establish whether there is a link between the temperature fluctuation and what is happening with the structure of the quay wall. For that reason, the data from the diaphragm walls of these five quay walls were analysed with the available measurements.

3.4. Combi wall analysis

In order to understand how the structural elements of the quay wall (diaphragm wall, MV-piles, SI-piles) respond to seasonal temperature fluctuations, except the anchor forces, the investigation of the combi wall is crucial.

Therefore, to verify the horizontal deformation of the combi walls, there are two types of measurements available. As mentioned above, the measurements were made using manual inclinometers and from the Shape Accel Array monitoring system. The difference between these two monitoring systems is that manual inclinometers have few measurements per year (1,2 or 3) while the SAA system measures everyday automatically. Of the five quay walls investigated, only the SIF quay wall has an SAA monitoring system.

Figures 3.10 and Figure 3.2 illustrate that the HHTT quay wall is divided into 4 sections A, B, C and D.



Figure 3.10: Section B and section D from the HHTT quay wall

To understand how the combi wall moves, it is essential to know the dredging records during the construction period and how the manual inclinometer monitoring system works. Both are already answered in previous sections.

Figure 3.11 shows the deformation that the manual inclinometer measures since the construction of the quay wall. The red dotted line is the bottom of the concrete bar and the blue dotted line is where the anchor level is, according to the design records. The wall is moving as expected. This means that there is a fixed point where the anchors and the concrete bar where a hinge is created and the wall below that part is free to deform.

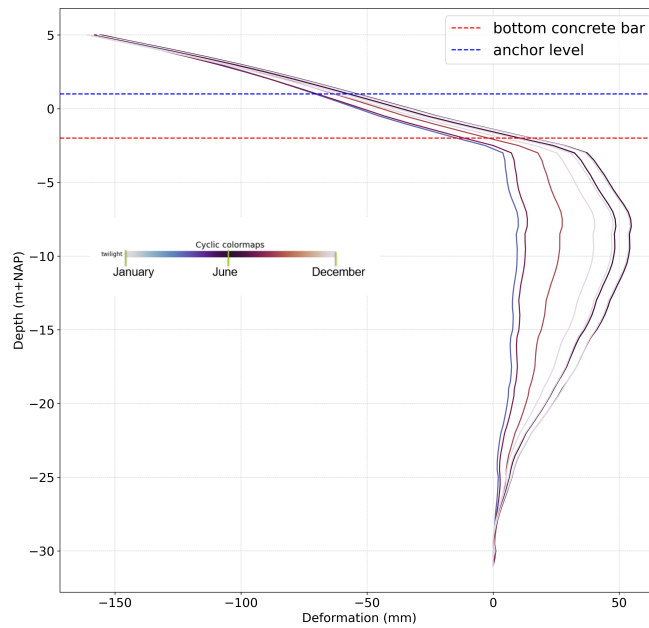


Figure 3.11: Combi wall deformation at section D01 at the HHTT quay wall

From Figure 3.11, the maximum deformation over the years is close to -5.0 m+NAP for section D. Therefore, the next figure illustrates how the wall moves through the years at a specific depth of -5.60 m+NAP.

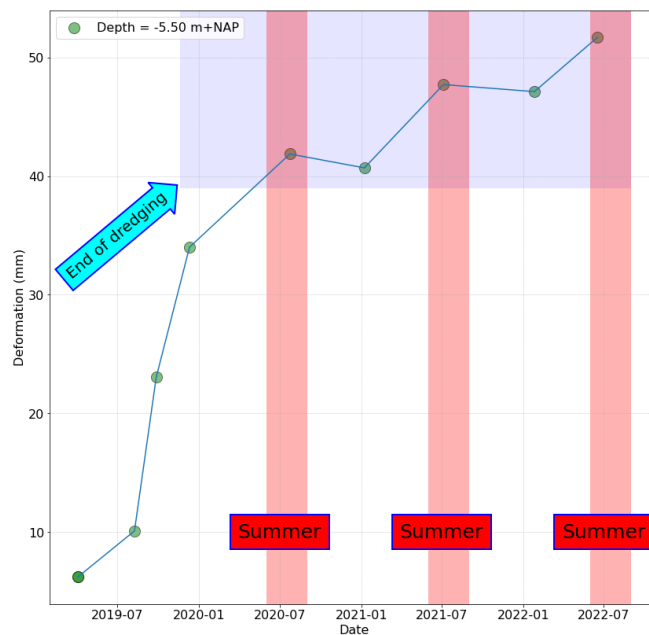


Figure 3.12: Combi wall deformation at section D01 for depth = -5.60m+NAP

During the dredging period, enormous wall displacements occur, which is expected because a huge volume of soil is removed in front of the wall. From 4/2019 to 12/2019 the wall deformed 27.80mm. However, after the dredging period, in the blue area of the graph in Figure 3.12, a seasonal fluctuation is visible. There is an increase in deformations during the summer period, which summer period is indicated with the red area, and a decrease in deformations during the rest of the period.

Table 3.3: Table of deformations for each measurement of combi wall at Section D-01 at depth = -5.50 m+NAP

Date	Deformation (mm)
24/07/2020	41.86
08/01/2021	40.69
05/07/2021	47.71
26/01/2022	47.12
17/06/2022	51.69

From Table 3.5 it is clear that there is a constant increase in deformations through the years. More specifically, the deformations increase during the summer measurements and decrease during the winter measurements.

This is the case along the whole platform of section D at the HHTT quay wall. Figure 3.14 illustrates the combined graph from four different subsections (1,3,5,7) in section D. The blue line, which corresponds to the right-hand side axis, displays the anchor forces. This verifies that, as already mentioned, there is a seasonal fluctuation for the anchor forces.

Table 3.4: Table of deformations for each measurement of combi wall at Section D-01 at depth = -5.50 m+NAP

Date	D01	D03	D05	D07
11/12/2019	34.01	99.11	4.43	128.51
24/07/2020	41.86	105.49	18.49	141.77
08/01/2021	40.69	101.95	15.05	138.56
05/07/2021	47.71	111.18	22.28	143.18
26/01/2022	47.12	104.98	21.82	142.17
17/06/2022	51.69	107.30	24.38	141.96

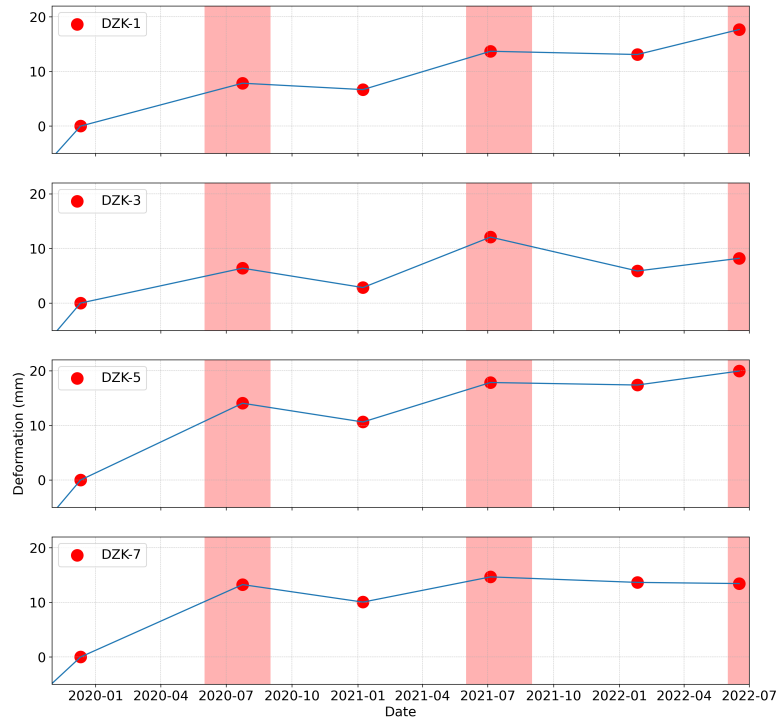


Figure 3.13: A combined graph with the deformations of the combi wall and the anchor forces from 11/2019 to 07/2022 at Section D

Table 3.5: Table of deformations for each measurement of combi wall at Section D-01 at depth = -5.50 m+NAP

Date	D01	D03	D05	D07
11/12/2019	0	0	0	0
24/07/2020	7.85	6.38	14.06	13.25
08/01/2021	6.68	2.84	10.62	10.05
05/07/2021	13.70	12.07	17.85	14.66
26/01/2022	13.10	5.87	17.39	13.65
17/06/2022	17.68	8.19	19.95	13.44

The red dots show the measured data from manual inclinometers. It is important to mention here that for this graph, the reference point is the end of the dredging period. This means that the graph presents how the wall moves after the dredging period.

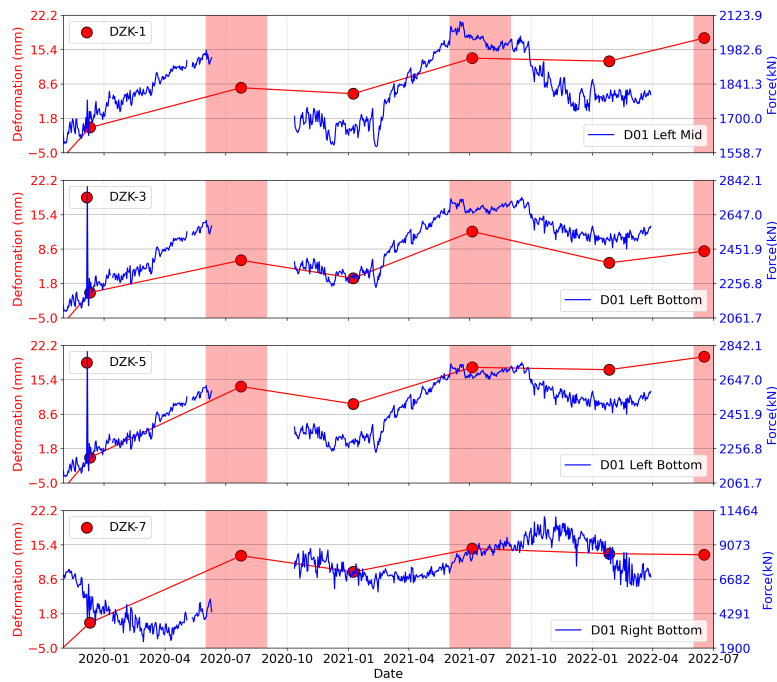


Figure 3.14: A combined graph with the deformations of the combi wall and the anchor forces from 11/2019 to 07/2022 at Section D

It is clearly visible that both the anchor forces and the horizontal movement of the diaphragm wall fluctuate seasonally. That means that the movement of the wall depends on the season according to the data. Therefore, during the summer period, an increase in horizontal deformations has been observed, which in combination with the increase in anchor forces means that there is a compound phenomenon. The wall is prone to move towards the sea; however, the MV-pile tends to keep the structure stable. For that reason, the tension capacity is activated and therefore an increase in the anchor forces is observed.

Regarding section B of the HHTT quay wall, the same pattern is observed Appendix.

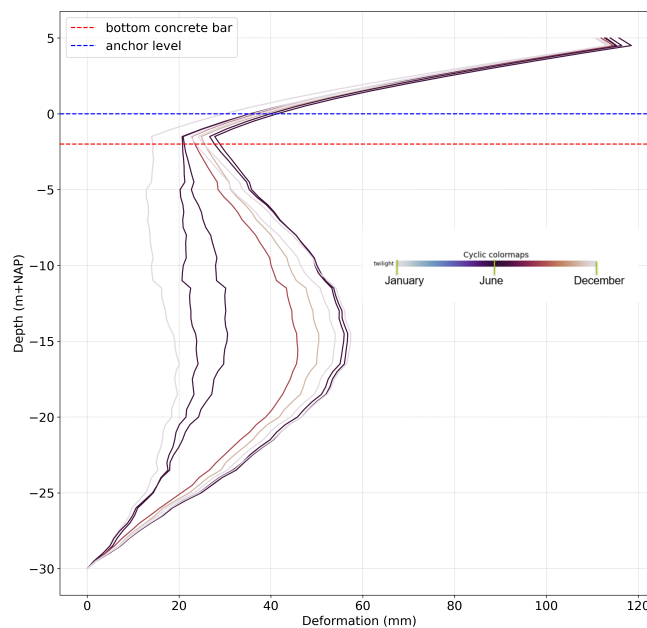


Figure 3.15: Combi wall deformation at section B03 at the HHTT quay wall

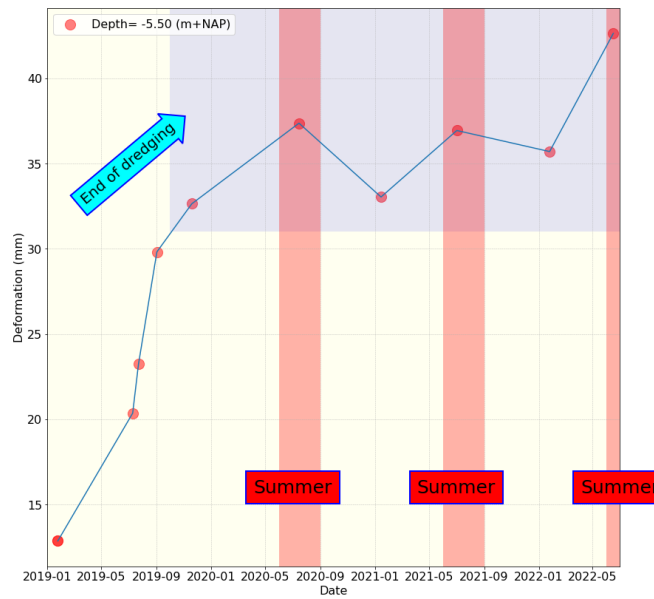


Figure 3.16: Combi wall deformation at section B03 for depth = -5.50m+NAP

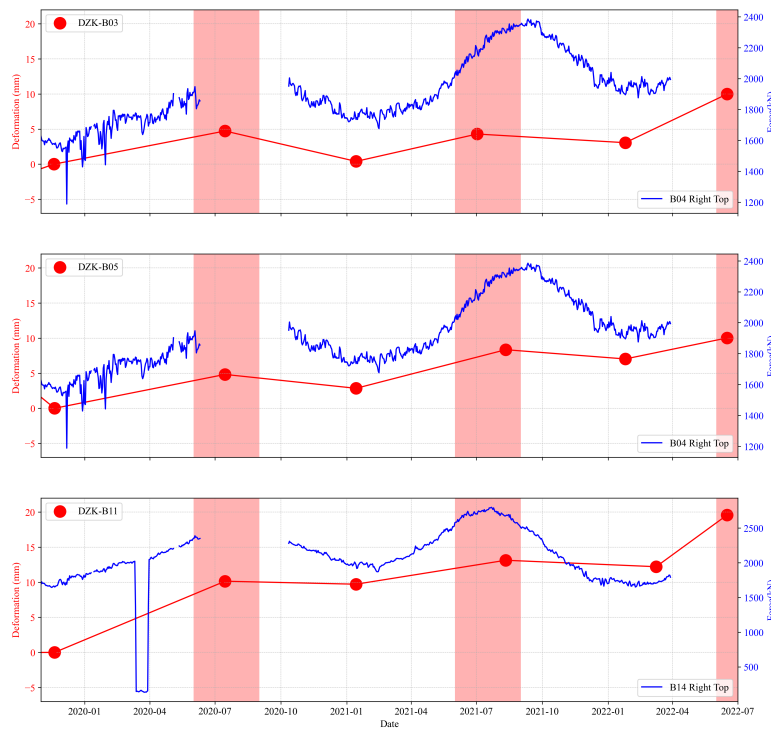


Figure 3.17: A combined graph with the deformations of the combi wall and the anchor forces from 11/2019 to 07/2022 at Section B

Figure 3.18 illustrates the daily measurements from the SAA monitoring system with respect to the horizontal deformation of the combi wall. However, the data are very noisy. After a cautious investigation of the satellite data for that period, nothing happened to explain this strange reaction of the wall.

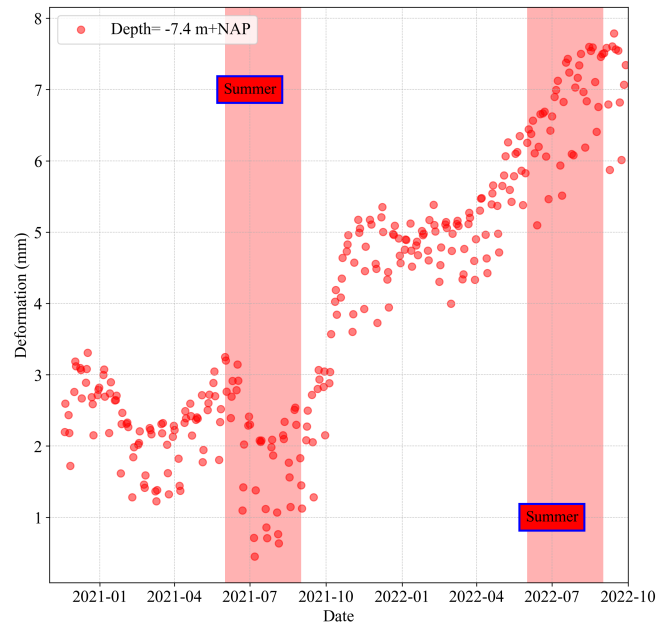


Figure 3.18: Deformations vs Time from P4 at the SIF quay wall

The most interesting part of the data is displayed in the graph below. Since February 2022 there are available data from the anchor forces of the wall. The pattern is again similar to the seasonal effect that was visible at.

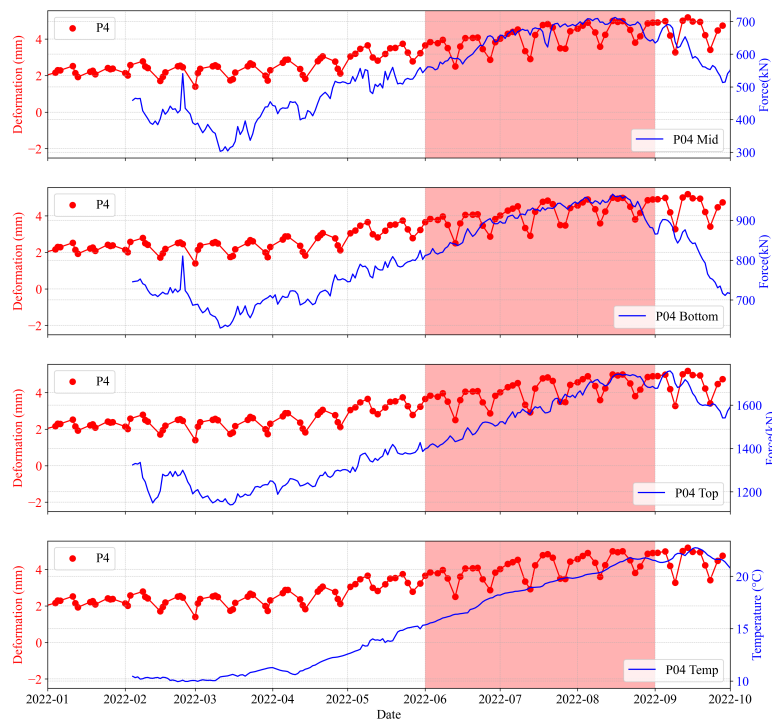


Figure 3.19: Deformations, anchor forces and anchor temperature vs time at SIF quay wall from 01/2022 to 10/2022

Another quay wall that was investigated with regard to the horizontal movements of the diaphragm wall is the Brammenterminal. The movement of the wall and the deformations are represented in Figure 3.20.

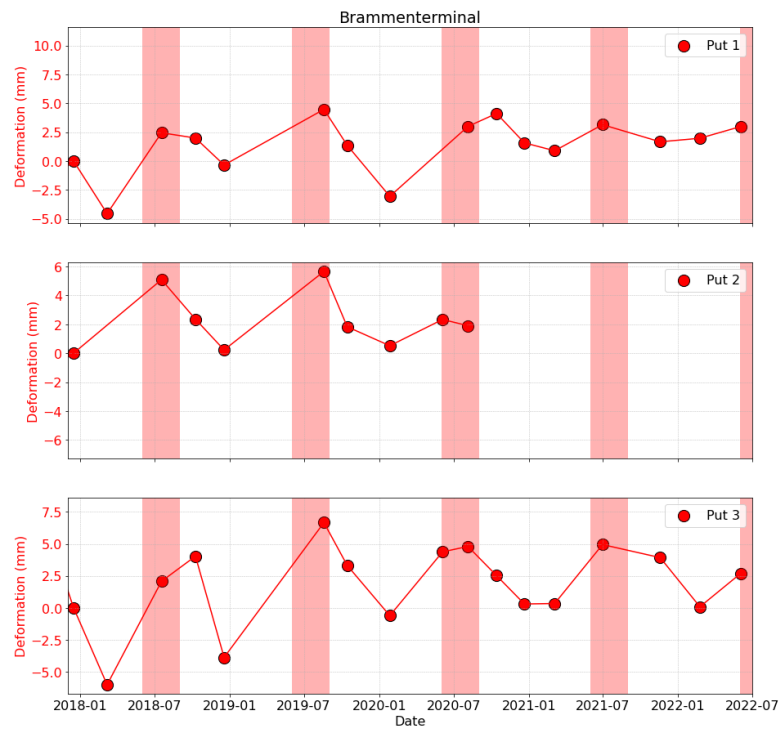


Figure 3.20: Deformations from the Brammenterminal from 2018 until today

The table A.2 illustrated the deformations for each specific day at the different sections of the Brammenterminal.

Table 3.6: Deformations for each measurement of combi wall at Section PUT-1 having as a reference measurement the 15/12/2017

Date	Deformation (mm)
15/12/2017	0
07/03/2018	-4.555
18/07/2018	2.45
09/10/2018	1.99
18/12/2018	-0.345
19/08/2019	4.475
15/10/2019	1.36
27/01/2020	-3.06
05/08/2020	2.995
14/10/2020	4.12
21/12/2020	1.575
05/03/2021	0.89
30/06/2021	3.15
18/11/2021	1.665
23/02/2022	1.975
03/06/2022	2.99

Table 3.7: Deformations for each measurement of combi wall at Section PUT-2 having as a reference measurement the 15/12/2017

Date	Deformation (mm)
15/12/2017	0
18/07/2018	5.08
09/10/2018	2.35
18/12/2018	0.225
19/08/2019	5.65
15/10/2019	1.825
27/01/2020	0.515
04/06/2020	2.33
05/08/2020	1.9

Table 3.8: Deformations for each measurement of combi wall at Section PUT-3 having as a reference measurement the 15/12/2017

Date	Deformation (mm)
15/12/2017	0
07/03/2018	-6.025
18/07/2018	2.07
09/10/2018	4.035
18/12/2018	-3.89
19/08/2019	6.665
15/10/2019	3.31
27/01/2020	-0.62
04/06/2020	4.375
05/08/2020	4.8
14/10/2020	2.515
21/12/2020	0.295
05/03/2021	0.33
30/06/2021	4.945
18/11/2021	3.925
23/02/2022	0.075
03/06/2022	2.695

3.5. Temperature analysis

Another quay wall that was investigated was the SIF quay wall. The difference between the HHTT and the SIF quay wall is that the latter has a different monitoring system. Figure 3.21 displays the location of the SIF quay wall and a cross section of the design records.

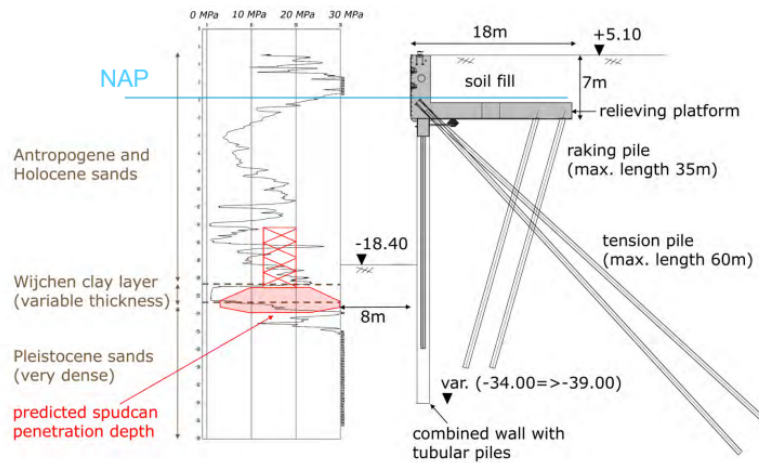


Figure 3.21: Cross section of SIF quay wall

Figure 3.22 illustrates the temperature that was measured from the combi wall. With regard to the literature and the available construction documents, the dredge level is at -18.4 m+NAP. Figure 3.22 shows that for the first 19 metres from +5m+NAP to -14m+NAP the temperature inside the sea is almost constant along the depth. Then, at depth = -14 m+NAP, when the seabed is reached, there is a change in temperature due to the soil. From -14 m+NAP until -21 m+NAP the temperatures, regardless of the season, converge to the constant value of $T = 11.75^{\circ}\text{C}$.

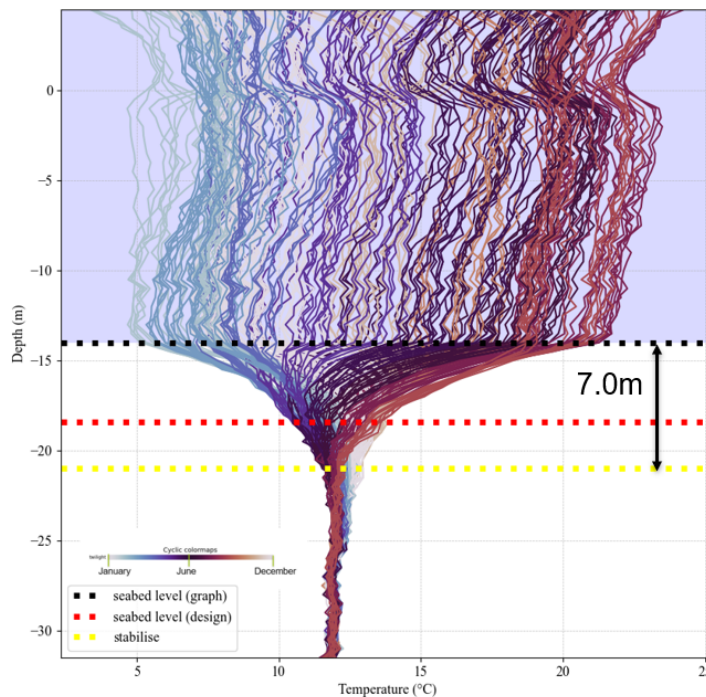


Figure 3.22: Temperatures from the combi wall of the SIF quay wall along the entire depth

In terms of literature, Figure 3.23 indicates the average monthly soil temperature distribution profile for Alexandria (Egypt). It can be found that in September, October, November, December, and January (winter season), the temperature profile begins with a low temperature at the surface and increases with depth. This high temperature at depth can be used for heating purposes. On the other hand, in February,

March, April, May, June and July the reverse occurred, which can be used for cooling purposes [21].

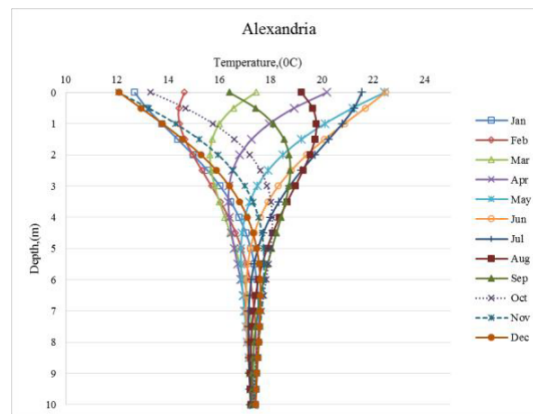


Figure 3.23: Temperatures along the depth during all the seasons in Alexandria, Egypt [21]

This is something that is expected to happen also at the Port of Rotterdam. Temperature measurements are available only for the SIF quay wall, along the diaphragm wall. Comparing Figure 3.22 and Figure 3.23, it is easy to observe that in the soil profile, both graphs follow the same pattern. From the surface level, the temperature will stabilise and converge at a constant temperature approximately after 7 metres.

Later, in chapter 5 where the results from the finite element model will be presented, there will be a comparison of the real data with the PLAXIS 2D model data in order to validate the result. If there is a stabilisation of the temperature approximately at a depth of 7m, then the model means that it works well, in terms of the thermal parameters.

3.6. Conclusions

The goal of this chapter was to determine whether there are sufficient measurement data of good quality which could be used to gain insight into the behaviour quay walls regarding the seasonal effect. This seems to be the case for the HHTT quay wall, SIF quay wall and Breammerterminal. A detailed summary of the measurement data that were available and analysed is given above. It is important to mention here that in order to analyse the movement of the combi walls and the anchor forces, there were selected sensors that were working properly and the measurements were familiar with what was expected as an output. However, a few sensors, which are not presented in this thesis illustrate a different response that is not congruent with common sense, and they were neglected from that research. Therefore, there is room for further research to understand why these sensors illustrate results which are not familiar with reality and obtain some conclusions.

After the analysis and the graphs that were already presented, it seems that the quay wall is reacting like a whole structure. This means that each structural element is individually affected by the temperature change, but the combi wall and the anchors move as a system. The seasonal phenomenon observed on the quay walls has similarities such as the cyclic loading effect. Thus, every summer it is observed an increase in the horizontal movement of the combi wall but then during the winter the wall is moving backward but not at the initial position. Therefore, over the years a cumulative deformation is observed. A characteristic of this phenomenon is that wall deformations are plastic and not elastic due to the fact that the wall is moving toward the sea but never reaching the reference point where the movement started. With unloads during winter, some recovery is observed, but it will never reach the initial stage.

This is the case at the HHTT quay wall which is a newly constructed quay wall. Therefore, could be the case that the deformations are observed due to the late response of the wall from the dredging period. On the other hand, at the Brammenterminal which is an older quay wall, the seasonal effect exists, but instead of plastic deformations the wall is moving backward to its initial position.

The red dots, the deformations of the combi wall, in the graphs above are constantly slightly increasing. This means that the wall is always moving towards the sea. However, this movement seems to be minor in the whole structure. This deformation is characterised as a minor effect, because the wall deformations that occurred during the dredging period are enormous compared to these ones. However, a careful and constant observation of the phenomenon is crucial to observe after a few years and more available cycles how much the wall is affected and whether the late deformations from the dredging period stopped or not.

4

Parameters for the model set up

In this chapter, the parameters that will be used in the finite element model (PLAXIS 2D) are explained. The goal is to predict the behaviour of the quay wall and the fluctuation of the temperature in the soil profile during the fluctuation of seasonal temperatures as best as possible. The model is then validated with the measurement data to determine how well the model is able to predict the behaviour of the quay wall.

4.1. Soil profile and geotechnical parameters

A soil profile will be designed for the HES Hartel Tank Terminal quay wall in the Port of Rotterdam. In particular, the soil profile will be for the section D of the HHTT quay wall for which the location is shown in Figure 4.1 and Figure 4.2 below.



Figure 4.1: The H.H.T.T quay wall



Figure 4.2: Section D at the HHTT quay wall is annotated with the yellow box

4.2. Site investigation

To investigate soil conditions and determine its design parameters, a desk study was performed to analyse CPTs around section D, see Figure 4.3.

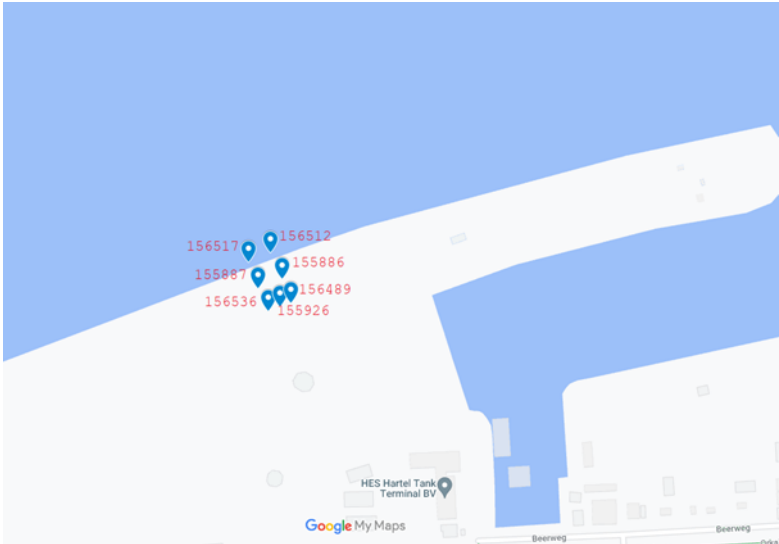
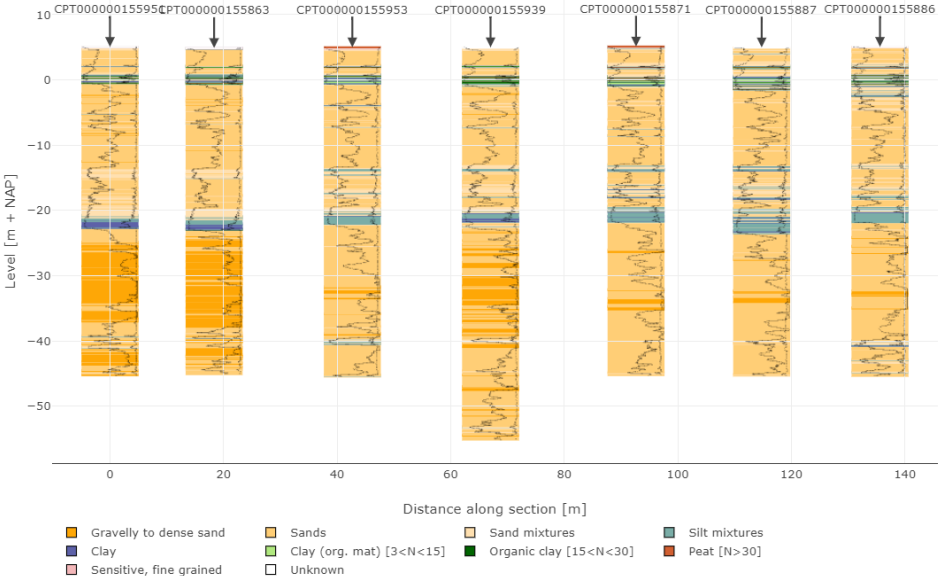


Figure 4.3: Location of the CPTs for the soil investigation at HHTT - section D [Dinoloket]

After an investigation of the area, the outcome of the CPTs looks similar. Therefore, it is unlikely that there will be a major change in the soil profile in this particular area. Therefore, for simplicity, only one CPT will be analysed to create a soil profile. Regarding the final soil profile, it looks very similar compared to other soil profiles that were used for similar research projects at the same location.

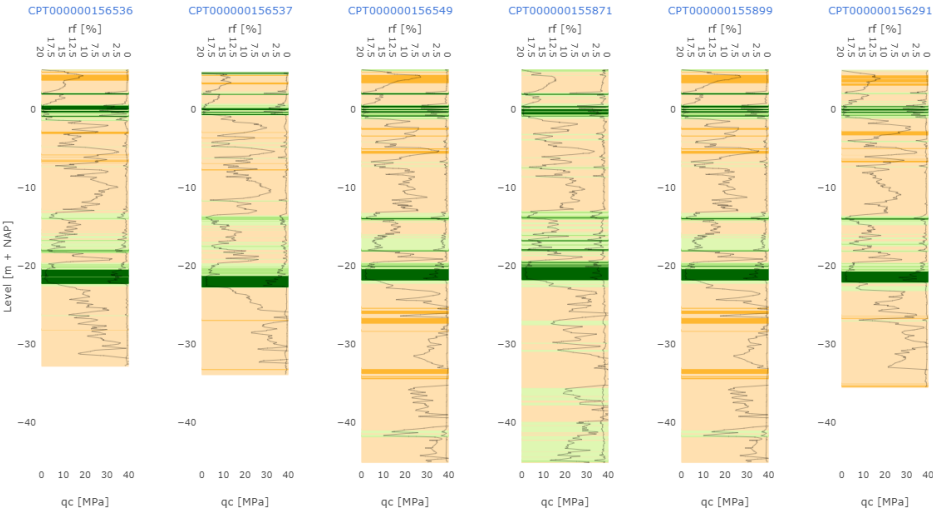


(a) Cross section of different CPTs at section D of HHTT quay wall along the sea



(b) Plan view of the CPTs that were selected at Section D of the HHTT quay wall

Figure 4.4: Section D of the HHTT quay wall along the coast



(a) Cross section of different CPTs at section D of HHTT quay wall along the land side of the quay wall



(b) Plan view of the CPTs that were selected at Section D of the HHTT quay wall

Figure 4.5: Section D of the HHTT quay wall along the coast

The CPT that was selected to be analysed is *CPT000000155926* .

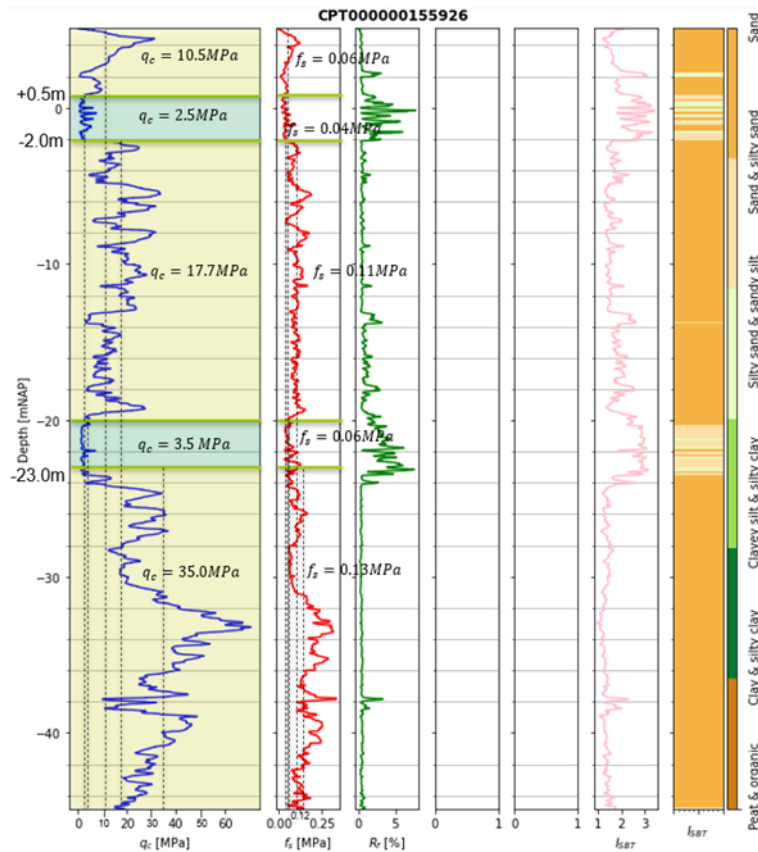


Figure 4.6: Modelled results for CPT 000000155926

From left to right, in Figure 4.6, it is illustrated the cone resistance q_c [MPa], the sleeve friction f_s [kPa] and the friction ratio R_f [%] over depth. Based on the cone resistance and sleeve friction distribution over depth of the CPT presented above in Figure 4.6, it is evident that from the ground surface +5.0 m+NAP to around a depth of -45.0 m+NAP, mostly sand layers of soil are present. However, there are also 2 thin clay layers from +0.5 m+NAP to -2.0 m+NAP and from -20.0 m+NAP to -23.0 m+NAP.

With regard to the CPT data, there are three main geological layers. The dredged sand that is until -13 m+NAP, then the Echteld formation from -13 m+NAP to -20 m+NAP, the Kreftenheye Wijchen Layer from -20 m+NAP to -23 m+NAP and then Kreftenheye thereafter. However, for simplicity in the modelling part and because the outcome will not be affected, the depth from -2m+NAP to -20m+NAP was considered as a sand layer.

Both cone resistance and sleeve friction are used to identify layers based on the Robertson's chart and Table 2b of Eurocode 7 (adjusted for Dutch soils, NEN9997). Moreover, as can be seen, the CPT data refer to depths up to -45 m+NAP. However, it can be conservatively assumed that the sand layer found can be extended to -55 m+NAP based on the provided borehole and CPT data from Dinoloket.

Tables 4.1 and Table 4.2 present the followed procedure. Different layers are defined based on the q_c [MPa] values, as shown in Figure 4.6.

The total and the effective stresses are calculated in the middle of each layer, and for this purpose, the saturated unit weight is assumed to be 20 kN/m^3 and the dry unit weight 17 kN/m^3 regardless of the type of soil. In addition to this, the ground surface is assumed to be at +5.0 m+NAP everywhere, while the water level is at +0.50 m+NAP. In this way, except for the first layer, all the others are considered fully saturated. Robertson graph, together with the nQ_c and nR_f values of each layer, are presented below.

The identification of the soil layers is then carried out according to Robertson's graph in 5, which has

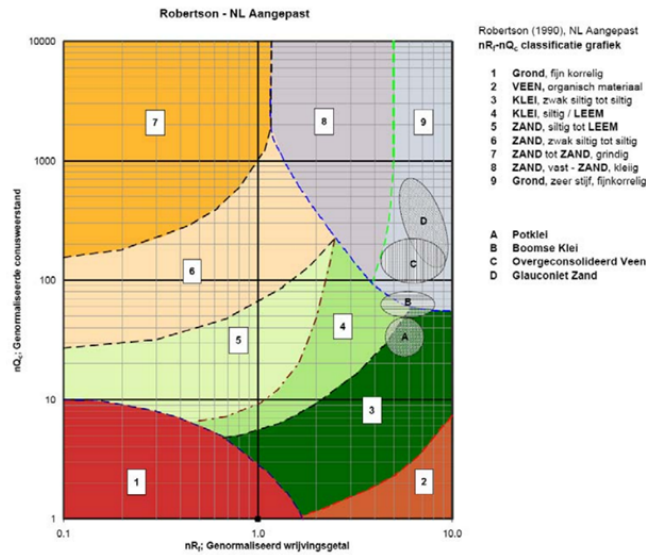


Figure 4.7: Graph for the identification of the soils [16].

been adapted to the Dutch circumstances. This interpretation is based on the normalised values of cone resistance nQ_c and friction number nR_f as input parameters.

Normalised values of the cone resistance nQ_c and the friction number nR_f are calculated from the measured frictional resistance f_s and the cone resistance q_c , if possible corrected for the pore pressure and the vertical effective and total soil tension according to the formulas below. In this particular site investigation $q_c = q_t$ due to the fact that the cone does not measure the pore pressure, as there is no filter for the water pressure to act on.

Normalised cone resistance:

$$nQ_c = (q_t - \sigma_{v0}) / (\sigma_{v0}) \quad (4.1)$$

Normalised friction number:

$$nR_f = (100 * f_s) / (q_t - \sigma_{v0}) \quad (4.2)$$

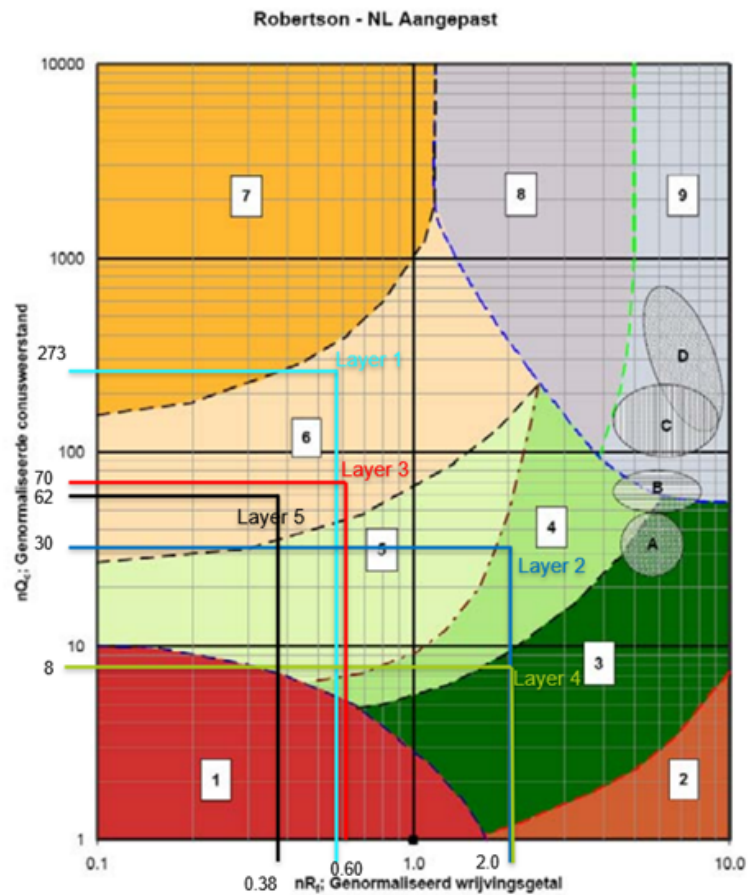


Figure 4.8: Soil identification regarding the Robertson graph

Table 4.1: Parameters based on the CPT values

Soil layer	Depth relative to NAP [m]	σ_v at the center of the layer [kPa]	σ_v at the center of the layer [kPa]	q_c [MPa]	f_s [MPa]	Friction ratio R_f [%]
1	5	38.25	38.25	10.5	0.06	0.5
2	0.5	101.5	79	2.5	0.05	2
3	-2	306.5	249	17.7	0.11	0.5
4	-20	506.5	346.5	3.5	0.06	3
5	-22	806.5	546.5	35	0.13	0.5

According to Robertson's chart, type 6 is sand, while type 4 and type 3 are clay layers.

4.3. Soil parameters

In geotechnical projects where the Finite Element Method (FEM) is used, the right selection of soil model parameters is crucial to make good predictions. Therefore, empirical formulas have been developed to derive the model parameters for the PLAXIS Hardening Soil model (HS) and the PLAXIS Hardening Soil model with small-strain stiffness (HS-small).

Table 4.2: Soil identification based on Robertson's graph

Soil layer	nQ _t	nF _r	Soil type based on Robertson's chart
1	273.5	0.6	Type 6
2	30.4	2.1	Type 4
3	69.9	0.6	Type 6
4	8.6	2.0	Type 3
5	62.6	0.4	Type 6

Table 4.3 , Table4.4 and Table 4.5 present the soil parameters of the five identified layers as implemented in the PLAXIS 2D program. The soil parameters are determined based on empirical correlations with the cone resistance (q_c) and the relative density (RD). This method is used mainly for sand layers. For clay layers, it is not very accurate to obtain soil parameters from CPTs. Therefore, the properties of the clay layers are obtained only from laboratory tests.

4.3.1. Volumetric unit weights

The unit weight of the soil layers is derived from the results of the laboratory volumetric weight tests, which can be found in the geotechnical laboratory report [3].

4.3.2. Relative density

The model parameters derived from the empirical formulas for the sand are based on the relative density. The strength and stiffness of coarse-grained soils, such as sand, largely depend on the in-situ density. It is common in geotechnical engineering to describe the in-situ density relative to the maximum and minimum density, the so-called Relative Density (RD).

Relative density is the measure of compactness of cohesionless soil. The relative density or density index is the ratio of the difference between the void ratios of a cohesionless soil in its loosest state and the existing natural state to the difference between its void ratio in the loosest and densest states.

Determining relative density is helpful in evaluating the compaction state of coarse-grained soils and also assessing the safe bearing capacity in the case of sandy soils.

$$DR = (e_{\max} - e)/(e_{\max} - e_{\min}) \quad (4.3)$$

Where,

e_{\max} = void ratio of coarse grained soil (cohesionless) in its loosest state.

e_{\min} = void ratio of coarse grained soil (cohesionless) in its densest state.

e = void ratio of coarse grained soil (cohesionless) in its natural existing state in the field.

The void ratio is a ratio between the volume of the solid soil particles and the volume of the void between the soil particles. Jamiolkowski [9] proposed a correlation between the q_c value and the relative

density RD.

$$RD = \frac{1}{C_2} * \frac{q_c}{C_0 * p_a * \left(\frac{\sigma'_v}{p_a}\right)^{C_1}} \quad (4.4)$$

Where,

q_c : the cone resistance

p_a : the atmospheric pressure

σ'_v : the vertical effective stress

C_0, C_1, C_2 : empirical constants. The sand layers are assumed to be normally consolidated, in that case the empirical constants are $C_0=17.68$, $C_1=0.5$ and $C_2=3.1$

Table 4.3: Unit weights and relative density of the soil layers

Soil layer	Depth relative to NAP [m]	$\gamma_{\text{unsat}} [kN/m^3]$	$\gamma_{\text{sat}} [kN/m^3]$	RD [%]
1	5	16.5	20	72.97
2	0.5	15.5	15.5	14.98
3	-2	16	19	59.60
4	-20	16.5	16.5	1.99
5	-22	16.5	20	68.91

4.3.3. Peak friction angle, dilatancy angle and cohesion

Regarding the peak friction angle ϕ'_p , there is a correlation of Mayne and Kulhawy [12] with the q_c value.

$$\phi'_p = 17.6 + 11 * \log\left(\frac{\frac{q_c}{p_a}}{\left(\frac{\sigma'_v}{p_a}\right)^{0.5}}\right) \quad (4.5)$$

According to empirical formulas to derive model parameters for sands [2], the dilatancy angle ψ , is determined from the relative density based on the equation below

$$\psi = -2 + (12.5 * D_r)/100[^\circ] \quad (4.6)$$

For clay layers, the effective cohesion is based on triaxial tests. The effective cohesion of the sand samples is assumed to be zero. However, to make the PLAXIS 2D model more stable, the cohesion of the sand layers is set to 1kPa.

4.3.4. Stiffness moduli

Table 4.4: Peak friction angle, dilatancy angle and cohesion values for the soil layers

Soil layer	$\phi'_p [^\circ]$	$\psi [^\circ]$	$c [kN/m^2]$
1	42.13	7.12	-
2	34.30	-	8.00
3	40.15	5.45	-
4	35.90	-	10.00
5	41.53	6.61	-

Mayne and Kulhawy [12] provide a correlation between the constrained tangent stiffness modulus E_{oed} , q_c values and the RD in normally consolidated coarse-grained soils.

$$E_{oed} = q_c * 10^{(1.09 - 0.0075 * RD)} \quad (4.7)$$

The stiffness moduli in the HS model are stress-dependent. Therefore, in the equation below, the constrained stiffness modulus is converted to a reference stress level using p_{ref} which is set at 100 kPa.

$$E_{oed}^{ref} = E_{oed} / (\sigma'_v / p_{ref})^m \quad (4.8)$$

According to Brinkgreve [2], considering $p_{ref} = 100 kPa$, the reference stiffness formulas are:

$$E_{50}^{ref} = 60000RD / 100 [kN/m^2] \quad (4.9)$$

$$E_{oed}^{ref} = 60000RD / 100 [kN/m^2] \quad (4.10)$$

$$E_{ur}^{ref} = 180000RD / 100 [kN/m^2] \quad (4.11)$$

The reference constrained tangent modulus, E_{oed}^{ref} , and the reference unloading/reloading stiffness modulus, E_{ur}^{ref} , for the sand layers, are derived from the reference constrained tangent modulus E_{oed}^{ref} by the following relations:

- For sand layers:

$$E_{50}^{ref} = E_{oed}^{ref} \quad (4.12)$$

$$E_{ur}^{ref} = 3 * E_{50}^{ref} \quad (4.13)$$

- For clay layers:

$$E_{50}^{ref} = 2 * E_{oed}^{ref} \quad (4.14)$$

$$E_{ur}^{ref} = 3 * E_{50}^{ref} \quad (4.15)$$

4.3.5. Power parameter

The power parameter m accounts for the stress-dependency of the stiffness moduli. The rate of stress dependency, m , is observed to be negatively correlated with the density. The following formula was proposed by Brinkgreve et al. in 2010 [2].

$$m = 0.7 - (D_r/320)[-] \quad (4.16)$$

The values in Table 4.6 are from the Mayne and Kulhawy [12] method because with the method from Brinkgreve [2] the values were lower and according to some available data from other researchers these values were underestimating the properties of the soils.

Table 4.5: Stiffness parameters for the soil layers

Soil layer	E_{oed} [MPa]	E_{oed}^{ref} [MPa]	E_{50}^{ref} [MPa]	E_{ur}^{ref}	m [-]
1	37	58	58	172.99	0.47
2		3	5	15.00	1.00
3	78	49	49	146.07	0.51
4		3	6	18.00	1.00
5	131	58	58	172.53	0.48

The values for clay layers (2,4) in 4.6 are obtained from laboratory tests. Therefore, there are not calculated with the empirical correlations. There is also a table with all the parameters that will be used in PLAXIS 2D and some remarks at the APPENDIX.

4.4. Geotechnical cross section

Figure 4.9 summarises the simplified soil profile based on the above mentioned soil investigation and is used herein to design the soil model for PLAXIS 2D.

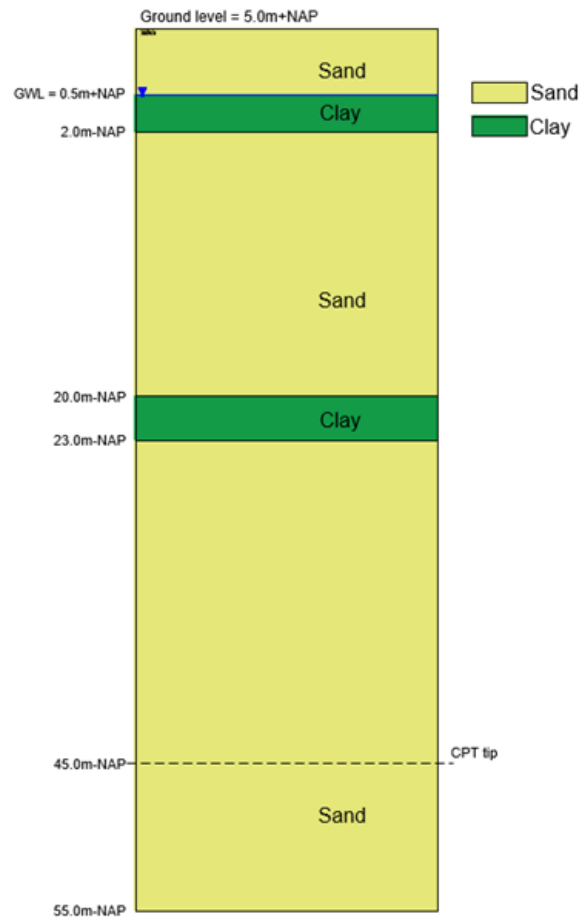


Figure 4.9: Simplified soil profile of at the section D of HHTT quay wall

4.5. Structure parameters

The applied structural elements and their properties are presented in Table 4.6. The table below shows the structural elements of Sections D1 and B4 of the HHTT quay wall.

** For the stiffness properties of the structural elements, lower, mean and upper values are presented. ** The cross-sectional area and the moment of inertia for each element are derived from another research project in the same area. However, in the table below, I have my own calculations.*

4.6. Structural elements in PLAXIS 2D

The combined wall is constructed of alternating tubular piles and triple PU28 sheet piles. Therefore, the width of the locks of the combined wall, which are welded on the tubular piles, should be considered as well. The type of the locks is C9. Hence, the total width is 1420mm (tubular piles of the combi wall) + 1800mm (width of the sheet piles PU28) + 2*37mm (lock C9) = 3.294m.

In PLAXIS the combined wall is modelled as a plate element because it is a continuous wall. However, the plate element in PLAXIS has no cross-sectional area and thus has zero bearing capacity. Therefore, an option in order to avoid unrealistic large vertical deformations due to punching behaviour, is to restrict a soil volume surrounding the bottom of the plate element. The relieving platform and the concrete bar

Table 4.6: Table with the structural element parameters of the HHTT quay wall

Element	Tubular piles combined wall	3 x PU 28 sheet piles combined wall	MV - piles (HEB600)	SI - piles	Floor relieving platform	Front wall relieving platform
Dimensions [mm]	D _{outer} :1420	Width:1800 Height:454	Width: 300 Height: 600	D _{steel tube} : 609 D _{screw tip} : 850	Width: 16800 Height: 1750	Width: 2200(B4) / 2800 (D1) Height:7000
Thickness steel [mm]	B4 : 24 D1 : 19	-	Flange: 30 Web: 15.5	10 (steel tube)	-	-
Centre to centre distance [mm]	3295	3295	B4: 3845 D1: 3295	Perpendicular: 3000 parallel 3295	-	-
Material quality	X70 (steel)	S355GP (steel)	S420M (steel)	Steel: S355 J2H Concrete: C35/45	C35/45 (concrete)	C35/45 (concrete)
Youngs Modulus *10 ⁶ [kPa]	E _{max} = 210 E _{mean} = 200 E _{min} = 190	-	steel: see left concrete: see right	-	E _{uncracked} =30 E _{mean} = 20 E _{cracked} = 10	
Cross-sectional area [mm ² /m]	B4:31955 D1:25380	120	B4:7025 D1:8195	steel:5715 concrete: 82715	175 * 10 ⁴	B4 : 220 * 10 ⁴ D1 : 280 * 10 ⁴
Moment of Inertia [mm ⁴ /m]	B4: 7786*10 ⁶ D1 : 6228 * 10 ⁶	323 * 10 ⁶	B4: 45 * 10 ⁶ D1 : 520 * 10 ⁶	steel: 256 * 10 ⁶ concrete : 1794 * 10 ⁶	446615 * 10 ⁶	B4 :887333 * 10 ⁶ D1 : 1829000 * 10 ⁶

are also modelled as plate elements. The SI-piles and MV-piles are modelled with embedded beam elements. The bearing capacity of the SI-piles F_{max} and the friction capacity T_{max} are estimated with the equations below.

$$F_{max} = a_p * q_b * A_{tip} \quad (4.17)$$

$$T_{max} = a_s * q_s * A_{circumference} \quad (4.18)$$

In these equations, a_p and a_s are pile factors which are equal to respectively 0.63 and 0.009, q_b and q_s are the base and shaft cone resistance with are set equal to respectively 10 MPa and 15 MPa. The area of the pile tip is 0.56 m² and the circumference area is 2.67 m².

Therefore, F_{max} =3.528 kN/m and T_{max} =3.604,5 kN/m.

The table from fig:Input parameters for plate elements illustrates the input parameters for the plate elements having as reference, the values from the Table 4.6. Moreover, Table 5.3 summarises how the structural elements will be modelled in PLAXIS 2D.

4.7. Definition of the material properties

The thermal properties of a material describe its ability to retain and conduct heat. The parameters that describe this phenomenon are: the heat capacity, the thermal conductivity and the thermal diffusivity.

The heat capacity of a material is the amount of heat that is required to raise its temperature by 1 degree [1].

The specific heat capacity of the solid material, C_s , is a parameter that describes the amount of energy (heat) that can be stored in the solid material (ie, the soil particles) per unit of mass. It is specified as the unit of energy per unit of mass per unit of temperature. The higher the specific heat, the more energy it takes to increase the temperature of the material [15].

The equation for calculating the heat capacity (C) is as follows:

$$C = 1/m(c_s * m_s + c_w * m_w + c_i * m_i + c_a * m_a) \quad (4.19)$$

Where C is the heat capacity [kJ/(kJ*K)], m is the total mass [kg] and the subscripts s, w, i and air stand for solids, water, ice and air. Total saturation and unfrozen conditions are assumed, simplifying the equation to:

$$C = 1/m(c_s m_s + c_w m_w) \quad (4.20)$$

The Thermal conductivity of the solid material, λ_s , is a parameter that describes the rate of energy (heat) that can be transported in the solid material (i.e. the soil particles). It is specified in the unit of power per unit of length per unit of temperature. The higher the conductivity, the more energy is transported, resulting in a faster propagation of a change of temperature in the material [15]. Generally, heat transfer is highest in solids, then in liquids and finally in gasses.

The Density of the solid material, ρ_s , is the parameter that describes the density of the soil particles, material expressed in the unit of mass per unit of volume [15].

Thermal expansion coefficients, α , describe how much the material expands (or elongates) when the temperature increases. In other words, the thermal expansion coefficient is the (change of) strain per unit of temperature. If the thermal expansion is isotropic, all coefficients are equal, but PLAXIS 2D can also handle anisotropic thermal expansion in the x, y, and z directions. Instead of entering linear thermal expansion coefficients, a single value can be specified for volumetric thermal expansion, considering isotropic expansion [15].

The rise in temperature is dependent on the heat capacity and the bulk density of the soil [1].

$$a = k/(C * \rho) \quad (4.21)$$

The vapour diffusion coefficient, Dv , governs the diffusion of vapour in the material. A value of zero disables the mass flux of the vapour in the material [15].

The thermal diffusion enhancement factor, fTv , influences the dependence of the temperature on the mass flux of vapour. A zero value means that the mass flux of the vapour is only governed by the

variations in the pore pressure [15].

Regarding the thermal functions that were used in PLAXIS 2D, the following descriptions are based on [14]. The thermal function describes the variation of the temperature over time. PLAXIS offers 3 ways to specify a function: as a harmonic, a linear and by means of a table. Only the table function is used in this thesis. This table can be defined in either the thermal functions window or be imported as a .txt file. In both cases, the table consists of two columns; the first column is the time in days and the second column holds, depending on the type of function, the Temperature [K] (temperature function), the HeatFlux [kW/m²] (heat flux function) or the Δ HeatTotalFlux [kW/m³] (heat total flux function). In this particular thesis, the table that was inserted were the temperatures from the KNMI station at Hook van Holland.

Table 4.7: Thermal properties of soil types and other components [24]

Material	Heat capacity (C_s)[kJ/(t * K)]	Thermal conductivity (λ)[kW/(m * K)]	Density (ρ_s)[t/m ³]	Volumetric thermal expansion coefficient (solids) α [1/K]
Clay	2357.14	0.00090	1.40	$1.02 * 10^4$
Sand	1666.66	0.00259	1.80	$1 * 10^4$
Steel	475.16	0.04450	7.85	$11 * 10^4$
Concrete	800	0.0021	2.50	$1 * 10^{-6}$

Plate		EA [kN/m]		EI [kNm ² /m]		v [-]	Weight [kN/m/m]
		B4	D1	B4	D1		
Tubular piles + sheet piles combined wall	mean	6.42E+06	5.10E+06	1.62E+06	1.31E+06	0	0
	min	6.09E+06	4.85E+06	1.54E+06	1.24E+06		
	max	6.74E+06	5.35E+06	5.36E+00	1.38E+06		
Tubular piles combined wall	mean	6.39E+06	5.08E+06	1.56E+06	1.25E+06	0	0
	min	6.07E+06	5.08E+06	1.48E+06	1.18E+06		
	max	6.71E+06	5.33E+06	1.64E+06	1.31E+06		
Cast iron saddle	-	$210 * 10^9$	$210 * 10^9$	$210 * 10^9$	$210 * 10^9$	0	0
Floor relieving platform	mean	3.50E+07	-	8.93E+06	-	0.2	17.5
	cracked	1.75E+07	-	4.47E+06	-		
	uncracked	5.25E+07	-	1.34E+07	-		
Front wall relieving platform	mean	4.40E+07	5.60E+07	1.77E+07	3.66E+07	0.2	B4: 35.2 D1: 44.8
	cracked	2.20E+07	2.80E+07	8.87E+06	1.83E+07		
	uncracked	6.60E+07	8.40E+07	2.66E+07	5.49E+07		

Figure 4.10: Table with the input parameters for plate elements

5

Set up and validation of the developed model

This chapter describes the development of the geotechnical model in PLAXIS 2D. Also, this chapter will answer the research question: "How can the temperature effect be modelled using geotechnical finite element methods like PLAXIS 2D?". A good understanding of the influence of the thermal component is vital for interpreting the computations correctly and comparing these with the real measurements. The chapter starts with a brief recap of the model setup and the definition of the initial and boundary conditions. Subsequently, the validation is started by comparing the temperature fluctuation of a simple model with the measured temperature of the SIF combi wall. After this, model validation is carried out by comparing the model output deformation of the combi wall after the dredging period with data from manual inclinometers at the HHTT quay wall. After validation, a new analysis is performed using the model and the heating input to see the influence of thermal fluctuations on PLAXIS 2D. Finally, an investigation was carried out into the impact of climate change and the corresponding increase in temperature fluctuations on the behaviour of the quay wall.

5.1. Set up of the geotechnical model in PLAXIS 2D

The Finite Element Method (FEM) describes the soil and structural behaviour of a model by solving a series of partial differential equations. These partial differential equations do not have an exact solution and, therefore, cannot be solved analytically, and thus, they are solved numerically. In this project, the PLAXIS software package is used to perform FEM calculations. PLAXIS has 2-Dimensional (2D) and 3-Dimensional (3D) packages in which FEM calculations can be performed. In this research project, only the PLAXIS 2D package was used.

The advantages of FEM models like PLAXIS 2D are that these models can model complex geometries including soil-structure interaction, calculate soil deformations, calculate anchor forces and model temperature effects. The main disadvantages of FEM models are the large number of input parameters required, relatively long calculation times and the required level of knowledge about soil behavior.

5.1.1. Drainage type

The selection of the drainage type depends on the permeability of the material and the type of loading conditions, rapid or very slow. Therefore, sand is a coarse grained soil, so this is calculated according to the drained method. The other present soil type, clay, is an impermeable soil, so it is calculated according to the undrained method. Table 5.1 illustrates the type of drainage type for each

soil material.

Table 5.1: Constitutive model and drainage type for each soil material

Material	Constitutive model type	Drainage type
Sand	Hardening soil	Drained
Clay	Hardening soil	Undrained

5.1.2. Temperature input

With respect to temperature input, PLAXIS uses some thermal functions. The following descriptions are based on the PLAXIS reference manuals [15] and [14]. The thermal function describes the variation of the temperature over time. Thermal functions describe the variation with time of quantities such as temperature. A temperature function can be assigned to the thermal flow boundary conditions and to the air temperature as defined in the climate model condition. Temperature is defined in units of temperature [15]. PLAXIS offers 3 ways to specify a function.

- Harmonic function
- Linear function
- Import a table

Only the table option is used in this research project. The first column is the time in days and the second column is the Δ Temperature [K] [15]. Δ Temperature parameter, specified in units of temperature, represents the increase or decrease in temperature in the time interval for the current calculation phase. Therefore, together with the time interval, this parameter determines the rate of increase or decrease in temperature. In this particular research, later it will be presented which values were used for the Δ Temperature column.

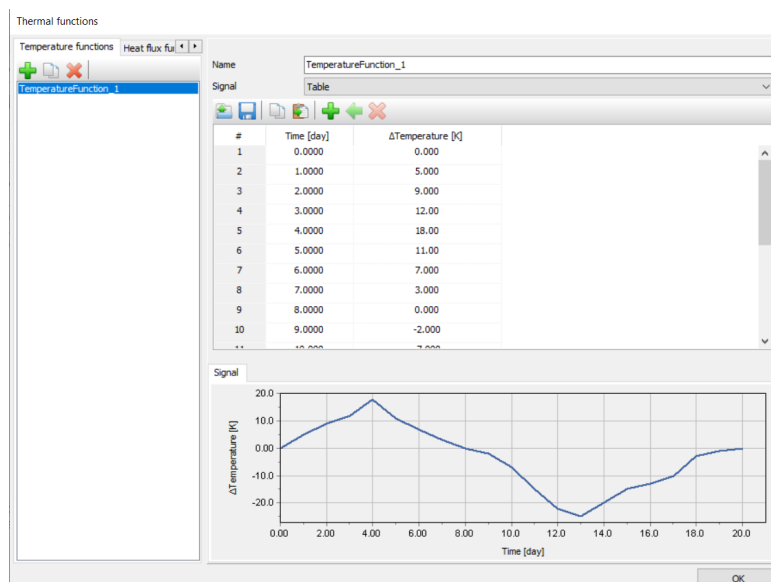


Figure 5.1: Tab sheet for filling the table for the temperature input of PLAXIS 2D

PLAXIS 2D has 5 steps before the model runs and executes the calculations. So far, there has been a discussion about the first four steps. Therefore, to complete the model, 4 phases were used in the staged

construction step.

Based on the literature and having information from other research projects for this particular project, the construction process is divided into multiple phases. However, the goal of this research is to investigate what is happening in the quay wall during its lifetime and not how the wall responds during the construction stages. Thus, the construction stages that were used for this research model are listed below.

- *Phase 0* → Initial phase - geometry input
- *Phase 1* → Installation of combi wall, MV pile and SI piles
- *Phase 2* → Excavation of the soil in front of the quay wall (dredging period)
- *Phase 3* → Heating phase - temperature input

During the installation stage, Phase 1, all structural elements of the quay wall were constructed at the same time. Therefore, the combi wall is installed at the same stage as the MV pile and the 2 SI piles.

For the first 3 phases, the calculation type was plastic, while during the heating phase, the calculation type was fully coupled flow deformation, as illustrated in Table 5.2.

Table 5.2: Calculation types for each phase of the model in PLAXIS 2D

Phase	Calculation type	Pore pressure calculation type	Thermal calculation type
Initial	k0 procedure	Phreatic	Ignore temperature
Installation	Plastic	Phreatic	Ignore temperature
Excavation	Plastic	Phreatic	Ignore temperature
Heating	Fully coupled flow deformation	Transient groundwater flow (automatic)	Use temperatures from the previous phase

5.1.3. Calculation types

With respect to the calculation type used, the PLAXIS 2D Reference Manual refers to the following types.

The ignore temperature option means that no temperature distribution is calculated and the temperature effects are ignored.

With the option of using temperatures from the previous phase, it is assumed that the initial temperature distribution in the current phase is equal to the temperature distribution at the end of the parent phase. This option can be used to indicate that the calculation kernel should use the temperature distribution of the previous step (phase) as input for the current deformation analysis according to the PLAXIS 2D reference manual [15].

In this particular project, where it is used the 'Fully coupled flow deformation analysis', with respect to the PLAXIS 2D reference manual, the option of using temperatures from the previous phase must be selected to take into account temperature effects. In this case, the temperature of the previous phase is only used to initialise the temperature at the beginning of the current phase, but it may still change during the phase as a result of a time-dependent change in thermal flow boundary conditions. This is the case because, in the heating phase, the input of the thermal function is the air temperature [15].

5.1.4. Project properties

The project properties that are initially specified play a crucial role in the model output. In particular, the reference temperature dominates the result.

In projects like this that involve the temperature, the input of a reference temperature is required. The reference temperature is the temperature on the ground surface in the case that no specific thermal conditions are given here. By default, the reference temperature is set to 293.1K(=20°C) [15]. However, according to the measured data, the soil temperature of the Port of Rotterdam area is 11.7°C according to Figure 3.22.

5.1.5. Boundary conditions

Thermal calculations require a set of thermal boundary conditions to be specified, which can be imposed on the model to define the temperature distribution on the geometry [15]. A brief description of the boundary conditions used is provided below.

- Closed
- Temperature
- Inflow
- Outflow
- Convention

When the Closed option is assigned to a boundary, no heat flux can occur across it. In other words, the boundary is perfectly insulated. This boundary condition is similar to the 'natural' boundary condition. This means that if no thermal boundary condition is applied at a model boundary, or the thermal boundary condition is inactive, then the boundary is a closed thermal boundary. A closed thermal boundary is only considered at external model boundaries or at 'internal' boundaries between active and inactive clusters [15].

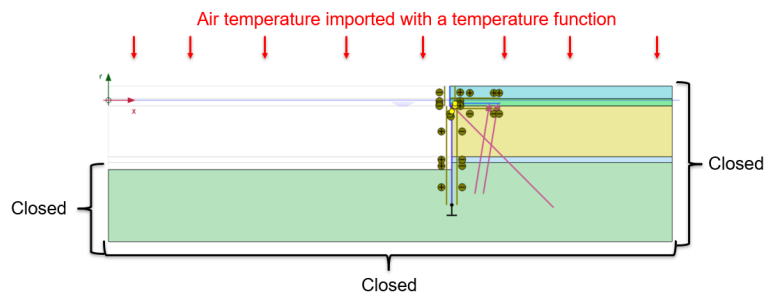


Figure 5.2: Boundary conditions that used for the heating phase in PLAXIS 2D

Therefore, the boundary conditions on the sides and at the bottom of the model are closed. At the top, the boundary condition is the time dependent temperature function which uses the air temperatures from the meteorological station KNMI at hook van Holland. Figure 5.3 illustrates the values that were used for different types of analysis. Moreover, Figure 5.2 illustrates the boundary conditions that were used.

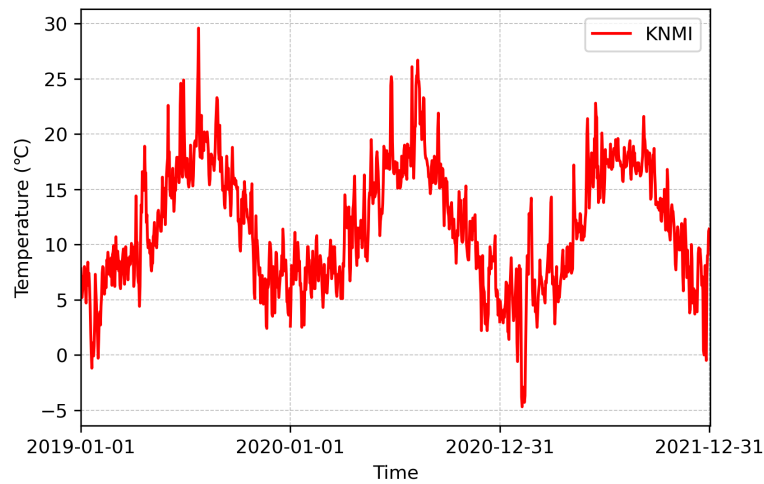


Figure 5.3: Air temperatures from KNMI station

The climate option can be used for thermal calculations to specify a general convective condition based on weather conditions (air temperature). The climate condition is applied to all the boundaries that represent the ground surface [15]. Additionally, with the climate option, the user can select the thermal function that they want to use. In this particular project, different thermal functions were used, which will be explained later.

Correct modelling of the geometries of the soil and structural elements is crucial to get a correct result. The table below illustrates how the structural elements were modelled in PLAXIS 2D.

Table 5.3: Structural elements applied on the quay wall

Structural elements	PLAXIS 2D
combined wall	plate element
SI - piles	embedded beam row
MV - piles	embedded beam row
relieving platform	plate element
concrete bar (floor)	plate element

The plate elements in FEM do not provide any end bearing. Therefore, the end bearing of a front wall should be modelled separately. This can be achieved by introducing a fixed-end anchor or by introducing a perpendicular plate. In this particular project, the fixed-end anchor was selected. However, this method has its limitations. By applying a fixed-end anchor, the stresses below the pile tip are not incorporated but 'disappear' into the fixed-end anchor and out of the model. Stress increase in the direct vicinity of the wall or pile tip will therefore unjustly be neglected.

5.2. Description of the Geometry

For the validation of the model, three different models will be used. The soil and structural parameters for these three models were obtained in Chapter 4. Figures 5.4a, 5.4b and 5.4c illustrate these models.

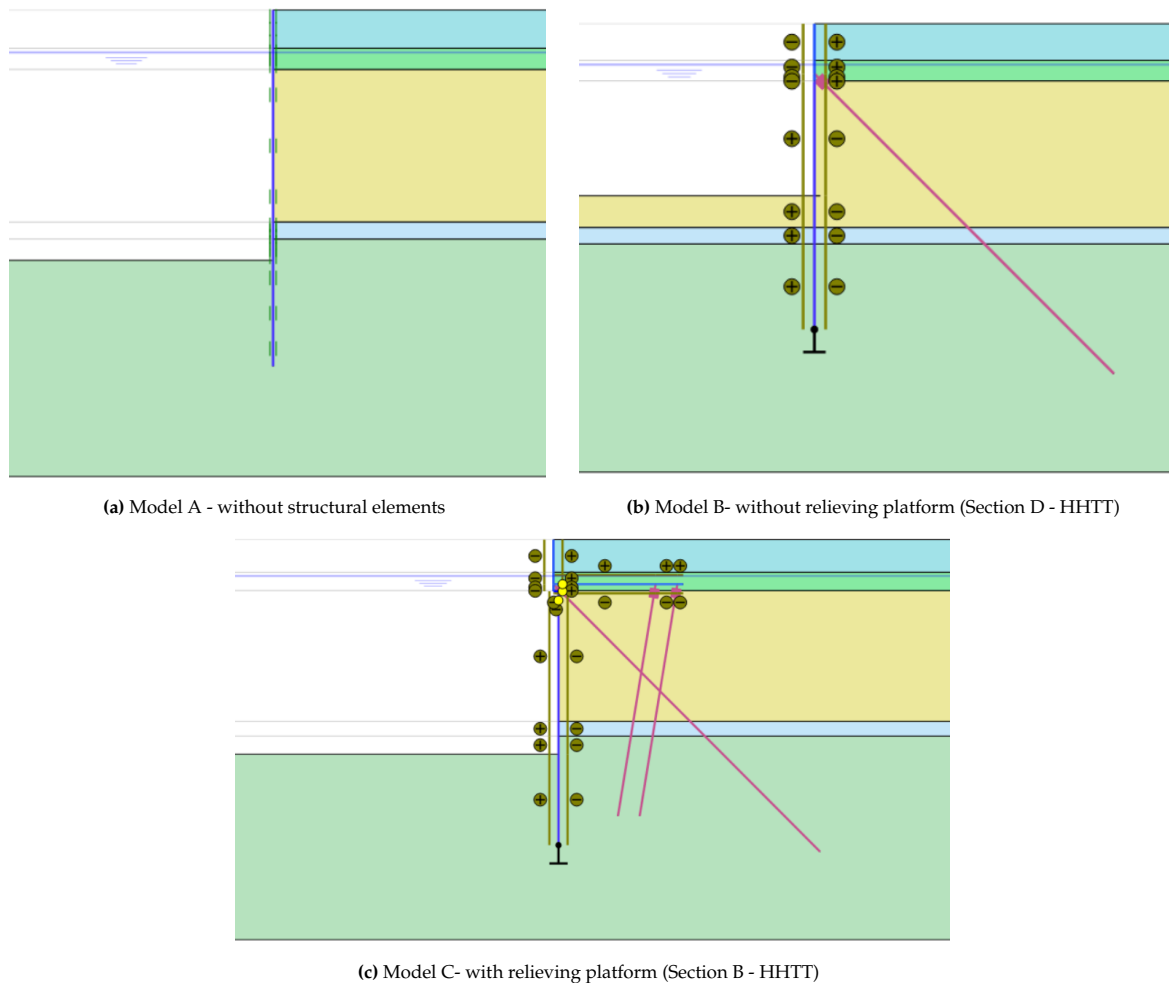


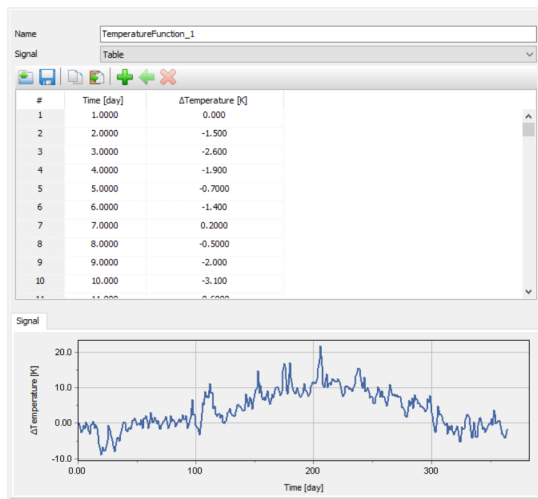
Figure 5.4: Different models in PLAXIS 2D

Three different models were created for the investigation and validation of the heating effect. The first, which is the simplest, includes the geometry of the soil profile and a line displacement instead of a quay wall. The second model is a quay wall, but without a relieving platform such as the section D of the HHTT quay wall. The third and most complicated model is with a quay wall and a relieving platform, like section B of the HHTT quay wall. For simplicity, since now in this project, the models in Figure 5.4a, Figure 5.4b and Figure 5.4c will be called models A B and C, respectively.

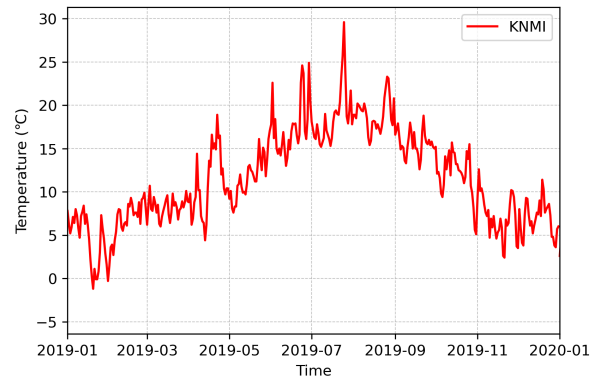
5.3. Validation of the developed model

5.3.1. Analysis with model A

The first goal of the validation is to verify if the model understands correct the temperature input. A detailed analysis will be conducted of how the soil profile reacts to the seasonal fluctuation of the temperature. This validation will take place with the simplest model, model A. Figure 5.5a shows the input temperature, which is the temperature over the duration of one year with the reference temperature on day 0, 280.9 K (7.8 °C).



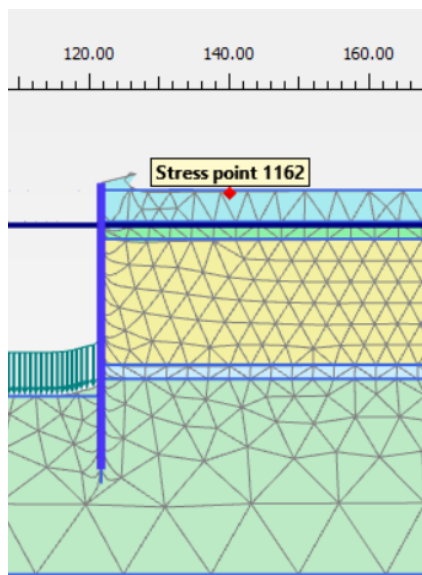
(a) Temperature function for input of 1 year temperatures



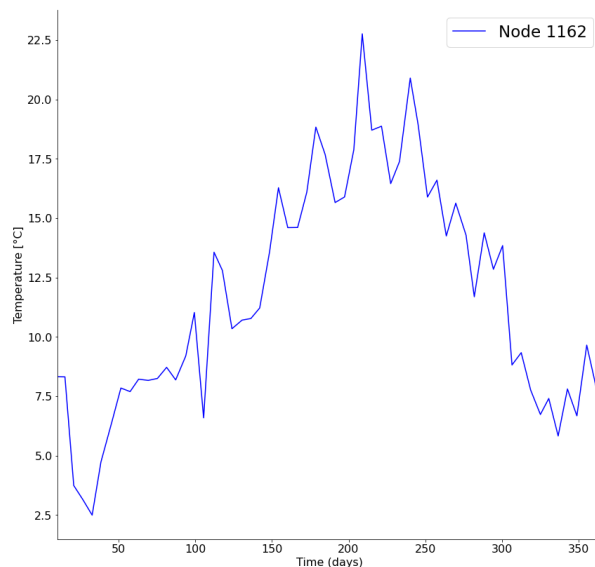
(b) Air temperatures from 01/2019 to 01/2020

Figure 5.5: Input temperature in PLAXIS 2D

For validation, a point was selected on the surface of the model. This point is the stress point 1162 ($x = 140.0\text{m}$, $y = 5.0\text{m}$) as illustrated in Figure 5.6a. The output of the model is illustrated in Figure 5.6b. The temperature on the surface is exactly what the input was. Therefore, the model "understands" the input perfectly.



(a) Stress point 1162 at the surface of the model A in PLAXIS 2D



(b) Temperature vs Time output for the stress point 1162 at the surface of the model A in PLAXIS 2D

Figure 5.6: Temperature at the stress point 1162

The next step to verify that the model works well, is to illustrate how the temperature affects the soil body of the model. Having as reference the figure from the SIF quay wall Figure 3.22, the goal is to check what the depth is that the temperature stabilises in the PLAXIS model and what is happening in the water domain and if PLAXIS realistically understands the temperature input.

For that reason, different stress points along the entire depth of the model were selected. From the surface level to the bottom of the model. The same process was also carried out for different stress points under the seabed. The following figures illustrate the stress points and the model output.

Although at Figure 5.7 it is not easy to understand which stress point is located where, they are selected along the whole depth for a better illustration of the results.

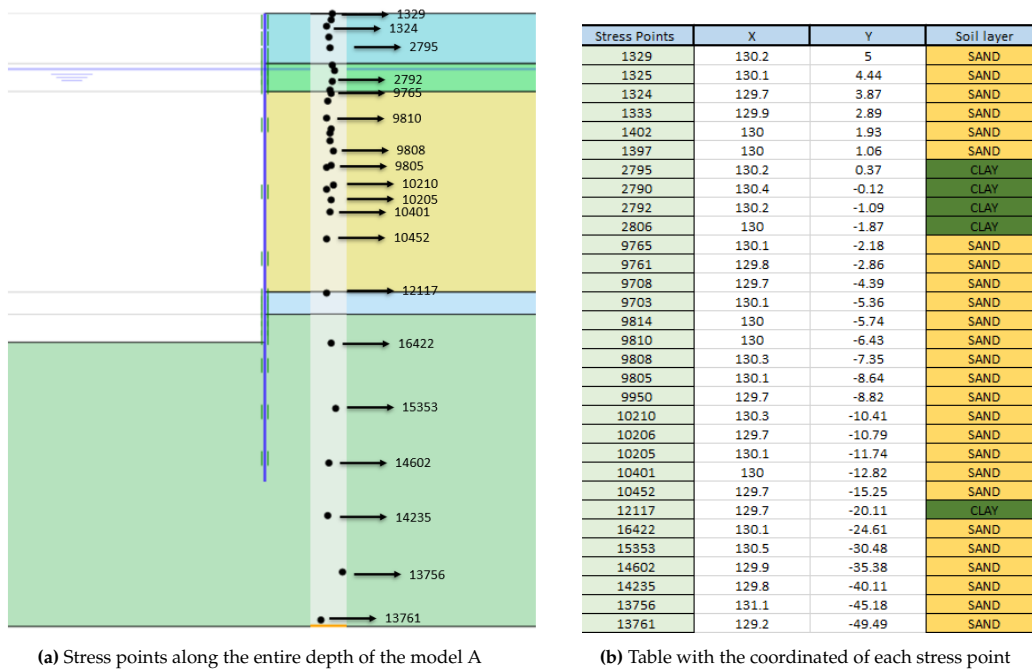


Figure 5.7: Depth vs Temperature for 1 year of the model A

For these 31 stress points, the temperature was calculated for 1 year, taking as input the data from Figure 5.5. The output of these calculations along the entire depth of the model is illustrated in Figure 5.8. PLAXIS 2D during the calculations divided the 1 year period into a certain amount of steps (63). Therefore, the lines in Figure 5.8 represent different moments in 1 year. The lines that start from the left side of the figure represent the winter period on the other had the lines which start from the right side of the graph represent the summer period.

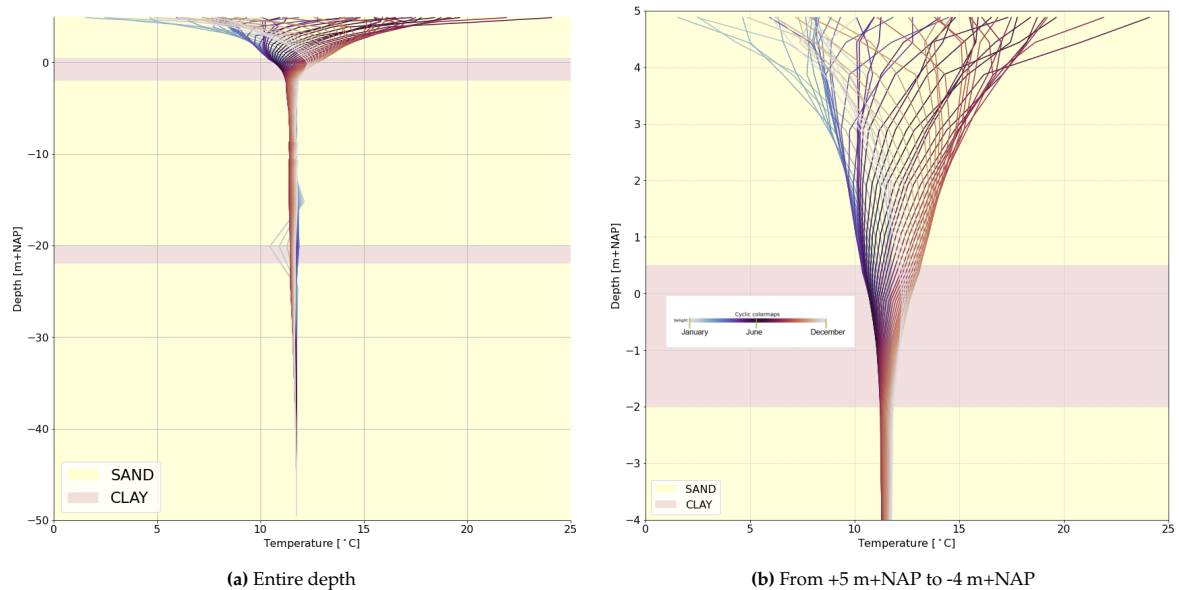


Figure 5.8: Depth vs Temperature for 1 year of the model A

Regarding Figure 5.8, it is visible that the depth at which the temperature stabilises in the soil body is approximately at a depth of -2 m+NAP. Therefore, approximately 7 metres from the surface level, from +5 m+NAP to -2 m+NAP, are enough to stabilise the temperature at 11.7 °C.

According to the measured data from the SIF quay wall Figure 3.22, the depth that is needed to stabilise the temperature is approximately 7 metres. Therefore, the model satisfies what the real data provide during the analysis. Hence, the model is validated in terms of how PLAXIS 2D "understands" the thermal function.

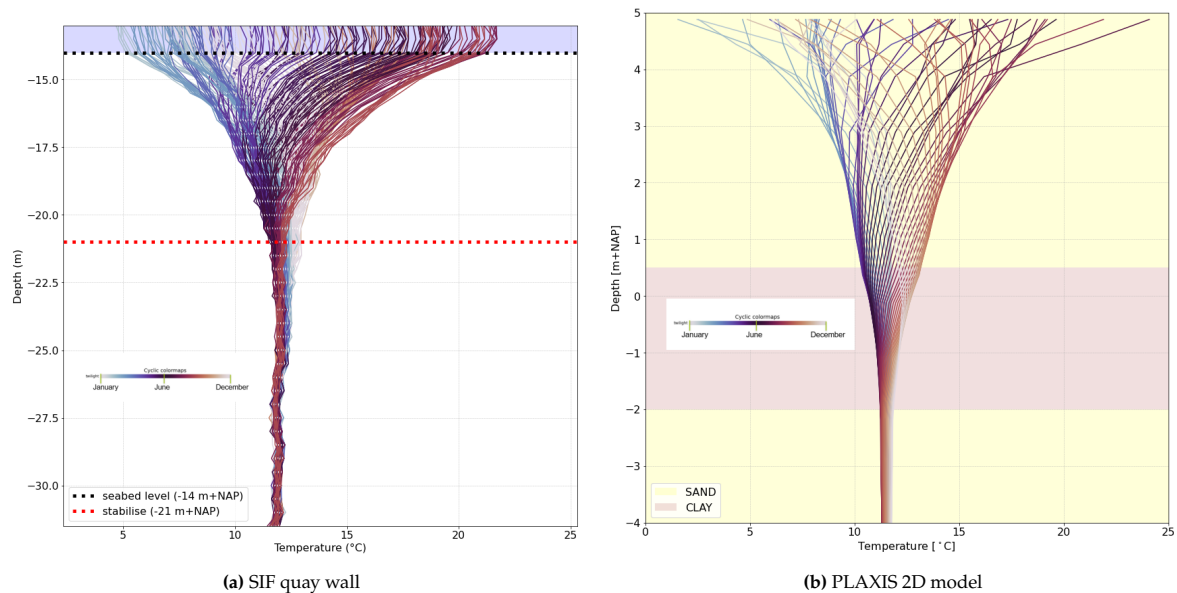


Figure 5.9: Real data from combi wall at the SIF quay wall compared with model A in PLAXIS 2D

Moreover, the water domain reacts realistically. From the aforementioned investigation, the domain below the seabed was examined and the reaction is similar to Figure 5.9a. This means that along the water the temperature remains approximately the same, and then the stabilisation depth is similar to what is happening at the surface level. According to Figure 5.10 the blue line, which is the seabed temperature, never reaches the peaks and the lows that the surface temperature reaches. This means that it is slightly decreased through the water domain, but is almost the same. This is also what is happening in reality.

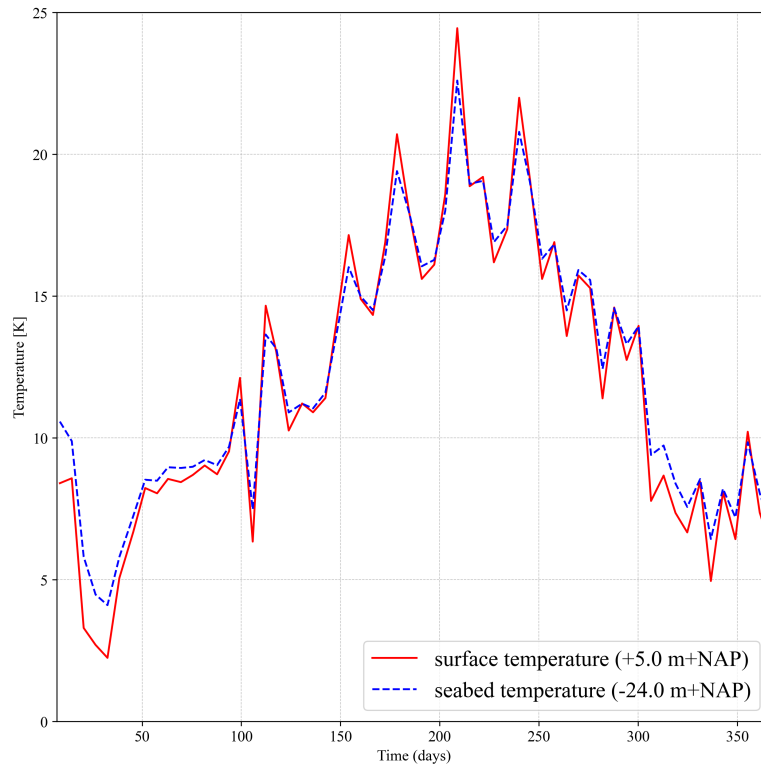


Figure 5.10: Temperature at the surface of the model and at the seabed of the model

5.3.2. Analysis with model B

The next goal, now that the model is perfect with respect to thermal input, is to validate if the model responds correctly with the added structural elements. Model B is a model only with the combi wall and the MV pile. Therefore, it is similar to section D of the HHTT quay wall. A way to verify that the model works well is to compare what is the reaction of the combi wall after the dredging period and to compare the wall deformations with the real data. Therefore, for the validation of the model, the output of the dredging phase will be used. Then the heating phase will follow.

The deformation from the combi wall in section D01 at the HHTT quay wall, after the dredging period, was 34.01mm. In PLAXIS 2D model B, after dredging, the maximum deformation of the plate, which represents the combi wall, was 40.89mm. Therefore, having these results, which are very close, the conclusion is that model works well.

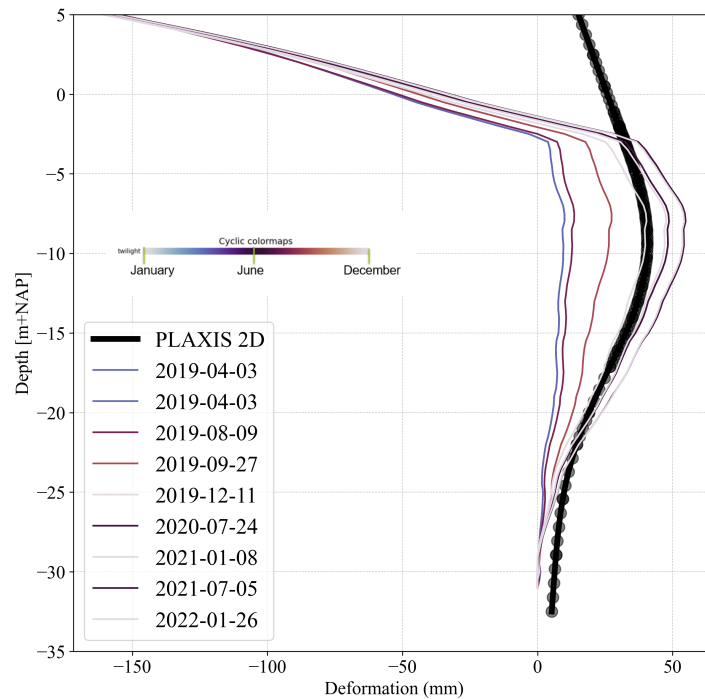


Figure 5.11: Comparison between the real measurements from Section D01 at the HHTT quay wall and the results from PLAXIS 2D model B

Regarding the deformations of the diaphragm wall, the dredging records of the quay wall during construction are vital. Therefore, as mentioned in M.Sc. Thesis from [19], the dredging period in section B4 ended on 23/10/2019 Figure A.1 and in section D1 ended on 19/11/2019 Figure A.1a.

5.3.3. Analysis with model C

Model C is similar to section B of the HHTT quay wall. Therefore, model C consists of a combi wall with a relieving platform, 1 MV pile and 2 bearing piles (SI-piles). As mentioned before, for the analysis with model B, a way to validate if the model works well is to compare the deformations of the combi wall of the model with the real data from the HHTT quay wall after the dredging period.

The deformation of the combi wall in section B03 at the HHTT quay wall, after the dredging period, was 49.27mm at depth = -13.6 m+NAP. In PLAXIS 2D model C, after dredging, the maximum deformation of the plate, which represents the combi wall, was 54.57mm. Therefore, having these results, which are very close, the conclusion is that the model works well. The measurements show deformations of the same magnitude with the numerical model in both cases, with and without a relieving platform. Therefore, the performance is relatively good.

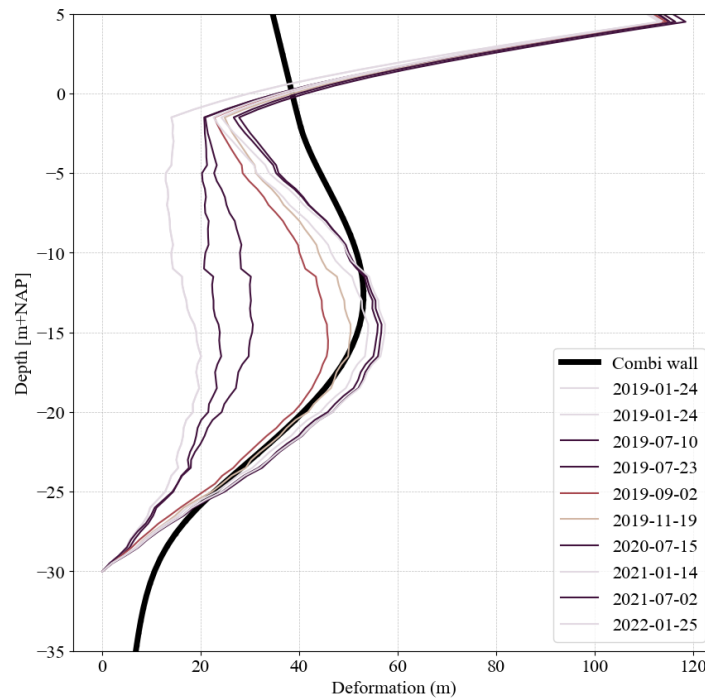


Figure 5.12: Comparison between the real measurements from Section B03 at the HHTT quay wall and the results from PLAXIS 2D model C

5.4. Heating phase

Now that the validation of the models has ended and it was concluded that they work well, the new heating phase will be added. Two different scenarios were tried to execute. The first scenario is a seasonal cycle effect, but instead of adding 365 days, the cycle that was used as an input in PLAXIS was 20 days. This is happening because in PLAXIS it was not possible for that model to execute the analysis for more than 100 days as input. This is a downfall of the model which have been developed for this research, that long-term time effects are not accounted for.

The other scenario is again with a time of 20 days in PLAXIS, but with the impact of climate change. Regarding the worst scenario of the IPCC climate models [23], there will be an increase of 4.5°C in temperature. Regarding Figure 1.1 from Chapter 1, the temperature will increase in the next few years. Also, it is relevant with the quay walls, because the lifetime of a quay wall is approximately 50 years and the climate models illustrate an increase in the next 50 years. Figure 5.13 illustrates the aforementioned scenarios.

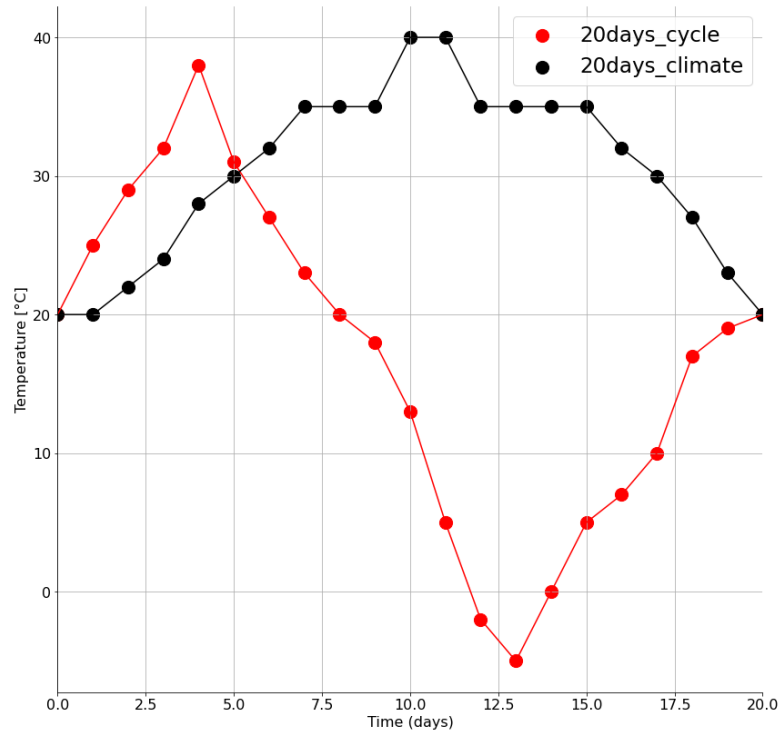


Figure 5.13: Two different scenarios for the heating phase of the model

For the analysis of the heating phase, various parameters and effects are taken into account. However, the next figures will present only the deformation of the combi wall in both scenarios along the entire depth of the wall and the anchor forces from the MV-pile along the entire length of the MV pile. This is happening because there will be a comparison with the available measurements.

For the analysis of the results, few nodes were chosen from the combi wall and the MV pile. Tables 5.4 and 5.5 illustrate these nodes. More information on the nodes and the coordinates of each node is available in the appendix in figure B.3.

Table 5.4: Coordinates of the Nodes from the model with relieving platform

Structural elements	Node	X	Y
Combi wall	3996	121.8	-2.70
	2444	121.8	-5.66
	5165	121.8	-11.91
	6395	121.8	-15.20
	7835	121.8	-25.28
MV Pile	17130	121.1	-1.13
	17134	121.54	-1.56
	17155	125.1	-5.09
	17156	125.4	-5.42
	17172	134.5	-14.54
	17195	151.0	-31.03

For model C, which is the model with the relieving platform, there were obtained the following graphs for the deformation of the combi wall and the axial forces of the MV pile.

Table 5.5: Coordinates of the Nodes from the model without relieving platform

Structural elements	Node	X	Y
Combi wall	597	121.1	-2.10
	3921	121.1	-5.48
	7291	121.1	-16.10
	8927	121.1	-25.44
MV Pile	13839	121.1	-1.13
	13845	122.45	-2.48
	13860	126.61	-6.64
	13883	135.75	-15.77
	13899	144.19	-24.22

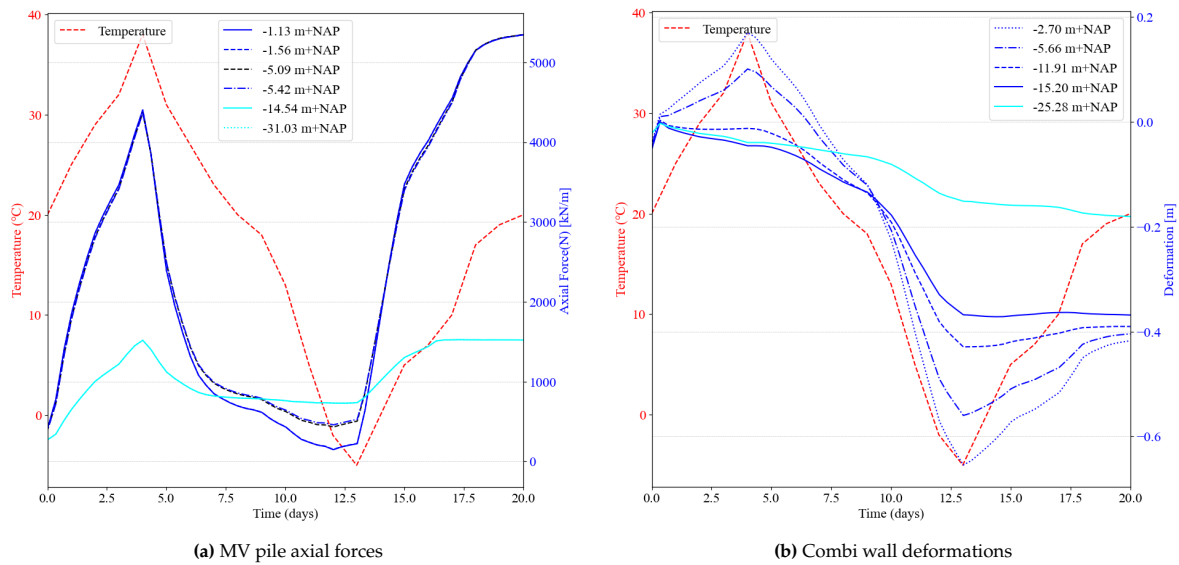


Figure 5.14: Model with relieving platform and with the cycle input approach

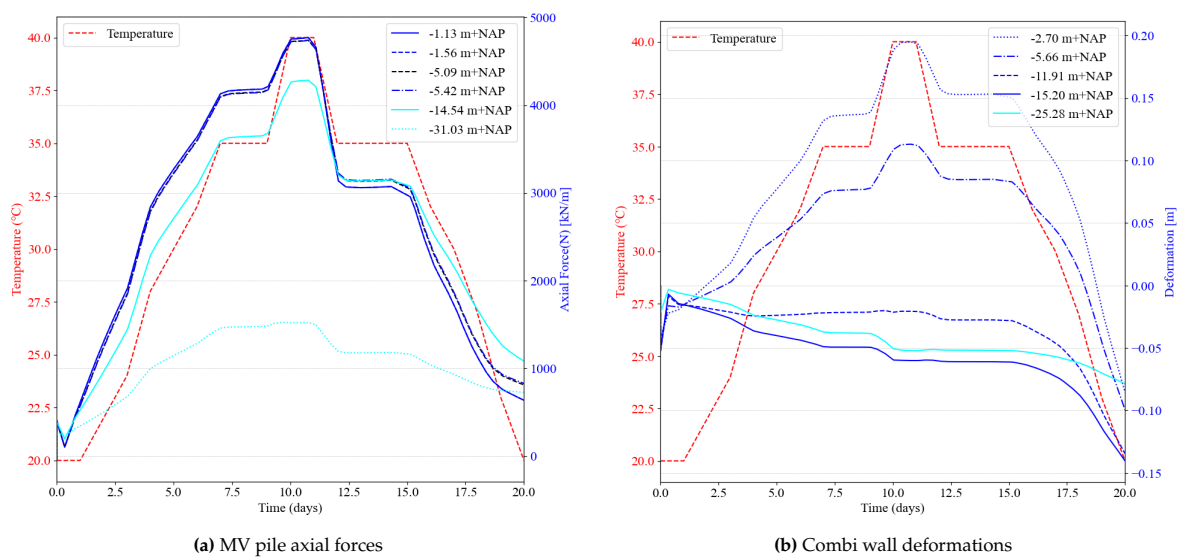


Figure 5.15: Model with relieving platform and with the climate input approach

Here it is visible that the increase of the anchor forces follows the increase of the temperature. In addition, during the decrease in temperature, the anchor forces decrease. However, the amount of increase and decrease, which is approximately 3500kN is much higher than the real measured data.

Regarding the combi wall, the deformations are much higher than was expected. Moreover, the movement of the wall is the opposite of what was expected as a result. An explanation for this could be that the influence of the temperature is happening locally and not along the entire domain. Therefore, a huge expansion is taking place in the combi wall, which is not representative of reality.

For model B, which is without the relieving platform, the following graphs were obtained for the deformation of the combi wall and the axial forces of the MV pile.

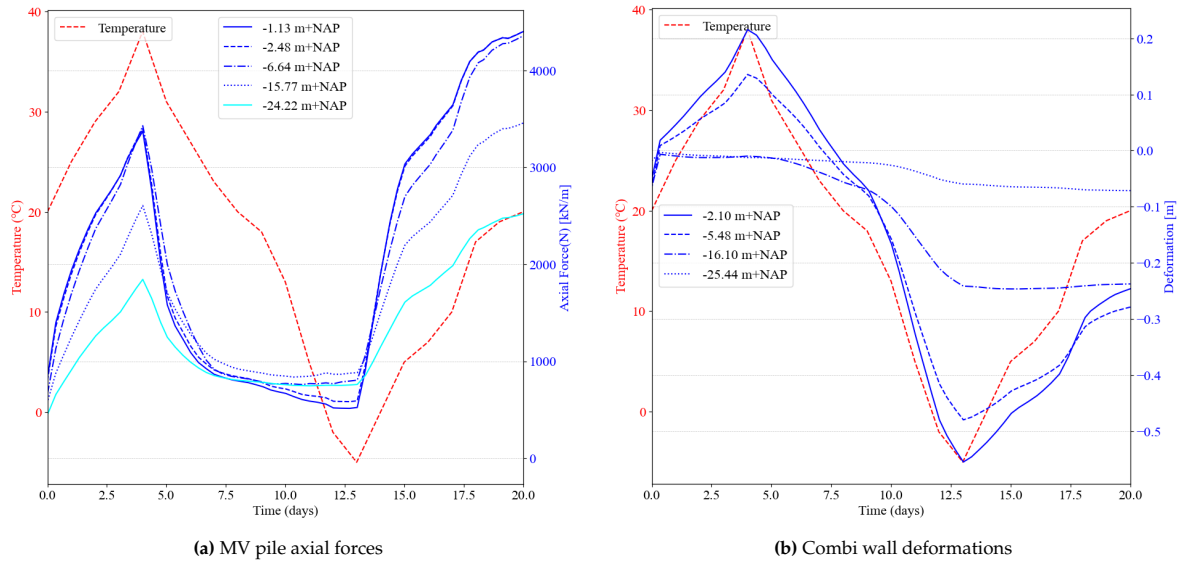


Figure 5.16: Model without relieving platform and with the cycle input approach

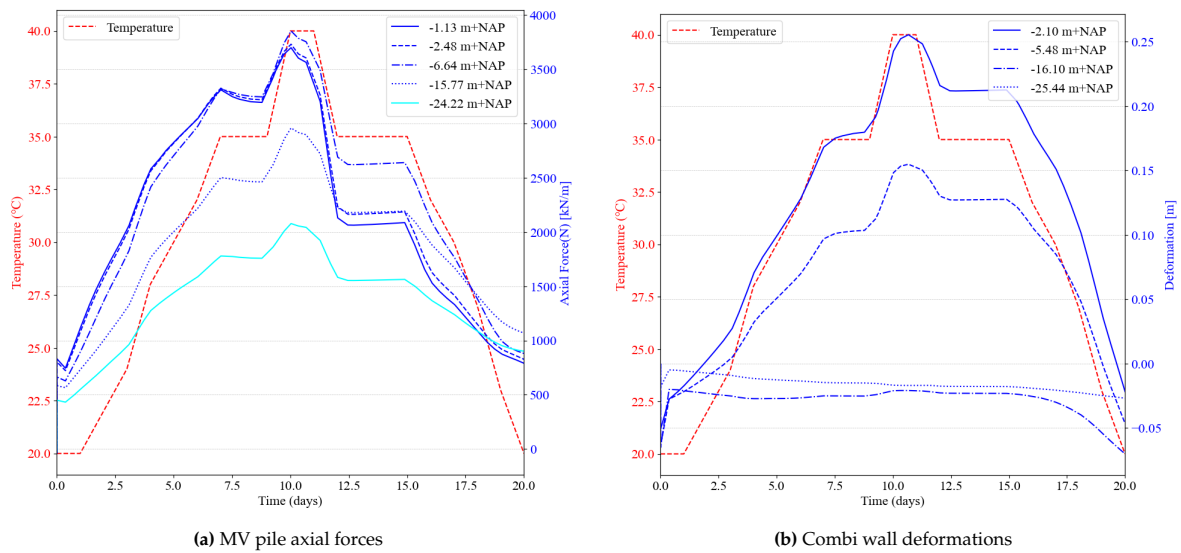


Figure 5.17: Model with relieving platform and with the climate input approach

The model with the relieving platform or the model without it reacts in the same way. In the scenario where the cycle effect was imported, there is an increase and a decrease of the anchor forces. However,

instead of moving towards the sea during the increase in temperature, the wall is moving towards the land side. Therefore, there is room for improvement for the model.

Another approach that was also examined was to add each month in the heating phase as a different construction stage. However, the results were again similar to the results above.

Another thing that should be mentioned is that with regard to the impact of climate change, it is visible that an increase in temperature could cause massive deformations. As already mentioned, there is room for improvement for the model; however, the massive increase in deformations should be considered for further investigation.

5.5. Sensitivity analysis of the thermal parameters

The sensitivity analysis was performed to verify how the parameters will affect the model and how sensitive the temperature distribution is with respect to an increase or decrease of these parameters. For the analysis, the simple model, model A, will be used. The analysis that will take place will have the sensitivity analysis $-/+ 25\%$.

Table 5.6: Sensitivity analysis input parameters

<i>Sand parameters</i>	75%	100%	125%
C_s [kJ/(t*K)]	1250.25	1667	2083.75
λ [kW/(m*K)]	0.0019425	0.00259	0.0032375
α [1/K]	0.000075	0.0001	0.000125
<i>Clay parameters</i>	75%	100%	125%
C_s [kJ/(t*K)]	1767.75	2357	2946.25
λ [kW/(m*K)]	0.000675	0.0009	0.001125
α [1/K]	0.0000765	0.000102	0.0001275

The parameters that were examined for the sensitivity analysis are the heat capacity, the thermal conductivity and the volumetric thermal expansion coefficient. A conclusion after the sensitivity analysis, where the results are in Appendix, is that the larger the specific heat, the more energy it takes to increase the temperature of the material. It is visible that comparing the values of Figure B.4a with the values of Figure B.4c, the temperature stabilises faster when there were used the values which were increased by 25%. Moreover, the higher the conductivity, the more energy is transported, resulting in a faster propagation of a change of temperature in the material. With respect to the sensitivity analysis of the thermal expansion coefficient, there was no change, which is exactly what was expected to happen. However, another conclusion is that no significant changes are visible with the sensitivity analysis that took place.

5.6. Concluding remarks

In this chapter, the models created in PLAXIS 2D were validated. This was done by comparing the results of the models with the real measured data from the quay walls. However, given the discrepancy during the heating phase, the model is characterised as not sufficient for calculating the thermal cycle effect with accuracy. Furthermore, a sensitivity analysis of how the model reacts with increasing and

decreasing thermal parameters was performed.

Additionally, it was not possible to model the cycle effect in the PLAXIS 2D model. As was mentioned in Chapter 3, the observations in the field data illustrate a cycle effect. This cycle effect indicates some plastic displacement of the combi wall, because the trend over the years is moving upward. This phenomenon could also be related to the ratcheting phenomenon. However, this could not be captured in the numerical model because of the limitation in time.

6

Conclusions and Recommendations

6.1. Conclusions

The Port of Rotterdam Authority has already addressed the urgent need to focus on asset management. They equip their new quay walls with modern sensors and have developed a quay wall monitoring system for their existing assets. These quay walls are called smart quay walls and the measurement data used for this project were obtained from a database of these smart quay walls. In terms of research, this database with actual monitoring data from these structures could be extremely beneficial in the future.

The seasonal effects of temperature fluctuations on quay walls are occurring. During the summer period, when there is an increase in temperature, the wall moves toward the sea, whereas in the winter period, the wall moves backward to the land side. Since in the design of the quay wall, the cycle movement of the combi wall due to seasonal fluctuation is not taken into account, this could have an impact on the stability of the wall in the future.

In particular, in Section D01 of the HHTT quay wall, the wall moves 7mm toward the sea each summer and 2mm backward during the winter period. In sections D05 and D07, the combi wall moves 4mm to 7mm toward the sea and 2mm back to its initial position. Similar is also the movement in section B of the HHTT quay wall. The SIF quay wall from January 2022 to August 2022 moved 3mm toward the sea, and now it seems that it started moving backward. Regarding the anchor forces, the fluctuation of the MV piles A11, B14 and C02 per cycle is 300kN. The difference from January to August is approximately from 700kN to 550kN.

However, older quay walls, like the Brammenterminal, deform from 4 to 10 mm per season, but it approximately moves back to its initial position. This means that the seasonal fluctuation of the quay wall is elastic and not plastic like the HHTT quay wall deformation.

Since this seasonal effect tends to increase only the displacements of the HHTT combi wall, which is a new quay wall, while the displacements from older quay walls like the Brammenterminal fluctuate seasonally but remain constant throughout the years, a conclusion comes through. The seasonal phenomenon exists, but instead of having an increase in the displacements of the wall over the years, there is an expansion of the materials (steel and concrete) during the summer period, which tends to move the wall towards the sea, and a contraction of the materials during the winter period where the wall moves back to its initial position.

In particular, if this cycle effect at the HHTT quay wall tends to increase the displacements of the combi wall for many years, this fact could also cause severe degradation to the quay wall through plastic deformation, ratcheting. Ratcheting is a progressive, incremental inelastic deformation characterized by a shift of the stress-strain hysteresis loop along the strain axis [17]. Furthermore, due to climate change, with an increase in temperature during the summer period, there will be greater temperature fluctuations. These larger cycles could cause more degradation, and finally over a long time could affect the lifetime of a quay wall.

However, this is not the case at the moment for HHTT the quay wall. The increase in the deformations of the quay wall is due to the fact that the construction of the combi wall took place three years ago, in 2019, and there is a delay in the deformations that were caused during the dredging period.

The numerical model that was created does not understand the heating and cooling phases, as was expected. Although the model works perfectly without the heating phase, when the heating phase is activated, the wall moves in the opposite direction, as was expected. The FEM that was created could not understand the cycle effect as expected. An explanation is that the model cannot absorb the input temperature so quickly over a period of 20 days. Another explanation is that the steel and concrete of the quay wall are expanding so rapidly, due to the local increase in temperature, and the result is not valid.

It is important to mention that in order to analyse the movement of the combi walls and the anchor forces, there were selected specific sensors that were working properly and the measurements were familiar with what was expected as an output. However, a few sensors which are not presented in this thesis, illustrate a different response that is not congruent with common sense. Consequently, they were neglected from that research. Therefore, there is room for further research to understand why these sensors illustrate results that are not familiar with reality and make some new conclusions.

The part of FEM of this project is an area for further research and a better understanding of how FEM works with the heating input could contribute better to future predictions due to climate change. Regarding sensitivity analysis, the influence of each thermal parameter on the behaviour of the soil was examined. In general, geotechnical parameters typically show significant influence; therefore, knowledge of how parameter selection can influence the outcome of a FEM simulation can provide insight into the reliability of the obtained simulation results. However, the conclusion after the sensitivity analysis is that the thermal parameters did not have a dominant effect on the output. This conclusion is drawn with caution since, as mentioned, the model needs improvement.

This thesis aimed to explain whether the increase in anchor forces seasonally has an effect on the entire quay wall by performing a data analysis of available measurements. The research question that this thesis report aims to answer is as follows:

What is the influence of seasonal temperature fluctuation on a quay wall and how could this be modelled using finite element method models like PLAXIS 2D?

To help answer the research question, several sub-questions are formulated to guide the work of this thesis. Each sub-question and their respective answers are as follows:

What is the outcome of the installed monitoring system and how accurate are the results?

Regarding the measurement frequency of the HHTT quay wall, inclinometer measurements were performed several times during the construction process. However, after the dredging period, there are few measurements per year (1-2-3). It would be more beneficial for research projects if there were more measurements.

Furthermore, the seasonal increase in relative horizontal deformations was small, approximately 5 millimetres per season. Even though the usability of these measurements is limited as the possible error in the measurements has a similar magnitude, this pattern is replicated at different locations and of the

same magnitude. Therefore, the possibility of an error is unlikely. However, having more measurements could help to achieve a better, more accurate and precise result.

HHTT is the most well-instrumented quay wall. Deformations and anchor force measurements were used for this thesis. However, instead of the manual inclinometers that are used on the HHTT quay wall, the SAA is the best monitoring system because there are measurements every day. Therefore, also SAA measurements from the SIF quay wall were used to validate the phenomenon.

Moreover, the reference measurement of the FBG-sensors at the HHTT quay wall is only measured once. These sensors might not have been stabilised and could show signs of drift. If multiple reference measurements were performed, it would be possible to exclude that any drift occurs in the sensors and a more stable reference measurement is obtained. Last but not least, to avoid strange picks and shifts in the measurements, better monitoring systems should be maintained to avoid data gaps.

How do structural elements (diaphragm wall, combi wall, MV-piles, SI-piles) respond to seasonal temperature fluctuations?

At the HHTT quay wall, there is a movement of the wall during the summer period toward the sea, and during the winter period the wall moves backward. However, the wall, after its movement, never reaches the initial position. Therefore, this movement could be characterised as a plastic deformation and not as an elastic movement of the wall. Possibly, there is a delay in wall deformations that were caused by dredging during the construction period. Therefore, this movement will stop in the next years. However, it is highly recommended to continue measuring and analysing the movement of the wall to verify the assumption before.

Regarding the measurements, the movement of the wall is minor 5-10mm per cycle compared to the movement that occurred during the dredging period (50mm) in the construction phase of the quay wall. At the same time, because the wall is moving towards the sea, the anchor (MV-pile) reacts to that movement and is trying to keep the wall stable. Therefore, tension forces act on the MV-piles. For that reason, as the graphs that were presented in this research illustrate, there is an increase in the forces during the summer period and a decrease in the anchor forces during the winter period.

How can temperature effects be modelled using finite element models, e.g. PLAXIS 2D?

With the THM the heating phase of the quay wall could be modelled. Furthermore, an important factor is the correct boundary conditions and the reference values that will be used as input for the model. All of these were analytically explained in Chapter 5.

Although the model worked perfectly without the heating phase, the outcome of the heating phase was not the expected one. The main limitation of the FEM was that it was not able to model the cycle effect, and the results were not valid. Therefore, further research could be performed to achieve the optimal result. The model works well without the heating phase. Both models (with and without the relieving platform) accurately predict the wall deformation after the dredging period. (Graphs with deformations and graphs from PLAXIS 2D). However, the PLAXIS models could not understand cycle temperature effects.

To what extent should temperature effects be included in quay-wall engineering taking into account climate change effects

Regarding the output, the potential increase in temperature, according to the worst-case scenario of the ICPP, will have an impact on the wall. Both anchor forces and combi wall deformation will increase during a potentially long period of extended heat wave of 40°C. However, the result cannot be quantified due to the inaccurate outcome of the model. Moreover, higher temperature fluctuations could lead to larger cycles and cause degradation on the walls.

6.2. Recommendations

Based on the results regarding the match between the deformations of the combi wall of the quay wall and the increase and decrease of the anchor forces from the MV piles, the following topics are suggested for further research.

6.2.1. Measurement data

1. Examination of a greater number of season cycles for a more accurate and precise result.
2. Examination of the quay walls with either an SAA measurement system or with a greater amount of manual inclinometer measurements multiple times per year. SAA measurements are the most accurate and precise for analysing the cycle effect at the quay walls. Therefore, the installation of more SAA sensors for quay walls could contribute to a better result.
3. Weekly data analysis to determine when a sensor is not working properly to avoid data gaps.

6.2.2. FE modelling

1. Better input in PLAXIS in terms of temperature and calculation period, in order to better validate the seasonal fluctuation and the cycle effect.
2. The impact of climate change on the quay walls should be investigated in further research.
3. Perhaps other FEM models could better model the seasonal temperature fluctuation effect.

6.2.3. The overall contribution of this research study to the industry is summarised below

There is a seasonal effect with the movement of the quay wall and the increase and decrease in temperature. The wall is moving towards the sea during the summer period. However, the combi wall at the HHTT quay wall never reaches the initial position again, which means that even though the movement is minor (5-10mm), it seems that this cycle effect affects the wall.

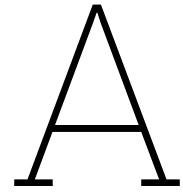
An educated guess, after this research project, is that the HHTT quay wall deforms due to a late response of the dredging period. However, if the deformations continue to increase per year for a few millimetres and with an increase of the temperature at the same time due to climate change, this could potentially influence the lifetime of a quay wall. Therefore, in the coming years a new study should be conducted to verify the effect. Cyclic loading effects can be more important than has been appreciated in design, particularly for quay wall structures that are exposed daily to huge loads. It is recommended that a graduated cyclic assessment process should be applied that starts with simple summary interaction diagrams and progresses, if required, to full analyses of site-specific soil-structure analyses considering local extreme heating and cooling loading conditions. Much work remains to be done before a proper understanding of the effects of cyclic loading due to temperature can be achieved; and this is an area for further research.

The thermal load on the combi wall is not a design parameter and is generally not investigated in detail. Therefore, it is strongly advised to conduct additional research. However, based on the findings from this research, it is concluded that the deformation resulting from the seasonal temperature fluctuation effect on a quay wall is not excessively large. This means that the primary objective of keeping the quay wall stable won't be compromised. This leads to the conclusion that the current design of a quay wall without taking into consideration the temperature is safe to be applied.

References

- [1] O. B. Andersland and B. Ladanyi. "An Introduction to Frozen Ground Engineering". In: *Springer Book Archive* Springer New York, NY (1994). URL: <https://doi.org/10.1007/978-1-4757-2290-1>.
- [2] R. Brinkgreve, Erjona Engin, and Harun Kürşat Engin. "Validation of empirical formulas to derive model parameters for sands". In: June 2010. ISBN: 978-0-415-59239-0. DOI: 10.1201/b10551-25.
- [3] A. Dijkstra. "Geotechnisch laboratoriumonderzoek, Project Hartel Tank Terminal te Rotterdam. Technical Report". In: *Wiertsema Partners Raadgevend Ingenieurs* (2017).
- [4] A. Fedorov et al. "Structural monitoring system with fiber Bragg grating sensors: Implementation and software solution". In: *Journal of Physics Conference Series* 594 (Mar. 2015), p. 012049. DOI: 10.1088/1742-6596/594/1/012049.
- [5] T. Gerber et al. "Monitoring Displacement vs. Depth in Lateral Pile Load Tests Using Shape Accelerometer Arrays". In: *17th International Conference on Soil Mechanics and Geotechnical Engineering (Alexandria)* (2016), pp. 2016–2019. DOI: 10.3233/978-1-60750-031-5-2016.
- [6] J. G. Gijt and M. L. Broeken. *Quay walls*. SBRCURnet Publication, 211E. CRC Press, 2014.
- [7] Stotaw Talbachew Hayle et al. "Reliable self-healing FBG sensor network for improvement of multipoint strain sensing". In: *Optics Communications* 499 (2021), p. 127286. ISSN: 0030-4018. DOI: <https://doi.org/10.1016/j.optcom.2021.127286>. URL: <https://www.sciencedirect.com/science/article/pii/S0030401821005356>.
- [8] B. Hurk and P. Siegmund. "KNMI'14: Climate Change scenarios for the 21st Century – A Netherlands perspective". In: *Scientific Report WR2014-01,KNMI* Version 26 (2014).
- [9] Michele Jamiolkowski, Diego Lo Presti, and Mario Manassero. "Evaluation of Relative Density and Shear Strength of Sands from CPT and DMT". In: Jan. 2003, pp. 201–238. ISBN: 978-0-7844-0659-5. DOI: 10.1061/40659(2003)7.
- [10] Jae-Min Kim et al. "Enhanced Strain Measurement Range of an FBG Sensor Embedded in Seven-Wire Steel Strands". In: *Sensors* 17 (July 2017), p. 1654. DOI: 10.3390/s17071654.
- [11] Jae-Min Kim et al. "Measurement of Prestressing Force in Pretensioned UHPC Deck Using a Fiber Optic FBG Sensor Embedded in a 7-Wire Strand". In: *Journal of Sensors* 2016 (July 2016), pp. 1–9. DOI: 10.1155/2016/8634080.
- [12] F.H. Kulhawy and Paul Mayne. "Manual on Estimating Soil Properties for Foundation Design". In: (Aug. 1990).
- [13] R. F. Obrzud and A. Truty. "The Hardening soil model – a practical guidebook". In: *Technical Report, Zace Services Ltd* (2018).
- [14] PLAXIS. "Reference Manual". In: *Bentley Systems International Limited, Dublin*. (1994).
- [15] PLAXIS. "Reference Manual". In: *Bentley Systems International Limited, Dublin*. (2022). URL: <https://communities.bentley.com/products/geotech-analysis/w/wiki/46137/manuals---plaxis>.
- [16] P. Robertson. "Soil classification using the cone penetration test". In: *Canadian Geotechnical Journal - CAN GEOTECH J* 27 (Feb. 1990), pp. 151–158. DOI: 10.1139/t90-014.
- [17] Joachim Rösler, Martin Baeker, and Harald Harders. *Mechanical Behaviour of Engineering Materials: Metals, Ceramics, Polymers, and Composites*. Jan. 2007. ISBN: 978-3-540-73446-8. DOI: 10.1007/978-3-540-73448-2.
- [18] T. Schanz, P.A. Vermeer, and P.G. Bonnier. "The hardening soil model: Formulation and verification". In: Jan. 2019, pp. 281–296. ISBN: 9781315138206. DOI: 10.1201/9781315138206-27.

- [19] O. Schouten. "Optimising the functionality of smart quay walls using measurement data obtained during the construction process". In: *M.Sc. Thesis TU Delft* (2020). URL: <http://resolver.tudelft.nl/uuid:1b827ff8-7b5f-4d6f-9c4f-b24f71203c98>.
- [20] Klaus Schwab. *The Global Competitiveness Report 2019*. Tech. rep. World Economic Forum, 2019, p. 666. URL: http://www3.weforum.org/docs/WEF_TheGlobalCompetitivenessReport2019.pdf.
- [21] Ahmed A. Serageldin et al. "Soil Temperature Profile for some New Cities in Egypt: Experimental Results and Mathematical Model". In: Aug. 2015.
- [22] Timothy Stark, Hangseok Choi, and Sean McCone. "Drained Shear Strength Parameters for Analysis of Landslides". In: *Journal of Geotechnical and Geoenvironmental Engineering - J GEOTECH GEOENVIRON ENG* 131 (May 2005). DOI: 10.1061/(ASCE)1090-0241(2005)131:5(575).
- [23] T.F. Stocker et al. "Climate Change 2013: The Physical Science Basis. Contribution of Working Group I to the Fifth Assessment Report of the Intergovernmental Panel on Climate Change". In: *Cambridge University Press, Cambridge, United Kingdom and New York, NY, USA* 1535 pp (2013).
- [24] J. Vries. "Quays Rather Than Boilers: Extracting Heat From Water and Soil Through Energy Sheet Piles". In: *M.Sc. Thesis TU Delft* (2021). URL: <http://resolver.tudelft.nl/uuid:2da05b2a-db22-4cfb-9a3d-fd8f33c5dcca>.



Data

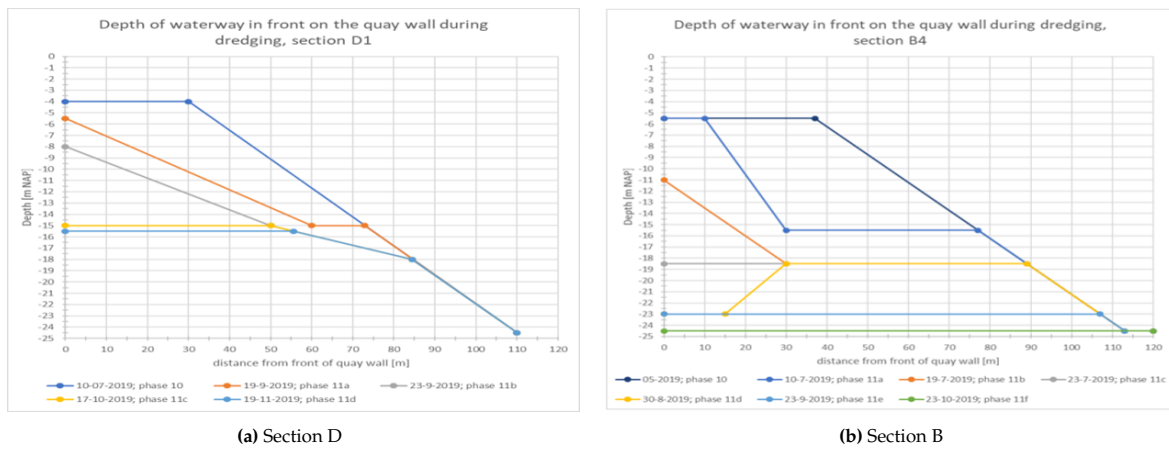


Figure A.1: Dredging records from section B and D at the HHTT quay wall [19]

Table A.1: Table of deformations for each measurement of combi wall at Section B-03 at depth = -5.50 m+NAP

Date	Deformation (mm)
24/01/2019	12.86
24/01/2019	12.86
10/07/2019	20.36
23/07/2019	23.24
02/09/2019	29.82
19/11/2019	32.64
15/07/2020	37.37
14/01/2021	33.04
02/07/2021	36.94
25/01/2022	35.70
16/06/2022	42.63

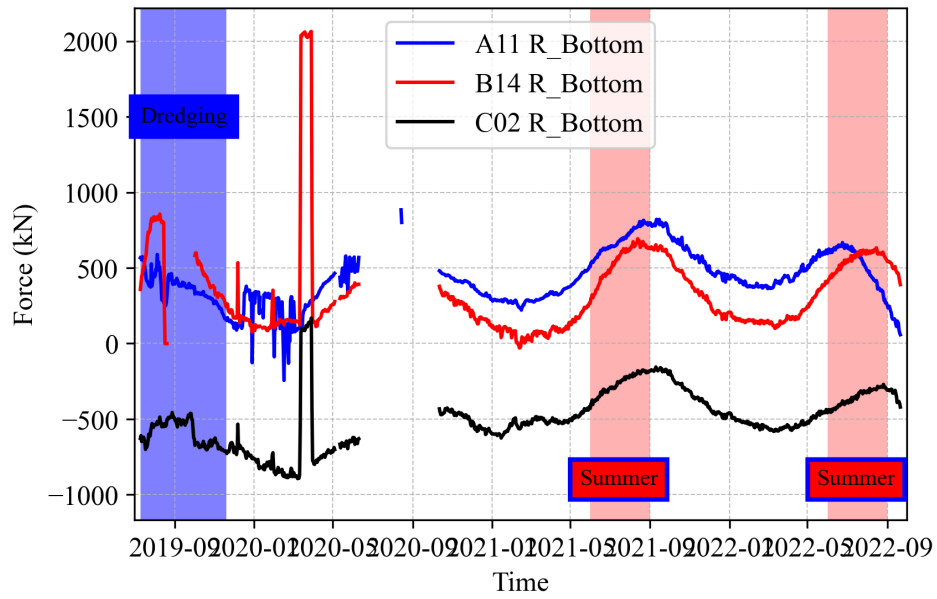


Figure A.2: Anchor forces from the right bottom sensor of the MV piles A11, B14 and C02 during the period from 11/2020 to 03/2022

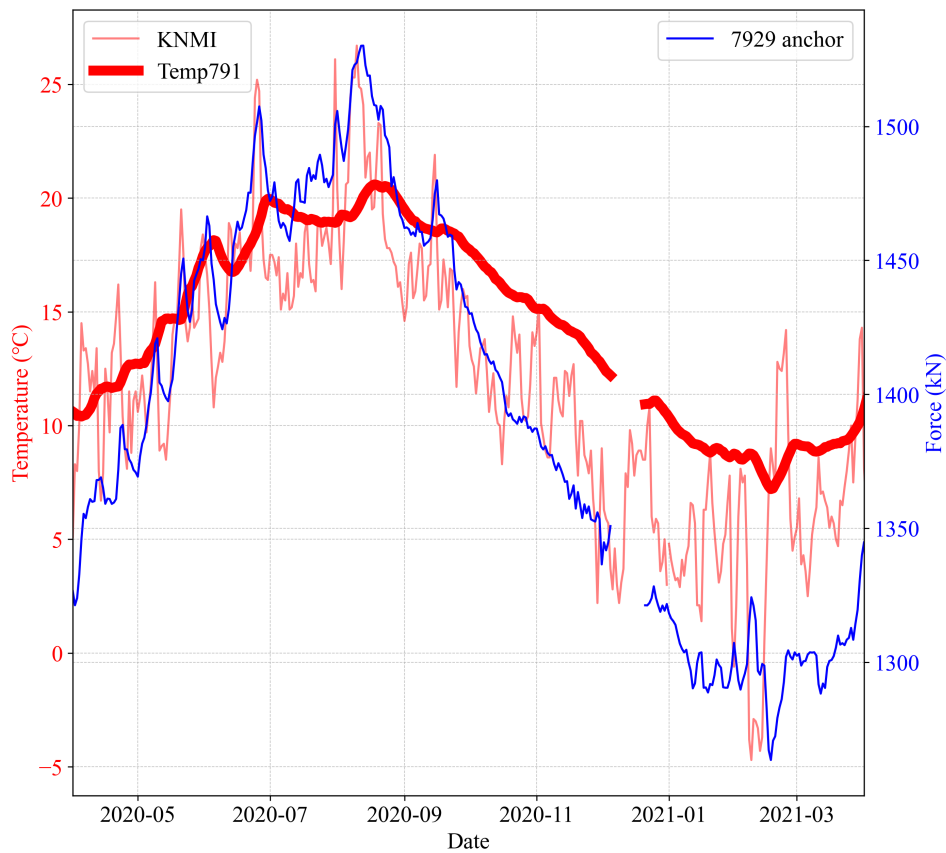


Figure A.3: Britanniehaven anchor 7929, temperature sensor 791 and KNMI temperatures from 05/2020 to 05/2021

Table A.2: Table of deformations for each measurement of combi wall at Section PUT-1

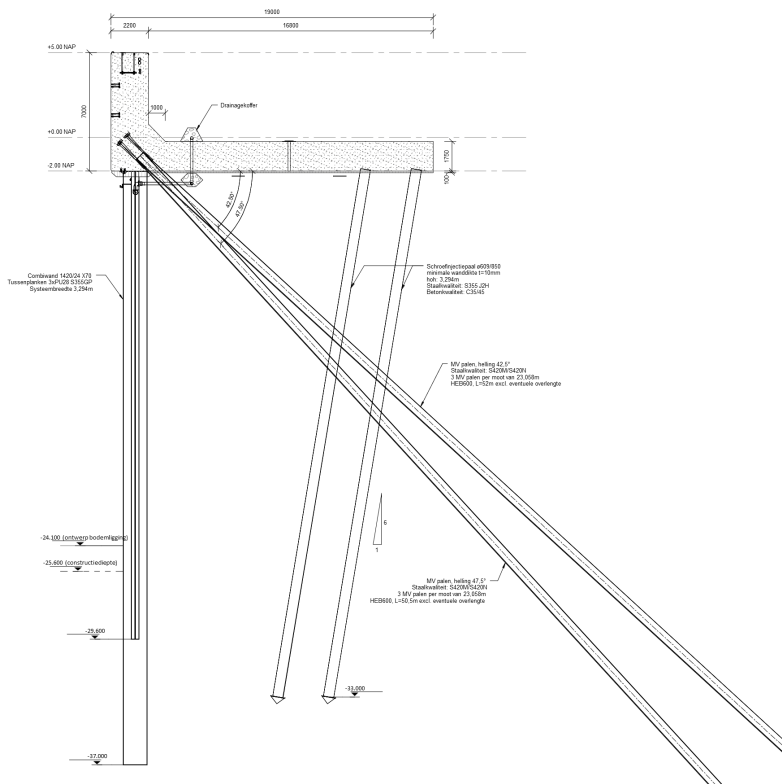
Date	Deformation (mm)
07/03/2018	103.145
18/07/2018	110.15
09/10/2018	109.69
18/12/2018	107.355
19/08/2019	112.175
15/10/2019	109.06
27/01/2020	104.64
05/08/2020	110.695
14/10/2020	111.82
21/12/2020	109.275
05/03/2021	108.59
30/06/2021	110.85
18/11/2021	109.365
23/02/2022	109.675

Table A.3: Table of deformations for each measurement of combi wall at Section PUT-2

Date	Deformation (mm)
17/12/2012	58.92
17/12/2012	58.92
06/05/2014	60.205
20/08/2014	64.38
28/11/2014	63.715
27/01/2015	57.475
02/04/2015	62.475
16/06/2015	63.125
30/11/2015	64.06
04/03/2016	62.335
01/07/2016	66.015
30/08/2016	67.3
29/11/2016	65.685
02/05/2017	63.855
18/07/2017	69.715
03/10/2017	62.785
15/12/2017	64.135
18/07/2018	69.215
09/10/2018	66.485
18/12/2018	64.36
19/08/2019	69.785
15/10/2019	65.96
27/01/2020	64.65
04/06/2020	66.465
05/08/2020	66.035

Table A.4: Table of deformations for each measurement of combi wall at Section PUT-3

Date	Deformation (mm)
07/03/2018	93.005
18/07/2018	101.1
09/10/2018	103.065
18/12/2018	95.14
19/08/2019	105.695
15/10/2019	102.34
27/01/2020	98.41
04/06/2020	103.405
05/08/2020	103.83
14/10/2020	101.545
21/12/2020	99.325
05/03/2021	99.36
30/06/2021	103.975
18/11/2021	102.955
23/02/2022	99.105
03/06/2022	101.725

**Figure A.4:** Section B HHTT

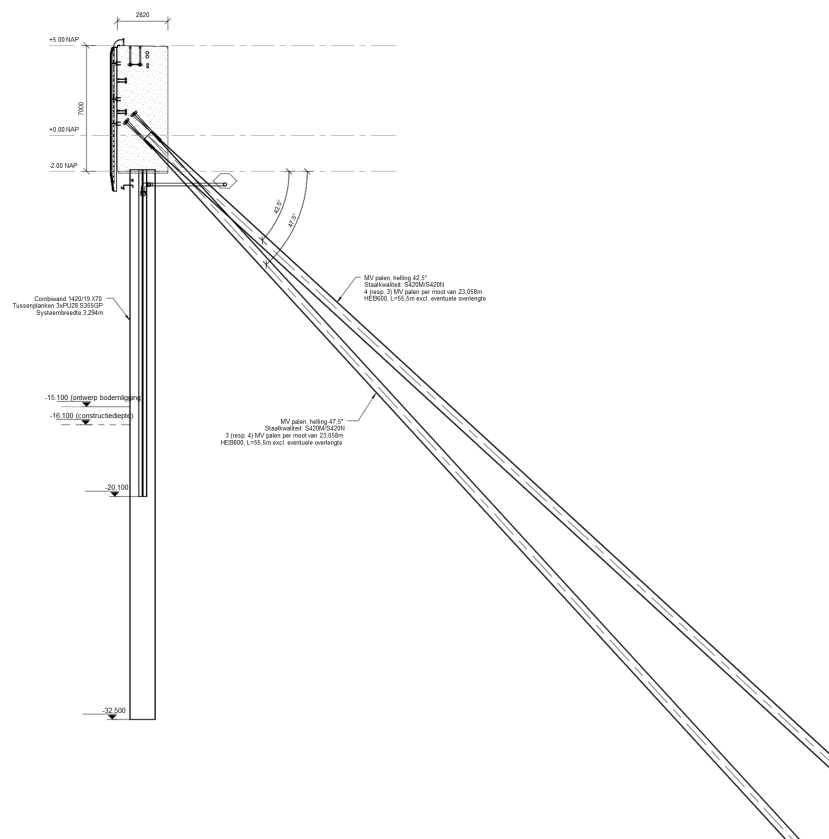
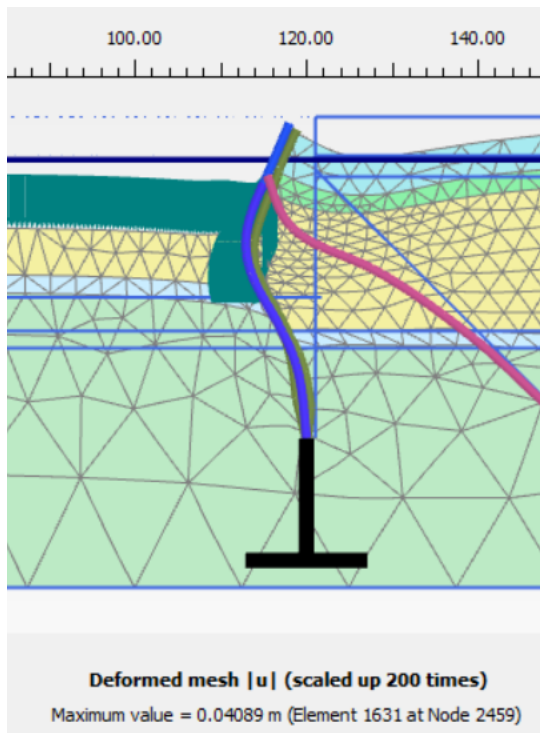


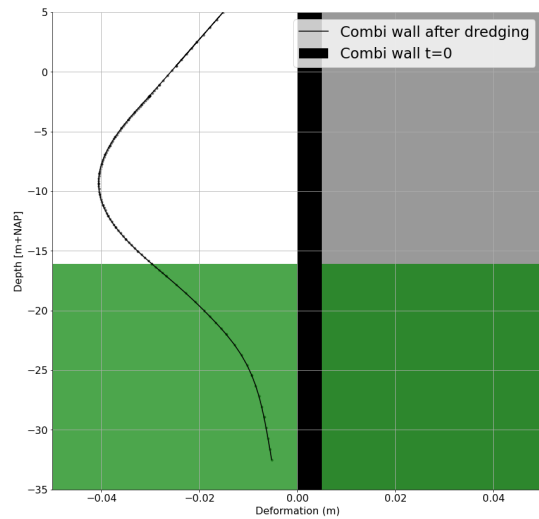
Figure A.5: Section D HHTT

B

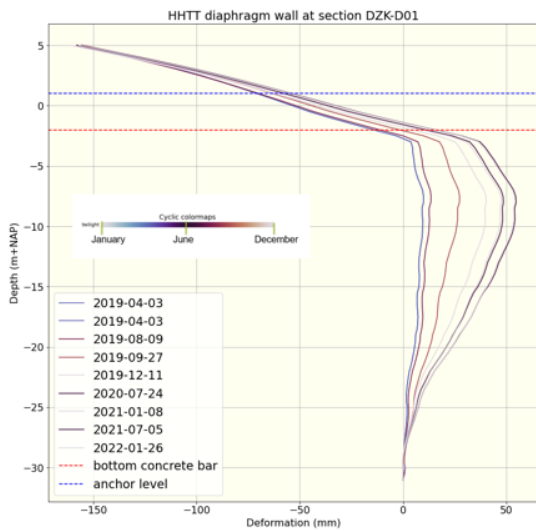
FEM



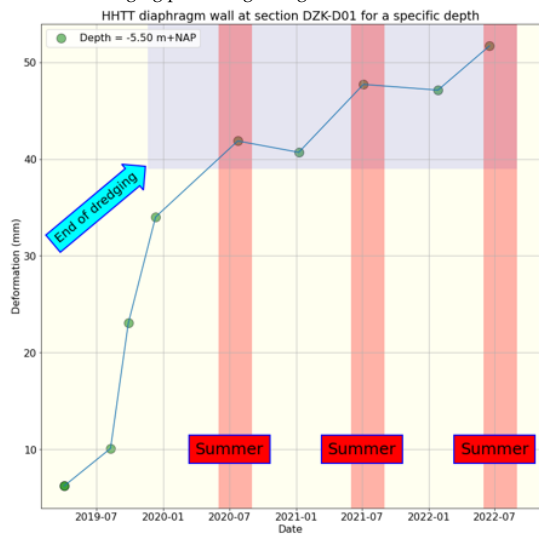
(a) Deformed mesh of the model without the relieving platform after the dredging period



(b) Deformation vs Depth of the combi wall before and after dredging period regarding PLAXIS 2D model

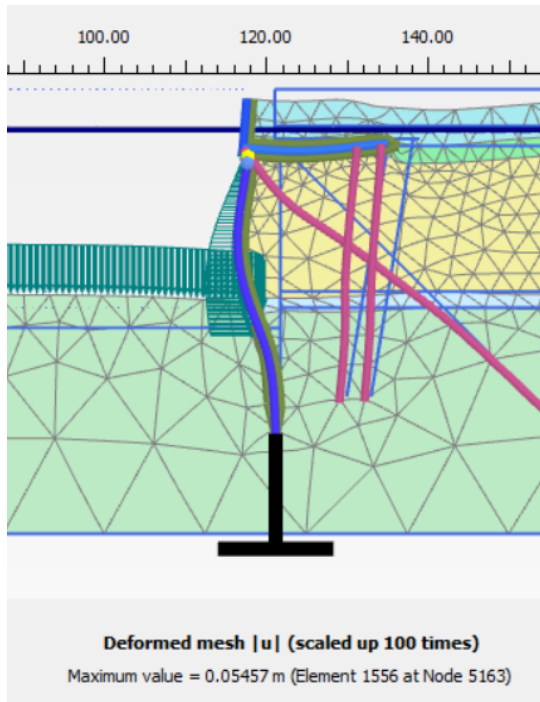


(c) Deformation vs Depth of the combi wall before and after dredging period regarding PLAXIS 2D model

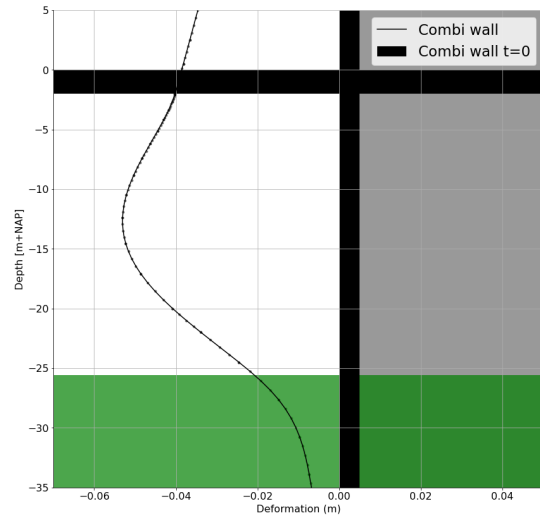


(d) Deformation vs Depth of the combi wall before and after dredging period regarding PLAXIS 2D model

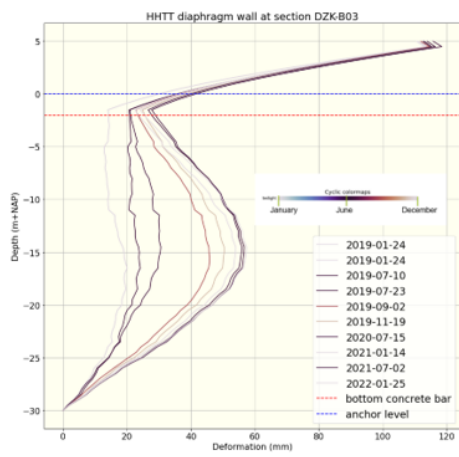
Figure B.1: Model without a relieving platform



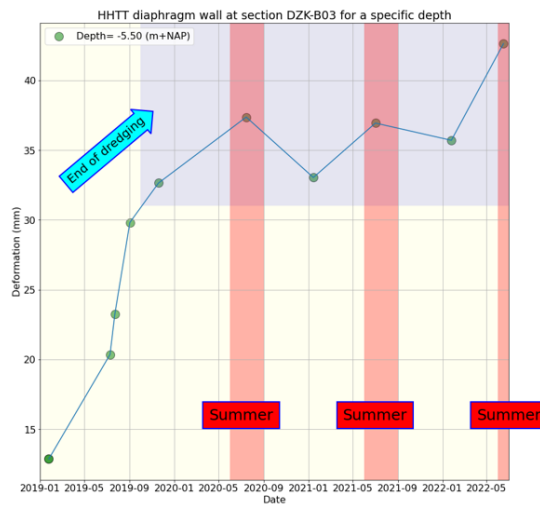
(a) Deformed mesh of the model without the relieving platform after the dredging period



(b) Deformation vs Depth of the combi wall before and after dredging period regarding PLAXIS 2D model



(c) Deformation vs Depth of the combi wall before and after dredging period regarding PLAXIS 2D model



(d) Deformation vs Depth of the combi wall before and after dredging period regarding PLAXIS 2D model

Figure B.2: Model without a relieving platform

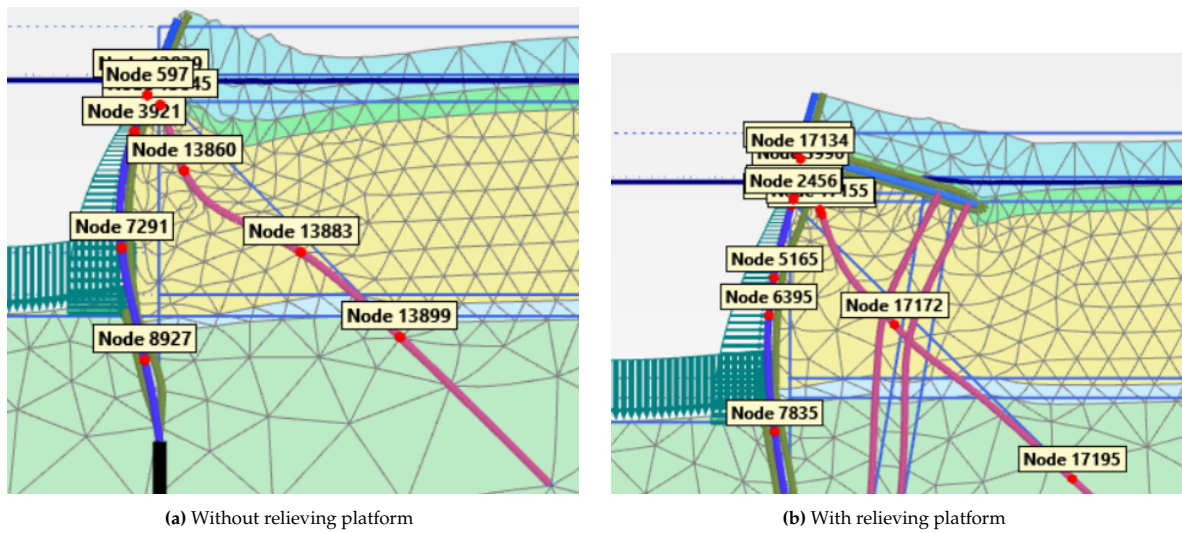


Figure B.3: Nodes for analysing the deformations of the combi wall and the axial forces of the MV pile

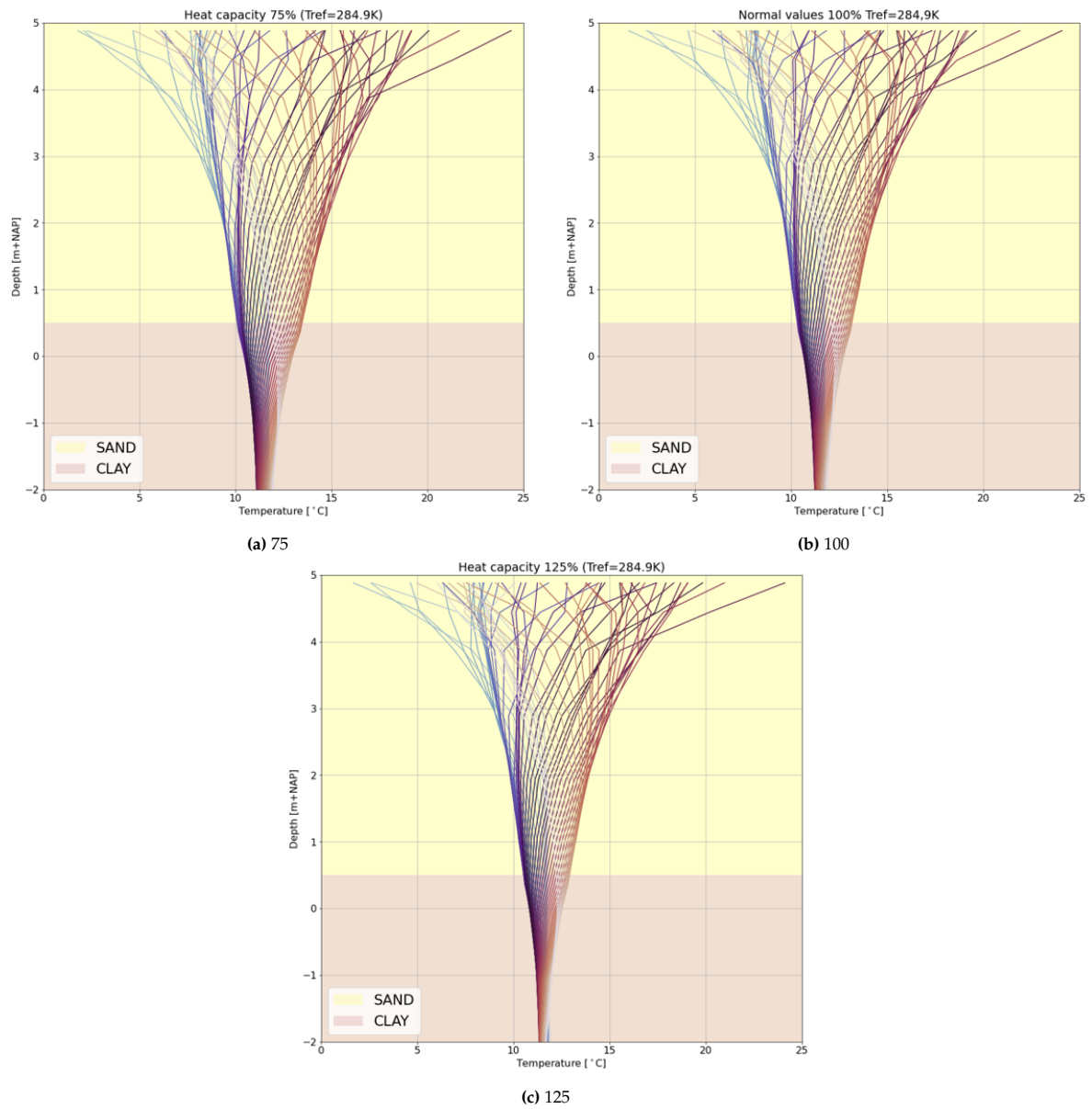


Figure B.4: Sensitivity analysis changing the value of the heat capacity

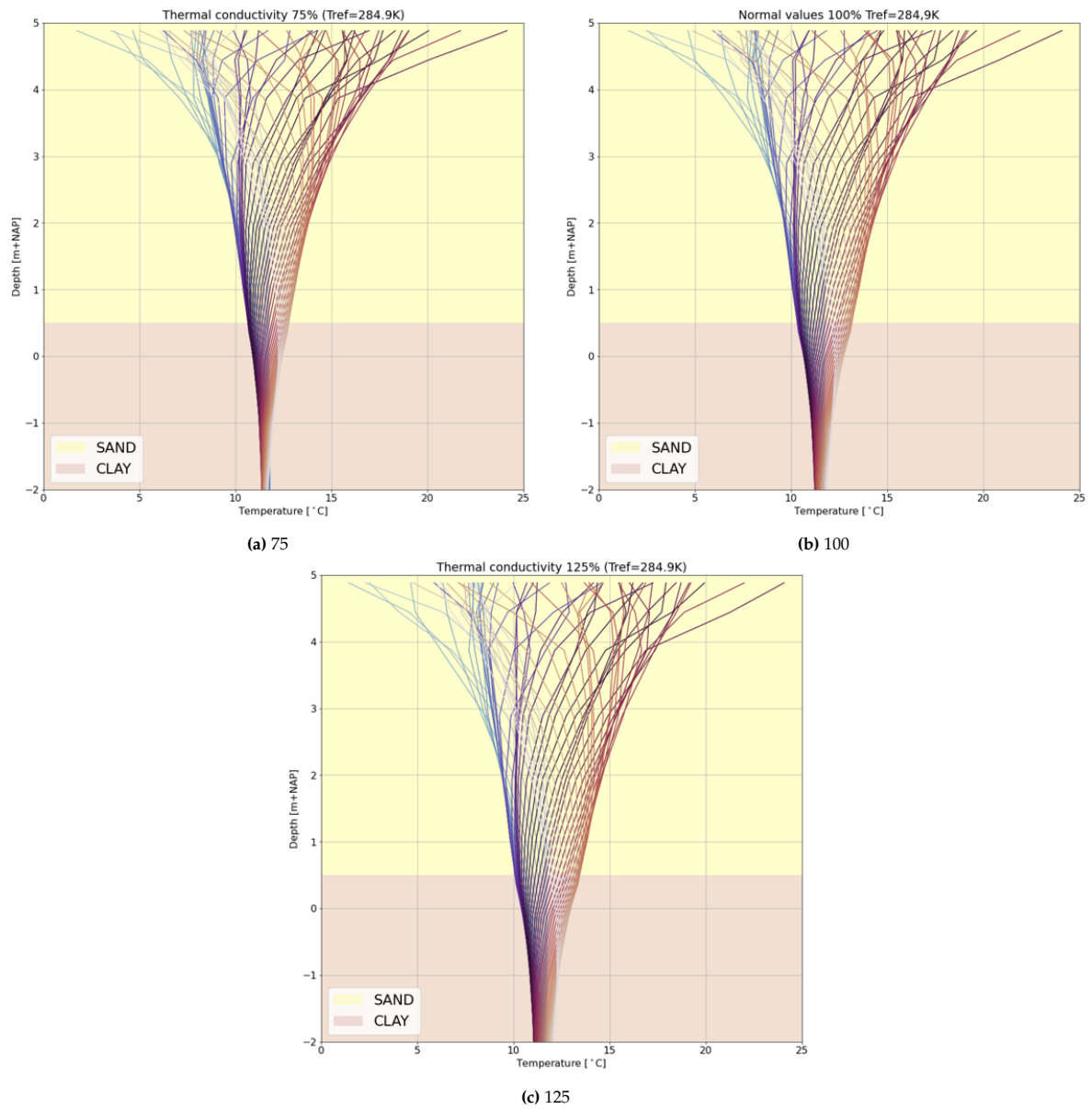


Figure B.5: Sensitivity analysis changing the value of the thermal conductivity